Title
THE LAMB SHIFT IN HELIUMLIKE URANIUM (u90+)

Author
Munger, C.T.

Publication Date
1987

Lawrence Berkeley Laboratory
UNIVERSITY OF CALIFORNIA

Materials & Molecular Research Division

THE LAMB SHIFT IN HELIUMLIKE URANIUM (U^{90+})

C.T. Munger, Jr.
(Ph.D. Thesis)

January 1987

Prepared for the U.S. Department of Energy under Contract DE-AC03-76SF00098

DISCLAIMER

The Lamb Shift in Heliumlike Uranium (U^{90+})

Charles T. Munger Jr.

(Ph. D. Thesis)

LBL 22640

Lawrence Berkeley Laboratory
University of California
Berkeley, California 94720

Abstract

I report an experimental value of 70.4 (8.3) ev for the one-electron Lamb shift in uranium, in agreement with the theoretical value of 75.3 (0.4) ev. I extract the Lamb shift from a beam-foil time-of-flight measurement of the 54.4 (3.4) ps lifetime of the $1s\,2p_{1/2}\,{}^3P_0$ state of heliumlike (two-electron) uranium.

This work was supported by the Director, Office of Energy Research: Office of Basic Energy Sciences, Chemical Sciences Division; and in part by the Office of High Energy and Nuclear Physics, Nuclear Science Division, of the U.S. Department of Energy under Contract No. DE-AC-03-76SF00098.

Dedication

I respectfully dedicate this thesis to my fellow Wiccamists, who would never have believed it; and to Dr. Gregory, who might.

Acknowledgements

Like the capstone of a pyramid this work rests on the accumulated labors of many. To the engineers, scientists and technicians of Lawrence Berkeley Laboratory and of the University of California, without whom not one stone would rest upon another, my thanks.

It is a special pleasure to thank my advisor Dr. Harvey Gould for his ideas, support and and encouragement; for his long hours of labor on this experiment; and for the opportunity to learn a trade from an ingenious and careful experimental physicist. I thank Mr. Roy Bossingham, Dr. Benedict Feinberg, Mr. Walter L. Kehoe, Dr. Richard McDonald, Professor Richard Mowat, and Dr. Alfred Schlachter for their assistance in running the experiment. I thank Professor Gordon W.F. Drake, Professor Walter R. Johnson, and Dr. Peter J. Mohr for many helpful discussions and for providing unpublished results. I especially thank the operators, staff and management of the Bevalac for making experiments with few-electron uranium possible.

This work was supported by the Director, Office of Energy Research: Office of Basic Energy Sciences, Chemical Sciences Division; and in part by the Office of High Energy and Nuclear Physics, Nuclear Science Division, of the U.S. Department of Energy under Contract No. DE-AC-03-76SF00098.

Table of Contents

The Lamb Shift in Heliumlike Uranium (U^{90+})

Chapter 1: General Overview

A possible failure of quantum electrodynamics (QED) to predict accurate radiative corrections to bound states at Z = 92 is not ruled out by its success at low Z. The largest contribution to the Lamb shift at Z = 92 comes from terms in the electron self-energy[1] which are high powers of $Z\alpha$ and which are invisible in experiments at low Z. Nor is a failure ruled out by precision measurements of the K x rays of neutral atoms, because the approximate many-electron problems yet solved on a computer differ from the true problem by the omission of terms whose effect on the $1s$ binding energy is at least 10% of the radiative shift of the $1s$ state[2]. Lamb shift measurements on high-Z electronic and muonic atoms are complementary because muonic atom measurements are sensitive to higher order vacuum polarization effects but not to self-energy effects[3].

We[4] report a value of 70.4 (8.3) ev for the one-electron Lamb shift in uranium. It is in agreement with the theoretical value[5,6] of 75.3 (0.4) ev based upon a calculation of the self-energy by Mohr[5]. We extract our Lamb shift from our beam-foil time-of-flight measurement of 54.4 (3.4) ps for the lifetime of the $1s\,2p_{1/2}\,{}^3P_0$ state of heliumlike uranium.

The $1s\,2p_{1/2}\,{}^3P_0$ state (Figure 1.1) is the only low-lying excited state found in

---

[1]G.W. Erickson, Phys. Rev. Lett. 27, 780 (1971); P.J. Mohr, Ann. Phys. New York 88, 26 (1974); P.J. Mohr, private communication.

[2]For the energies of $n = 2 \rightarrow 1$ transitions in neutral heavy elements a comparison between experiment and the predictions from the sum of the results of Multi-Configurational Dirac-Hartree-Fock codes and the hydrogenic K and L Lamb Shifts may be found in paper by Peter Mohr, *Lamb Shift in High-Z Atoms,* in *Relativistic Effects in Atoms, Molecules, and Solids,* G.L. Malli, editor; Plenum Press, New York, 1983, p. 145.

[3]For a review of strong field QED, see S.J. Brodsky and P.J. Mohr, in: *Structure and Collisions of Ions and Atoms.* ed. I.A. Sellin (Springer, Berlin, 1978), Topics in Current Physics, Vol. 5, p. 3.

[4]In this thesis the combined work of Dr. Harvey Gould and me is introduced with the pronoun "we"; work which is mine alone is introduced with "I".

[5]P.J. Mohr, Phys. Rev. Lett. 34, 1050 (1975); P.J. Mohr, Phys. Rev. A26, 2338 (1982).

[6]W.R. Johnson and G. Soff, Atomic Data and Nucl. Data Tables 33, 405 (1985).

hydrogenlike uranium or heliumlike uranium whose long lifetime allows its decay to be observed in vacuum downstream from the target in which it is produced. In heliumlike uranium the $1s\,2p_{1/2}\,{}^3P_0$ state decays 70% of the time to the $1s\,2s\ {}^3S_1$ state by an electric-dipole (E1) transition. This makes the $1s\,2p_{1/2}\,{}^3P_0$ lifetime sensitive to the $1s\,2p_{1/2}\,{}^3P_0$ - $1s\,2s\ {}^3S_1$ energy difference of 260.0 (7.9) ev (experimental value) and hence to the Lamb shift. At Z=92 the major contributions to the calculated Lamb shift are the self-energy[5] of 56.7 ev, the leading order term in the vacuum polarization[5,6] of -14.3 ev and the finite nuclear size correction[6] of 32.5 ev. In heliumlike uranium there is also a small screening correction to the radiative corrections - expected to be of order 1/Z times the self-energy[3,7]. For zero Lamb shift the $1s\,2p_{1/2}\,{}^3P_0$ - $1s\,2s\ {}^3S_1$ states would be split by the difference in the $1s_{1/2}$ - $2s_{1/2}$ and $1s_{1/2}$ - $2p_{1/2}$ Coulomb interactions. This splitting at Z = 92 has been calculated by Mohr[8] to be 330.4 ev; which agrees (1 ev) with the calculations of Lin, Johnson and Dalgarno[9] and of Drake[10]. The other significant decay of the $1s\,2p_{1/2}\,{}^3P_0$ state is to the $1s^2\,{}^1S_0$ ground state by a two-photon electric-dipole magnetic-dipole (E1M1) transition[10]. To obtain the Lamb shift we combine our measured $1s\,2p_{1/2}\,{}^3P_0$ lifetime and the calculated values for the E1M1 decay rate[10], the $1s\,2p_{1/2}\,{}^3P_0$ - $1s\,2s\ {}^3S_1$ E1 matrix element[11], and the $1s\,2p_{1/2}\,{}^3P_0$ - $1s\,2s\ {}^3S_1$ Coulomb splitting[8].

In our beam-foil time-of-flight measurement 0.7%[12] of a beam of 218 Mev/amu hydrogenlike uranium is converted to the $1s\,2p_{1/2}\,{}^3P_0$ state of heliumlike uranium by electron

---

[7]P.J. Mohr, in *Relativistic Effects in Atoms, Molecules, and Solids,* edited by G.L. Malli (Plenum, New York, 1983), p. 145.

[8]P.J. Mohr, Phys. Rev. A32, 1949 (1985); P.J. Mohr, in *Beam Foil Spectroscopy* edited by I.A. Sellin and D.J. Pegg (Plenum, New York, 1976), Vol 1, p. 97; P.J. Mohr, private communication.

[9]C.D. Lin, W.R. Johnson, and A. Dalgarno, Phys. Rev. A15, 154 (1977); F. Parpia, and W.R. Johnson, private communication.

[10]G.W.F. Drake, Nucl. Instrum. Methods in Phys. Research B9, 465 (1985); G.W.F. Drake, private communication.

[11]M. Hillery and P.J. Mohr, Phys. Rev. A21, 24 (1980); H. Gould, R. Marrus, and P.J. Mohr, Phys. Rev. Lett. 33, 676 (1974).

[12]This figure of 0.7% replaces the less precise statement of "about 0.5%" found in C.T. Munger and H. Gould, Phys. Rev. Lett. 57, 2927 (1986).

capture in a 0.9 mg/cm^2 Pd foil. Hydrogenlike uranium[13] is obtained from the Lawrence Berkeley Laboratory's Bevalac[14]. Downstream from the Pd foil we observe, not the 260 ev photon from the $1s\,2p_{1/2}\,{}^3P_0 \rightarrow 1s\,2s\ {}^3S_1$ transition, but instead the 96.01 kev x ray[6,8] from the subsequent fast decay of the $1s\,2s\ {}^3S_1$ state to the $1s^2\,{}^1S_0$ ground state. The 96.01 kev x ray is much easier to detect than the 260 ev photon, and the $1s\,2s\ {}^3S_1$ lifetime[9] of 10^{-14} s has no effect on the measured $1s\,2p_{1/2}\,{}^3P_0$ lifetime provided sufficient time is allowed for the initial $1s\,2s\ {}^3S_1$ population to decay.

Figure 1.2 shows a spectrum recorded by one of our Ge x-ray detectors collimated to view emission perpendicular to the uranium beam at a point 0.67 cm downstream from the Pd foil. The 96.01 kev x ray from the $1s\,2p_{1/2}\,{}^3P_0$ -fed $1s\,2s\ {}^3S_1 \rightarrow 1s^2\,{}^1S_0$ decay is Doppler shifted and appears as a peak at 77.76 (0.18) kev. We identified this peak by its correct time dilation (transverse Doppler shift) and exponential decay at two different beam energies, 218 Mev/amu and 175 Mev/amu (here determined from the operating conditions of the Bevalac and corrected for energy loss in foils); by the dependence of the Doppler broadened peak width on the angular acceptance of the detector; by the yield[15] using foils of different Z and thickness; by the peak's absence when the foil is removed; and by the lack of any other long-lived, low-lying states of heliumlike uranium or hydrogenlike uranium besides the $1s\,2p_{1/2}\,{}^3P_0$ state.

The height of the peak above background was found by a maximum-likelihood fit of a quadratic to the background. The decay curve (Figure 1.3), which spans 2.7 decay lengths, is a maximum-likelihood fit of a single exponential to the data. The reduced χ^2 for the fit is

---

[13]H. Gould, D. Greiner, P. Lindstrom, T.J.M. Symons, and H. Crawford, Phys. Rev. Lett. 52, 180 (1984) (Errata, 52, 1654 [1984]).

[14]J.R. Alonso, R.T. Avery, T. Elioff, R.J. Force, H.A. Grunder, H.D. Lancaster, J.R. Meneghetti, F.B. Selph, R.R. Stevenson, and R.B. Yourd, Science 217, 1135 (1982).

[15]W.E. Meyerhof, R. Anholt, J. Eichler, H. Gould, Ch. Munger, J. Alonso, P. Thieberger, and H.E. Wegner, Phys. Rev. A32, 3291 (1985); R. Anholt and W.E. Meyerhof, Phys. Rev A33, 1556 (1986).

0.89. The spectrum shown in Fig. 1.2 contributes to the first point at 0.67 cm in Fig. 1.3. The 1/e decay length is 1.182 (0.069) cm, and the 5.8% statistical error dominates our final error in the $1s\,2p_{1/2}\,^3P_0$ lifetime. We determine the beam velocity to be 0.5866 (44) c from the Doppler shift of the x ray from the $1s\,2s\ ^3S_1 \rightarrow 1s^2\,^1S_0$ transition. This velocity agrees with the value of 0.583 (2) c determined from the operating conditions of the Bevatron corrected for energy loss in foils. (We choose to use the Doppler shift determined value of the velocity which, although less accurate, is more direct.) Our value for the $1s\,2p_{1/2}\,^3P_0$ lifetime is 54.4 (3.4)ps. Other contributions to our 6.3% total lifetime error are: 1.2% in the determination of the beam velocity and time dilation using the transverse Doppler shift of the $1s\,2s\ ^3S_1 \rightarrow 1s^2\,^1S_0$ transition and 2.3% from the experimental upper limit to contamination of our signal by cascade feeding.

A disadvantage in using the $1s\,2p_{1/2}\,^3P_0$ - fed $1s\,2s\ ^3S_1 \rightarrow 1s^2\,^1S_0$ decay as a signal is that it makes the measured $1s\,2p_{1/2}\,^3P_0$ lifetime sensitive to repopulation of the $1s\,2p_{1/2}\,^3P_0$, $1s\,2s\ ^3S_1$ and $1s\,2p_{1/2}\,^3P_1$ states by cascade feeding from states of high principal quantum number n. States of heliumlike uranium with $n < 22$ will cascade to the $1s^2\,^1S_0$ ground state before we begin our measurement of the $1s\,2p_{1/2}\,^3P_0$ lifetime. But the population of states with $n \geq 22$ and high orbital angular momentum (l) can perturb our measurement by cascading down the chain of $l = n - 1$ yrast states. The population of these states however is very small and we are able to set an upper limit of 2.3% for their contribution to the measured decay length.

In heliumlike uranium there are four $J = j_1 + j_2$ (jj coupled) states of a $1s_{1/2}$ electron coupled to a nl electron: they are $J = l - 1$ and $J = l$ for a $1s_{1/2}$ electron coupled to a $nj = nl - 1/2$ electron, and $J = l$ and $J = l + 1$ for a $1s_{1/2}$ electron coupled to a $nj = nl + 1/2$ electron. We assume that the population of the $nj = nl + 1/2$ states and $nj = nl - 1/2$ are equal. This assumption is consistent with our observation of the intensities of the $n = 2$

state fine structure components of heliumlike and hydrogenlike uranium when we view the target directly and by the population of the $1s\,2p_{1/2}\,^3P_0$ state. (If the nj $= l + 1/2$ states have greater populations, our analysis overestimates the uncertainty due to cascades.) We also assume that for each nj electron the population of the two states of different J are equal. Surprisingly, the populations of the four different jj coupled states are only slightly redistributed in the cascade because the probability for making $\Delta J = 0$ or $\Delta j = 0$ transitions scales roughly as $0.5\ l^{-2}$ and therefore is very small at high l.

Cascades which have the potential to affect the measured decay length, besides those reaching the $1s\,2p_{1/2}\,^3P_0$, are those reaching the the $1s\,2p_{1/2}\,^3P_1$ and $1s\,2p_{3/2}\,^3P_2$ states: the $1s\,2p_{3/2}\,^3P_2$ state because it decays 30% of the time to the $1s\,2s\ ^3S_1$ state; and the $1s\,2p_{1/2}\,^3P_1$ state because its decay is not resolved from the $1s\,2s\ ^3S_1$ decay. We set a limit to the presence of these cascades by searching for the x ray which results[6,9] from both $1s\,2p_{3/2}\,^1P_1$ decay (100.6 kev) and from the 70% of the $1s\,2p_{3/2}\,^3P_2$ state which decay directly to the ground state (100.5 kev). The rates at which cascades enter the $1s\,2p_{1/2}\,^3P_0$, $1s\,2s\ ^3S_1$ and $1s\,2p_{1/2}\,^3P_1$ states are proportional to the intensity of this x-ray line. In Fig. 1.2 this x-ray line would appear as an isolated peak, Doppler shifted to 81.4 kev. The count rate from this supposed peak, after subtraction of the background, is plotted in Fig. 1.3 and is consistent with zero.

As both feeding of the $1s\,2p_{1/2}\,^3P_0$ state and blends from the $1s\,2s\ ^3S_1$ and $1s\,2p_{1/2}\,^3P_1$ states would be present from cascades, the effect upon the measured $1s\,2p_{1/2}\,^3P_0$ decay length would be positive for a constant or slowly decreasing cascade rate and negative for for a rapidly decreasing cascade rate. The bounds set by the data on the respective shifts are +3.2% and -1.4% respectively. These are smaller than the statistical error in the $1s\,2p_{1/2}\,^3P_0$ lifetime of 5.8% and we combine cascade uncertainties into a single error of 2.3%.

Possible cascades in the hydrogenlike fraction of our beam would feed the $2\,^2P_{3/2}$ and $2\,^2P_{1/2}$ states which are unresolved from the corresponding states in the heliumlike fraction. We find that if part of the cascades came from hydrogenlike uranium instead of heliumlike uranium the net effect of cascades on the measured $1s\,2p_{1/2}\,^3P_0$ lifetime would decrease. We have found it difficult to produce excited states of heliumlike uranium by direct excitation in a target and therefore we expect to produce only a negligible number of excited states of hydrogenlike uranium in our target.

From our $1s\,2p_{1/2}\,^3P_0$ lifetime of 54.4 (3.4)ps and Drake's calculated E1M1 decay rate[10] of 0.564(5) • 10^{10} s^{-1} we obtain a $1s\,2p_{1/2}\,^3P_0$ - $1s\,2s\ ^3S_1$ E1 decay rate of 1.273 (0.116) • 10^{10} s^{-1}. Using the dipole length formula for the E1 decay rate[11]: $A = 12\alpha k^3\,(Z\alpha)^{-2}\,[0.792+0.759/Z]^2$ ($h/2\pi = m = c = 1$) we find for k, the $1s\,2p_{1/2}\,^3P_0$ - $1s\,2s\ ^3S_1$ splitting, a value of 260.0 (7.9) ev. Subtracting the calculated Coulomb contribution[8] of 330.4 ev yields a Lamb shift of 70.4 (7.9) ev.

So far we have accounted only for experimental uncertainty; theoretical uncertainty comes from the effect of small terms omitted from the calculations. We estimate that a $Z^{-1}\,(Z\alpha)^2$ correction to the $1s\,2p_{1/2}\,^3P_0$ - $1s\,2s\ ^3S_1$ E1 matrix element, and a 1/Z correction to the E1M1 decay rate, contribute a total of $\approx$ 1 ev to our inferred $1s\,2p_{1/2}\,^3P_0$ - $1s\,2s\ ^3S_1$ splitting; that a term of $Z^{-2}\,(Z\alpha)^5$ or $Z^{-2}\,(Z\alpha)^6$ contributes $\approx$ 2 ev to the 330.4 ev Coulomb splitting of the $1s\,2p_{1/2}\,^3P_0$ - $1s\,2s\ ^3S_1$ states; and that a 1/Z screening correction to the self energy, vacuum polarization and finite nuclear size contributes $\approx$ 1 ev to the Lamb shift. These combine to give a separate theoretical error of 2.4 ev in our extracted value of the Lamb shift.

To sum up, we used the following steps to measure the Lamb shift in uranium: i.) Measured the decay length for the heliumlike uranium $1s\,2p_{1/2}\,^3P_0$ state using the beam foil

time-of-flight technique by observing the $1s\,2s\ ^3S_1 \rightarrow 1s^2\ ^1S_0$ x-ray transition. ii.) Determined the $1s\,2p_{1/2}\ ^3P_0$ lifetime by combining the measured $1s\,2p_{1/2}\ ^3P_0$ decay length with the beam velocity. iii.) Found the $1s\,2p_{1/2}\ ^3P_0 \rightarrow 1s\,2s\ ^3S_1$ E1 decay rate by combining the $1s\,2p_{1/2}\ ^3P_0$ lifetime with the calculated E1M1 decay rate[10] for $1s\,2p_{1/2}\ ^3P_0 \rightarrow 1s^2\ ^1S_0$. iv.) Found the $1s\,2p_{1/2}\ ^3P_0 - 1s\,2s\ ^3S_1$ energy splitting from the $1s\,2p_{1/2}\ ^3P_0 \rightarrow 1s\,2s\ ^3S_1$ E1 decay rate and the calculated E1 matrix element[11]. v). Found the uranium Lamb shift from the $1s\,2p_{1/2}\ ^3P_0 - 1s\,2s\ ^3S_1$ splitting and the calculated Coulomb interaction between the electrons[8]. Our final value of the uranium Lamb shift of 70.4 (8.3) is in agreement with the theoretical value[5,6] of 75.3(0.4) ev.

In the following chapters I discuss the experiment in more detail. The first three chapters contain theory. In Chapter 2 I review the calculation of the binding energies of the $n=2$ states of heliumlike uranium. I calculate the $1s\,2p_{1/2}\ ^3P_0 - 1s\,2s\ ^3S_1$ energy difference and show how it divides into the sum of the hydrogenlike uranium $2s_{1/2} - 2p_{1/2}$ interval (the Lamb shift) and a contribution from photon exchange between the bound electrons. I also discuss the theoretical ambiguities involved in extracting the Lamb shift from the measured $1s\,2p_{1/2}\ ^3P_0$ lifetime. In Chapter 3 I assemble the formula for the $1s\,2p_{1/2}\ ^3P_0$ decay rate which I invert to get the $1s\,2p_{1/2}\ ^3P_0 - 1s\,2s\ ^3S_1$ splitting and so the Lamb shift. I also calculate the decay rates of some other $n=2$ states which I need to set limits to certain systematic effects, notably the effect of cascades. In Chapter 4 I discuss the way cascades from initial states of high principal quantum number n would repopulate the $n=2$ states and affect our measurement. I show how the absence of a single 81.4 kev line in our spectra sets an limit to the effect of cascades on our measured $1s\,2p_{1/2}\ ^3P_0$ lifetime. This limit depends only on the known decay rates of the high-n states and does not depend on any calculation of what the initial population of the high-n states might be. I then show that recent calculations of the initial population of the high-n states predict that there is too little to have any

effect on our measured lifetime.

In Chapter 5 I describe our apparatus and the way we took data. I discuss the atomic and nuclear backgrounds which hinder beam-foil spectroscopy using a relativistic uranium beam, the measures we took to suppress them, and how well these measures worked in practice. In Chapter 6 I determine from our x-ray spectra both the beam velocity and the 1/e decay length of the $1s\,2p_{1/2}\,{}^3P_0$ state. I calculate the $1s\,2p_{1/2}\,{}^3P_0$ lifetime and our experimental limit to cascade feeding, which is our largest source of systematic error. In Chapter 7 I analyze our background and set limits to the intensity of the possible atomic and nuclear lines which lie near 77.8 kev and which could give a false contribution to our $1s\,2s\ {}^3S_1 \rightarrow 1s^2\,{}^1S_0$ signal peak. In Chapter 8 I show that the motion of our beam and the geometrical and electronic imperfections of our apparatus are a negligible source of systematic error. Finally in Chapter 9 I extract the Lamb shift from our measured $1s\,2p_{1/2}\,{}^3P_0$ decay rate, and discuss the significance of our measurement.

Chapter 2

Energy Levels and General Theory

The $1s\,2p_{1/2}{}^3P_0$ state of two-electron uranium is an exotic bound state of two relativistic, interacting particles which decays by the emission of two photons with a rate which radiative corrections increase by a factor of ~ 2. The analysis of such a system within QED demands a system of calculation which incorporates simultaneously both radiative corrections and the electrons' relativistic mutual interaction, because both contribute equally to the binding energies of the states. The needed system of calculation, based on the Furry picture of bound state quantum electrodynamics[1], is still being built. Some uncertainty in the value of the $1s\,2p_{1/2}{}^3P_0$ decay rate results because it is still necessary to introduce radiative corrections by hand into the calculation of the $1s\,2p_{1/2}{}^3P_0 \rightarrow 1s\,2s\,{}^3S_1$ electric dipole rate, instead of deriving the required corrections from the axioms of QED.

The structure of two-electron uranium can be solved for using the Furry bound state interaction picture of quantum electrodynamics, as outlined by Mohr [2, 3]. Because the interaction between the electrons' single charges is weak compared to each electron's interaction with the 92 charges of the uranium nucleus, the structure of two-electron uranium can be solved perturbatively by an expansion into Feynman diagrams. The characteristic coupling constant is $1/Z$, the ratio of the electron and nuclear charges, which is small ($\sim .01$) for $Z = 92$. This expansion is the generalization applying to relativistic systems of the $1/Z$ expansion for non-relativistic systems obeying the Schrodinger equation[4].

The first sets of diagrams[2,3] are shown in Figure 2.1. The double lines indicate an electron in a bound or continuum state of an external potential, instead of a plane-wave state

---

[1]A useful introduction to the theory may be found in S. S. Schweber, *An Introduction to Relativistic Quantum Field Theory*, Harper and Row, New York, 1961.

[2]P.J. Mohr, Phys Rev A32, 1949 (1985).

[3]P.J. Mohr, in *Relativistic Effects in Atoms, Molecules, and Solids*, edited by G.L. Malli (Plenum, New York, 1983), p. 145.

[4]An elementary introduction to $1/Z$ perturbation theory can be found in H. A. Bethe and E. E. Salpeter, *Quantum Mechanics of One- and Two- Electron Atoms*, Springer-Verlag, 1957. A review of its application to helium-

appropriate for an electron in free space. Precisely, the electron wavefunctions are those which correspond to the solutions of the Dirac equation for the electrostatic potential of a distributed nuclear charge, instead of the simple Coulomb potential $-Ze^2/r$. It is customary to report the result of a calculation which includes the effect of the finite extent of the nucleus as the sum of the result for a point nucleus and a nuclear size "correction", defined to be just the difference. I will follow this convention.

The zero order state of two bound electrons is an antisymmetrized product state of two jj coupled Dirac wavefunctions, represented by the first diagram in Figure 2.1. The total energy is just the sum of the Dirac equations energies for the individual one-electron bound states, which for a point nucleus are each given by the Sommerfeld formula[5] for a state with principal quantum number n and spin j:

$$E = \left[1 + \frac{(Z\alpha)^2}{(n - (j+\frac{1}{2}) + \sqrt{(j+\frac{1}{2})^2 - (Z\alpha)^2})^2} \right]^{-\frac{1}{2}} mc^2 \qquad 2.1$$

The next correction, $\sim 1/Z$ smaller, is represented by the set of three diagrams in Fig 2.1(b), representing single photon exchange between the bound electrons, and the vacuum polarization and electron self-energy shifts of the separate electrons. The vacuum polarization and the self energy contributions come suppressed by an extra factor of $(Z\alpha)^3$ relative to the contribution from simple photon exchange -- in general the more loops in a diagram, the more factors of $Z\alpha$ which appear -- but for Z = 92 one has $Z\alpha \sim 2/3$ and even many powers of $Z\alpha$ fail to reduce decisively the contribution of a diagram containing a loop compared to a diagram containing a simple photon exchange. One sees that radiative shifts and the shifts from the electrons' Coulomb interaction are roughly the same size and must be included simultaneously. The contribution of the diagrams in Figure 2.1 have been calculated for a point nucleus by Mohr[6], and the corrections due to the finite size of the ^{238}U nucleus have

like ions may be found in W. C. Martin, Phys. Scr. 24, 725 (1981).

[5]First derived by A. Sommerfeld using a relativistic version of N. Bohr's old quantum theory, and first derived from the Dirac equation by W. Gordon, Z. Physik 48, 11 (1928).

[6]P.J. Mohr, Phys. Rev. Lett. 34, 1050 (1975); P.J. Mohr, Phys. Rev. A26, 2338 (1982); P.J. Mohr, Phys. Rev. A32, 1949 (1985).

been calculated for the Sommerfeld binding energy, and for the vacuum polarization and self-energy, by Johnson and Soff[7]. The contributions of the separate diagrams are tabulated in Table 2.1, and the resulting energy differences complete to order 1/Z between the $1s^2\,{}^1S_0$, $1s\,2s\,{}^3S_1$, $1s\,2p_{1/2}\,{}^3P_0$ and $1s\,2p_{3/2}\,{}^3P_2$ states[8] are tabulated in Table 2.2.

Table 2.1 Contributions to U^{90+} Binding Energies [ev]

	State	Point Nucleus	Finite size correction
Dirac Binding Energy	1s 1/2	-132280.99(82)(a)	+193.8(25)
	2s 1/2	-34215.76(11)	+36.82(47)
	2p 1/2	-34215.76(11)	+4.30(05)
	2p 3/2	-29650.08(09)	+0.00
Electron Self-Energy	1s 1/2	+359.62(17)	-6.41(36)
	2s 1/2	+66.37(01)	-1.18(10)
	2p 1/2	+4.30(05)	-0.17(00)
	2p 3/2	+8.90(01)	-0.00(00)
Vacuum Polarization	1s 1/2	-93.22(89)	+4.32(07)
	2s 1/2	-16.54(15)	+0.83(02)
	2p 1/2	-2.81(04)	+0.09(00)
	2p 3/2	-0.11(00)	+0.00(00)
One-Photon Exchange	1 1S0	2271.58 (b)	
	2 3S1	+589.07 (c)	
	2 3P0	+923.38 (c)	
	2 3P2	+611.09 (b)	

Except where noted, the data are from W. R. Johnson and G. Soff, Atomic Data and Nuclear Data tables 33, 405 (1985).
(a)Sommerfeld formula. The uncertainty derives from the uncertainty in the fine structure constant and in the electron mass in units of ev, using the values from C.G. Wohl *et al*, Rev. Mod. Phys., Vol 56, No. 2, Part II, April 1984: $\alpha = 1/137.03694(11)$, m = 0.5110034(14) Mev/c^2.
(b)Interpolated from P.J. Mohr, Phys. Rev. A32, 1949 (1985). The fractional uncertainty in the interpolation is $\sim 0.05\%$. The error in the actual calculation is much less, $\sim$ 1 part in 10^6.
(c)P.J. Mohr, private communication.

[7]W.R. Johnson and G. Soff, Atomic Data and Nucl. Data Tables 33, 405 (1985). A yet more precise value than is used by these authors for the ^{238}U radius is now available from the work of Zumbro *et al*, Phys. Rev. Lett. 53, 1888 (1984). The greater precision is not needed to interpret this experiment.

[8]The $1s\,2s\,{}^1S_0$ state is not included in Tables 2.1 and 2.2 because the contribution of the diagram for the exchange of one photon has, to my knowledge, nowhere been published.

Table 2.2 U^{90+} transition energies to order 1/Z [ev]

State	1 1S0	2 3S1	2 3P0	2 3P2
1 1S0	0	96010.9(31)	96270.0(31)	100521.1(31)
2 3S1	-	0	259.06(56) (a)	4510.91(62)
2 3P0	-	-	0	4251.13(41)
2 3P2	-	-	-	0

(a)The more accurate value of 255.1 ev for this interval, including some higher order terms, is derived in the text.

The $1s\,2p_{3/2}\,^1P_1$ and $1s\,2p_{1/2}\,^3P_1$ states differ little in energy and can mix because they have the same J^π. In addition to calculating the energy shift to order 1/Z of the isolated $n=2$ levels Drake[9] has diagonalized the appropriate two-by-two matrix for the $1s\,2p_{3/2}\,^1P_1$ and $1s\,2p_{1/2}\,^3P_1$ states, including the exchange of one photon exactly and including some terms from the exchange of multiple photons. He reports that the energy splittings $1s\,2p_{3/2}\,^1P_1 - 1s\,2p_{3/2}\,^3P_2$ and $1s\,2p_{1/2}\,^3P_0 - 1s\,2p_{1/2}\,^3P_1$ are 74.7 ev and 113.7 ev respectively. For these splittings any difference would cancel between any different authors' treatments of the finite nuclear size, vacuum polarization and self-energy corrections the energies of the one-electron states. He also reports[10] a value for the $1s\,2s\,^1S_0 - 1s\,2s\,^3S_1$ splitting, for which any such differences also would cancel, of 258.8 ev These three splittings and the transition energies to order 1/Z from Table 2.2 have been used to construct the complete set of energy differences in Table 2.3. The absence of terms $\sim 1/Z^2$ limits the accuracy of the entries to the table to $\sim$ 10 ev for $n=2\rightarrow1$ transitions and to $\sim$ 5 ev for $n=2\rightarrow2$ transitions.

For the key $1s\,2p_{1/2}\,^3P_0$ and $1s\,2s\,^3S_1$ states the first two terms in the binding energies of order $1/Z^2$, with the smallest number of powers of $(Z\alpha)$, are known and can be used to get a better value for the key $1s\,2p_{1/2}\,^3P_0 - 1s\,2s\,^3S_1$ interval. These contributions are[11]

[9]G.W.F. Drake, Nucl. Instrum. Methods in Phys. Research B9, 465 (1985).

[10]G.W.F. Drake, private communication.

[11]P.J Mohr, *Hyperfine Quenching of the* $1s\,2p_{1/2}\,^3P_0$ *State of Helium-like Ions*, in *Beam Foil Spectroscopy 1, Atomic Structure and Lifetimes*, I.A. Sellin and D.J. Pegg, editors, Plenum Press, 1976.

Table 2.3. U^{90+} n =2 and n =1 transition energies [ev]

State	1 1S0	2 3S1	2 3P1	2 1S0	2 3P0	2 3P2	2 1P1
1 1S0	0	96101	96156	96270	96270	100521	100596
2 3S1	-	0	145	259	259(a)	4511	4586
2 3P1	-	-	0	114	114	4397	4472
2 1S0	-	-	-	0	0(b)	4397	4472
2 3P0	-	-	-	-	0	4251	4326
2 3P2	-	-	-	-	-	0	75
1 1P1	-	-	-	-	-	-	0

Energies for n = 2 → 1 transitions are accurate to ~ 10 ev.
Energies for n = 2 → 2 transitions are accurate to ~ 5 ev.
(a)The more accurate value of 255.1 ev for this interval, including some higher order terms, is derived in the text.
(b)The 2 1S0 and 2 3P0 levels are nearly degenerate.

$$\Delta E_{^3P_0} = -0.0729981 \frac{(Z\alpha)^2}{Z^2} - 0.307 \frac{(Z\alpha)^4}{Z^2} \qquad 2.2$$

$$\Delta E_{^3S_1} = -0.0474093 \frac{(Z\alpha)^2}{Z^2} - 0.042 \frac{(Z\alpha)^4}{Z^2} \qquad 2.3$$

The result is an extra -4.1 ev contribution to the 259.0 ev result of the calculation pursued only to $\sim 1/Z$, for a net $1s\,2p_{1/2}\,^3P_0 - 1s\,2s\,^3S_1$ splitting of 255.1 ev. Since all terms of order Z^{-2} up to $Z^{-2}(Z\alpha)^4$ are now included in this energy difference the largest missing term is at most of order $Z^{-2}(Z\alpha)^{-5}$, which would contribute $\sim$ 2 ev if its coefficient were of typical size (taken here to be ~ 0.36).

If QED is to fail to describe nature it will likely first fail to predict accurate radiative corrections, the calculation of which requires renormalizing the theory. A convenient way to analyze the $1s\,2p_{1/2}\,^3P_0$-$1s\,2s\,^3S_1$ interval is to divide it into the sum of the hydrogenic $2s_{1/2} - 2p_{1/2}$ interval (the Lamb shift) and a contribution from the exchange of photons between the bound electrons. The $2s_{1/2} - 2p_{1/2}$ interval includes with the effect of finite nuclear size the vacuum polarization and self-energy terms and so requires a renormalization to calculate; the contribution from the exchange of photons does not. Such a division ignores in heliumlike uranium a $\sim 1/Z$ correction to the n =2 vacuum polarization and self-energy corrections for the screening of the inner $1s$ electron. The resulting theoretical $2s_{1/2}$-$2p_{1/2}$ interval is 75.3 ev and the contribution from photon exchange is 330.4 ev.

Given that a systematic solution of the two-electron system for Z = 92 is possible in principle one can ask how far it can be pushed in practice. Summing analytically over electron intermediate states is far more difficult for a bound electron than for a free electron, because the intermediate states are complicated bound and continuum solutions to the Dirac equation instead of analytically simple plane waves. With the development of variational principles for the Dirac equation some such sums have been done numerically by replacing the actual integration over intermediate states by a finite sum over variationally determined pseudostates[12]. Whether this technique will make all such problems tractable is still unknown. A further complication is that the finite charge distribution of a uranium nucleus modifies the electrostatic potential from the simple Coulomb potential $-Ze^2/r$, and that using solutions for the *modified* potential will be essential to calculate correctly effects which are weighted near the origin -- notably, the effects of vacuum polarization and self-energy. The finite nuclear size contribution to the electron self energy, for example, is $\sim$ 1 ev out of a total of $\sim$ 55 ev. The quadrupole and even the hexadecapole charge moments of ^{238}U have been measured using muon spectroscopy[13], so the modified potential is known; incorporating this knowledge exactly, order by order in 1/Z, into the calculation may pose problems. Nonetheless it appears possible to pursue the calculation complete to order $1/Z^2$, which would yield a theoretical $1s\,2p_{\,1/2}\,^3P_0 - 1s\,2s\,^3S_1$ interval uncertain by only $\sim$ 0.05 ev. A meaningful comparison of theory and experiment may be possible at a precision equivalent to about 10^{-3} of the $2s_{\,1/2} - 2p_{\,1/2}$ Lamb shift.

---

[12]See, for example, J.D. Talman, Phys. Rev. Lett. 57, 1091 (1986); W.R. Johnson and J. Sapirstein, Phys. Rev. Lett. 57,1126 (1986); G.W.F. Drake, Phys. Rev. A 34, 2871 (1986); S.P. Goldman and G.W.F. Drake, Phys. Rev. A 24, 183 (1981); G.W.F. Drake and S.P. Goldman, Phys. Rev. A 23, 2093 (1981).

[13]J.D. Zumbro, E.B. Shera, Y. Tanaka, and C.E. Bemis, Jr; R.A. Naumann, M.V. Hoehn, W. Reuter, and R.M. Steffen, Phys. Rev. Lett. 53, 1888 (1984). They determine the rms charge radius ($<r^2>^{\frac{1}{2}}$) of ^{238}U to be 5.8604(23) fm. Describing the nuclear charge distribution in more detail they find for ^{238}U the quadrupole and hexadecapole charge moments Q_0 and H_0 to be 11.118(58) $e.b$ and 2.28(11) $e.b^2$, respectively. For a measurement of the moments of the deformed optical (nuclear) potential for ^{238}U by the scattering of polarized protons, and for references to the measurement of the ^{238}U charge moments by electron scattering and by Coulomb excitation, see also Y. Takenchi, H. Sakaguchi, M. Nakamura, T. Ichihara, M. Yosoi, M. Ieiri, and S. Kobayashi, Phys. Rev. C 34, 493 (1986).

Only the $1s^2\,{}^1S_0$ state of a two-electron system is stable. One can investigate the radiative decay of the $n=2$ states by including in the calculation diagrams which represent transitions from an original excited two-electron state to a $1s^2\,{}^1S_0$ final state accompanied by one or more photons. The $1s\,2p_{1/2}{}^3P_0$ state is forbidden by the conservation of angular momentum to reach a final $1s^2\,{}^1S_0$ state accompanied by one photon, so the first non-zero contribution to the decay rate is represented by a diagram with two photons in the final state. (The two photons must be of opposite parity.) The rate for this decay has been calculated by Drake[14]. The rate for decay into the two-photon continuum breaks into the sum of three parts: a rate A^{π} for the decay into a "true" two-photon continuum where the energy of neither photon is close to the energy splitting between the $1s\,2p_{1/2}{}^3P_0$ and either the $1s\,2s\,{}^3S_1$ or the $1s\,2p_{1/2}{}^3P_1$ state; and the rates for the separate electric dipole and magnetic dipole decays $1s\,2p_{1/2}{}^3P_0 \rightarrow 1s\,2s\,{}^3S_1$ and $1s\,2p_{1/2}{}^3P_0 \rightarrow 1s\,2p_{1/2}{}^3P_1$, as one would calculate them from the standard theory of radiative decay based on Fermi's Golden Rule[15]. Thus the total decay rate of the $1s\,2p_{1/2}{}^3P_0$ state is

$$A_{{}^3P_0} = A^{\pi} + A^{E1}{}_{{}^3P_0 \rightarrow {}^3S_1} + A^{M1}{}_{{}^3P_0 \rightarrow {}^3P_1} \qquad 2.4$$

The contribution of the magnetic dipole decay $1s\,2p_{1/2}{}^3P_0 \rightarrow 1s\,2p_{1/2}{}^3P_1$ to the total is so small it may be ignored. Using the standard dipole length formula for the electric dipole decay rate one has

$$A_{{}^3P_0} = A^{\pi} + \frac{4}{3}\alpha\frac{k^3}{c^2}\;|\,<{}^3P_0|\;\vec{r}_1+\vec{r}_2\;|\,{}^3S_1>\,|^2 \qquad 2.5$$

The scheme of the experiment is to measure the total decay rate of the $1s\,2p_{1/2}{}^3P_0$ state, and using Eq. 2.5 and the theoretical values for A^{π} and the matrix element $<|\,\vec{r}_1+\vec{r}_2\,|>$, to see the effect of radiative corrections on k, the $1s\,2p_{1/2}{}^3P_0 - 1s\,2s\,{}^3S_1$ splitting. The two-photon decay rate A^{π} is insensitive to small changes in the binding energies of any states and in particular to the radiative corrections to the energies, and the dipole

[14]G.W.F. Drake, Nucl. Instrum. Methods in Phys. Research B9, 465 (1985).

[15]One adaptation of this theory to the radiative decay of electrons obeying the Dirac equation may be found in I.P. Grant, J. Phys. B12, 1458 (1974).

matrix element is easily calculated. Is this scheme truly sound? There are two subtle difficulties.

The change in the $1s\,2p_{1/2}{}^3P_0 \rightarrow 1s\,2s\,{}^3S_1$ electric dipole decay rate due to radiative corrections, no doubt *part* of which may be attributed to a simple change in the energy splitting due to the Lamb shift, I take into account *only* by adjusting by hand the $1s\,2p_{1/2}{}^3P_0 - 1s\,2s\,{}^3S_1$ splitting k fed into Eq. 2.5. This would be correct if the increased splitting arose from some small added term in the two-electron Hamiltonian, but including radiative corrections thus is an uncertain procedure[16]. Radiative corrections are calculable only because of the delicate subtraction of infinities which occurs in the renormalization of QED; no one has yet condensed their effects into any effective Hamiltonian operator. Furthermore it cannot be true that the *only* effect of radiative corrections is to modify the state splitting one plugs into Fermi's Golden Rule, though this may be true *to some, so far unquantified, approximation.* To achieve full rigor the calculation of the two-photon decay rate should be done as a part of a Furry bound state calculation, so that radiative corrections to the binding energies and radiative corrections to the decay rates could be treated simultaneously and consistently. Such a calculation would make unnecessary my insertion by hand of radiative corrections into k and so into the calculation of the $1s\,2p_{1/2}{}^3P_0$ decay rate. Until this is done I rest the interpretation of the experiment on an assumption:

The change in the $1s\,2p_{1/2}{}^3P_0 \rightarrow 1s\,2s\,{}^3S_1$ electric dipole decay rate due to radiative corrections can be calculated as if the increased $1s\,2p_{1/2}{}^3P_0 - 1s\,2s\,{}^3S_1$ splitting arose from a small extra term in the two-electron Hamiltonian.

A similar assumption is implicit in a calculation of the response of the hydrogen $2s$ and $2p$ states to an external field, if the calculation includes the hydrogen $2s - 2p$ Lamb shift interval – assuredly a radiative correction – as a simple energy denominator in stationary or

[16] I thank Dr. Peter Mohr for pointing out this subtlety.

time-dependent perturbation theory. For the the Stark mixing of the $2s$ and $2p$ states in one-electron ions Hillery and Mohr[17] have shown that the predictions of such naive calculations for the resulting quenched $2s$ decay rate are in fact matched, to order α in the radiative corrections and for weak electric fields, by the results of a rigorous calculation based on the Furry picture of quantum electrodynamics. So I can be confident, if not absolutely certain, that a similar assumption will lead to similarly correct predictions for the decay of the uranium $2s$ and $2p$ states. Here I leave the matter.

The second problem concerns an apparent lack of gauge invariance in the way the $1s\,2p_{1/2}\,^3P_0 \rightarrow 1s^2\,^1S_0$ electric dipole decay rate is calculated[18] in Eq. 2.5. Gauge invariance guarantees that the length and velocity formulas for electric dipole decay rates must yield identical results. In the non-relativistic limit the two formulas are

$$\Gamma^{length} = \frac{4}{3}\alpha k^3{}_{^3P_0-{}^3S_1} \,|\, \langle {}^3P_0 |\ \vec{r}_1+\vec{r}_2\ | {}^3S_1 \rangle \,|^2 \qquad 2.6$$

$$\Gamma^{velocity} = \frac{4}{3}\alpha k^1{}_{^3P_0-{}^3S_1} \,|\, \langle {}^3P_0 |\ \vec{v}_1+\vec{v}_2\ | {}^3S_1 \rangle \,|^2 \qquad 2.7$$

Suppose the effect of the radiative corrections is indeed equivalent to the effect of some added small term in the two-electron Hamiltonian. I calculate the change in the $1s\,2p_{1/2}\,^3P_0 \rightarrow 1s^2\,^1S_0$ E1 decay rate using the dipole length formula in Eq. 2.5, keeping the original unperturbed wavefunctions in the matrix element and modifying only the energy in the phase space factor k^3. A paradox seems to appear because the same approach using the dipole velocity formula must give a different prediction, because the rate calculated from the velocity formula scales as k^1, not k^3. What happened to gauge invariance? And which dependence on k, if either, is correct?

Gauge invariance, and the equivalence of the two formulas, will be maintained order by order in perturbation theory only if the changes made by a perturbation to both the energy splitting k *and* to the wavefunctions are kept. So I should expect that if I ignore the changes

[17]M. Hillery and P.J. Mohr, Phys. Rev. A 21, 24 (1980).

[18]For calling my attention to this subtlety I am again indebted to Dr. Peter Mohr.

in the wavefunctions the length and velocity formulas will give different answers. Ignoring the change in the wavefunctions in the velocity formula makes a large error because the velocity matrix element for the unperturbed $1s\,2p_{1/2}{}^3P_0$ and $1s\,2s\,{}^3S_1$ wavefunctions nearly vanishes, while the length matrix element does not. To see the effect look at the electric dipole decay $1s\,2p_{1/2}{}^3P_0 \rightarrow 1s\,2s\,{}^3S_1$ in a high-Z Schrodinger system where the Hamiltonian H is

$$H + H_0 + H_C \tag{2.8}$$

where

$$H_0 = \left[\frac{p_1^2}{2m} - \frac{Ze^2}{r_1^2}\right] + \left[\frac{p_2^2}{2m} - \frac{Ze^2}{r_2^2}\right] \tag{2.9}$$

$$H_C = \frac{e^2}{|\vec{r}_1 - \vec{r}_2|} \tag{2.10}$$

and where the Coulomb interaction Hamiltonian H_C is a small perturbation $\sim 1/Z$ smaller than H_0. The commutation relation

$$\vec{v}_1 + \vec{v}_2 = \frac{2\pi i}{h}\,[H, \vec{x}_1 + \vec{x}_2] \tag{2.11}$$

guarantees the exact equivalence of the dipole length and velocity formulae

$$\Gamma^{length} = \frac{4}{3}\alpha k^3{}_{BA}\,|<B\,|\,\vec{r}_1+\vec{r}_2\,|\,A>|^2 \tag{2.12}$$

$$\Gamma^{velocity} = \frac{4}{3}\alpha k^1{}_{BA}\,|<B\,|\,\vec{v}_1+\vec{v}_2\,|\,A>|^2 \tag{2.13}$$

for an electric dipole transition between any states B, A.

To zeroth order in H_C the $1s\,2p_{1/2}{}^3P_0$ and $1s\,2s\,{}^3S_1$ states are degenerate. The commutation relation Eq. 2.11 applied to the $1s\,2p_{1/2}{}^3P_0$ and $1s\,2s\,{}^3S_1$ states gives

$$<{}^3P_0|\,\vec{v}_1 + \vec{v}_2\,|{}^3S_1> = \frac{2\pi i}{h}\left[E_{{}^3P_0} - E_{{}^3S_1}\right] <{}^3P_0|\,\vec{x}_1 + \vec{x}_2\,|{}^3S_1> \tag{2.14}$$

That is, while the length element is finite the velocity element vanishes to zeroth order in H_C. Since the $1s\,2p_{1/2}{}^3P_0$ and $1s\,2s\,{}^3S_1$ states are split to first order in H_C, or equivalently to first order in 1/Z, the length formula Eq. 2.6 predicts the $1s\,2p_{1/2}{}^3P_0 \rightarrow 1s\,2s\,{}^3S_1$ rate will then scale as $k^3 \sim 1/Z^3$. The velocity formula Eq. 2.7 also gives this $1/Z^3$ scaling, but only one factor of 1/Z comes from the factor k^1. Two come from the admixtures $\sim 1/Z$ of other

states into the zero-order $1s\,2p_{1/2}{}^3P_0$ and $1s\,2s\,{}^3S_1$ wavefunctions by the perturbation H_C. Thus the dipole length formula gives the correct scaling ($\sim k^3$) when it is used with a matrix element calculated with zero-order wavefunctions, but the velocity formula does not, and the latter's apparent $\sim k^1$ dependence is illusionary.

Now add to the Hamiltonian H a second perturbation H' where H' is designed to mimic the effect of radiative corrections on the $1s\,2p_{1/2}{}^3P_0 - 1s\,2s\,{}^3S_1$ splitting. Provided H' is local, that is, provided $[H', \vec{r}_1 + \vec{r}_2] = 0$, the commutation relation Eq. 2.11 still holds. Perturbation theory shows the fractional error in the change in the $1s\,2p_{1/2}{}^3P_0 \rightarrow 1s\,2s\,{}^3S_1$ rate due to H', made by dropping in the length formula the corrections due to H' in the $1s\,2p_{1/2}{}^3P_0$ and $1s\,2s\,{}^3S_1$ wavefunctions, to be roughly $<H'>/<H_0>$, where the brackets denote typical magnitudes or energy splittings. The fractional error made using the velocity formula is roughly $<H'>/<H_C>$ -- about a factor of Z larger. Estimating $<H'>$ to be $\sim$ 50 ev, the $2s - 2p$ self-energy splitting; $<H_C>$ to be $\sim$ 250 ev, the $1s\,2p_{1/2}{}^3P_0 - 1s\,2s\,{}^3S_1$ energy difference; and $<H_0>$ to be $\sim$ 20 kev, the $n=3$ to $n=2$ difference[19], I find the errors made in the length and velocity formulas by neglecting the change in the wavefunctions to be respectively 0.3% and 30% of the true change in the $1s\,2p_{1/2}{}^3P_0 \rightarrow 1s\,2s\,{}^3S_1$ rate.

This argument supports my use of the length instead of the velocity formula in Eq. 2.5, but it is obviously not conclusive. I should use a Dirac instead of a Schrodinger Hamiltonian; but since the Dirac $2s_{1/2}$ and $2p_{1/2}$ states are degenerate and since the zeroth order velocity matrix element still vanishes I doubt anything essential changes. A less repairable weakness is that I do not know the form of an appropriate Hamiltonian H' which would mimic the effect of radiative corrections; furthermore if such a Hamiltonian exists it may not prove local (commute with $(\vec{r}_1+\vec{r}_2)$) as I have assumed[20]. Still, while ultimately there is no substitute for a rigorous calculation of the $1s\,2p_{1/2}{}^3P_0 \rightarrow 1s\,2s\,{}^3S_1$ decay rate within the Furry

[19]For the $1s\,2p_{1/2}{}^3P_0$ and $1s\,2s\,{}^3S_1$ states there are no other $n=2$ states of the same J^π, so the nearest admixable states have $n=3$.

formulation of QED, I assert there is no reason to suppose this less rigorous calculation will prove to be wrong.

[20]For this criticism, too, I am indebted to Dr. Peter Mohr.

Chapter 3

Calculation of Key Decay Rates

In this chapter I re-examine the two-photon decay rate of the $1s\,2p_{1/2}{}^3P_0$ state and derive the exact formula corresponding to Eq. 2.5 which I will use to extract the $1s\,2p_{1/2}{}^3P_0$ – $1s\,2s\,{}^3S_1$ splitting from the measured total decay rate of the $1s\,2p_{1/2}{}^3P_0$ state. As discussed in chapter 2, this requires a separate calculation using Fermi's Golden Rule of the electric and magnetic dipole decays $1s\,2p_{1/2}{}^3P_0 \rightarrow 1s\,2s\,{}^3S_1$ and $1s\,2p_{1/2}{}^3P_0 \rightarrow 1s\,2p_{1/2}{}^3P_1$. I also calculate the branching ratios for the electric dipole and magnetic quadrupole decays of the $1s\,2p_{3/2}{}^3P_2$ state, $1s\,2p_{3/2}{}^3P_2 \rightarrow 1s\,2s\,{}^3S_1$ and $1s\,2p_{3/2}{}^3P_2 \rightarrow 1s^2\,{}^1S_0$, which I need in Chapter 4 to calculate the sensitivity of the measured $1s\,2p_{1/2}{}^3P_0$ decay rate to a possible repopulation of the $n=2$ states by cascades. Finally I calculate the change in the $1s\,2p_{1/2}{}^3P_0$ decay rate if the ^{238}U nucleus acquires a spin in a close Coulomb collision, to show that even if some $1s\,2p_{1/2}{}^3P_0$ states in the beam have lifetimes quenched by the resulting magnetic hyperfine interaction that there will be no change in the $1s\,2p_{1/2}{}^3P_0$ lifetime found by my time-of-flight measurement.

The principal decay modes of the $n=2$ states, and rough values for the decay rates, of hydrogenlike and heliumlike uranium are displayed in the Grotian diagrams in Figures 3.1 and 1.1. In obtaining more accurate values or the transition rates one is aided by the fact that except for weak admixtures, $\sim 1/Z$, of other configurations the bound state wavefunctions are just j-j coupled and antisymmetrized products of Dirac single-particle wavefunctions. I use units where $\hbar/2\pi = m = c = 1$.

Decays of the $1s\,2p_{1/2}{}^3P_0$ state: the electric dipole rate $1s\,2p_{1/2}{}^3P_0 \rightarrow 1s\,2s\,{}^3S_1$.

Because the transition energy is small the long-wavelength approximation is adequate; the length form of the decay rate formula is

$$A_{E1} = \frac{4}{3}\alpha\frac{k^3}{c^2} \mid <B \mid \vec{r} \mid A> \mid^2 \qquad 3.1$$

where k is the energy difference between states B ,A . For the $1s\,2p_{1/2}{}^3P_0 \rightarrow 1s\,2s\,{}^3S_1$ transition this simplifies to

$$A_{E1} = 12\,\alpha\frac{k^3}{c^2}\,(Z\alpha)^{-2}\left[\Omega + \frac{b}{Z}\right]^2 \qquad 3.2$$

where $\Omega \rightarrow 1$ as $(Z\alpha) \rightarrow 0$ and involves a radial integral over the large and small components of Dirac wavefunctions, and b represents the first correction to the matrix element for the mixing in of other configurations by the Coulomb interaction. The integral Ω is:

$$\Omega_{{}^3P_0 \rightarrow {}^3S_1} = \frac{(Z\alpha)}{3\sqrt{3}}\int_0^\infty [g_{2s_{1/2}}(x)\, g_{2p_{1/2}}(x) + f_{2s_{1/2}}(x)\, f_{2p_{1/2}}(x)]\, x^3 dx \qquad 3.3$$

where the large and small radial functions g and f are defined defined according to the conventions of Rose.[1] The functional form of Ω for the $1s\,2p_{1/2}{}^3P_0 \rightarrow 1s\,2s\,{}^3S_1$ transition is especially simple:

$$\Omega_{{}^3P_0 \rightarrow {}^3S_1} = \left(\frac{\varsigma+1}{2}\right)\left[\frac{2\varsigma+1}{3}\right]^{1/2} \sim 1 - \frac{5}{12}(Z\alpha)^2 - \frac{11}{144}(Z\alpha)^4 - \cdots \qquad 3.4$$

Here quantity ς is defined by

$$\varsigma \equiv \sqrt{1-(Z\alpha)^2} \qquad 3.5$$

For Z=92 Eq. 3.4 gives

$$\Omega_{{}^3P_0 \rightarrow {}^3S_1} = .79189 \qquad 3.6$$

The correlation correction constant b for the $1s\,2p_{1/2}{}^3P_0 \rightarrow 1s\,2s\,{}^3S_1$ transition is [2]

$$b = +.759 \qquad 3.7$$

For the moment I will treat the energy difference k in Eq. 3.2 as known and solve for A_{E1}; later to interpret the experiment I will invert this procedure. Using the value from Table 1.3 for the energy difference k ,

---

[1] M. E. Rose, *Relativistic Electron Theory,* Wiley, New York, 1961.

[2] H. Gould, R. Marrus and P.J. Mohr, Phys. Rev. Lett. 33, 676 (1974).

$$k_{^3P_0-^3S_1} = 255.16\ ev \tag{3.8}$$

the resulting value for the $1s\,2p_{1/2}{}^3P_0 \rightarrow 1s\,2s\,{}^3S_1$ decay rates is

$$A^{E1}{}_{^3P_0\rightarrow{}^3S_1} = 1.2023\bullet 10^{10}\ s^{-1} \tag{3.9}$$

Consider the error in this rate arising from missing terms in the dipole matrix element. There are relativistic corrections to the correlation correction, itself of order Z^{-1}, which are of therefore leading order $Z^{-1}(Z\,\alpha)^2$. With an unknown coefficient estimated as 1.0, these would contribute $\simeq 0.50\%$ to the matrix element and so $\simeq 1.0\%$ to the rate. There is also a correction for the finite wavelength of the emitted radiation. Examining the formulae of Grant[3] , one sees that this enters as an overlap of the small and large components of the Dirac wavefunctions; it contributes $\sim (Z\,\alpha)^2 < kx >$, where x is the size of the uranium ion. Estimating $x \sim a_0/Z$ where a_0 is the Bohr radius, this contributes $\simeq 3\bullet 10^{-4}$ to the matrix element for $1s\,2p_{1/2}{}^3P_0$ decay. If k were known exactly the rate (Eq. 3.9) derived from Eq. 3.2 would be accurate to $\pm \simeq 1\%$. Equivalently if the rate were known exactly in Eq. 3.2 the energy k could be derived to $\pm \simeq 0.3\%$. The error is a factor of 3 smaller because k depends on the cube root of the decay rate. For $k \sim 250$ ev the uncertainty would be ~ 1 ev.

The magnetic dipole decay rate $1s\,2p_{1/2}{}^3P_0 \rightarrow 1s\,2p_{1/2}{}^3P_1$.

For this rate I need only an estimate so I evaluate the required M1 matrix element using Schrodinger wavefunctions and the non-relativistic form of the M1 operator. The formula for an allowed M1 transition between states A ,B is

$$A^{M1} = \frac{1}{3}\alpha\frac{k^3}{c^2} \mid < A \mid \vec{L} + 2\vec{S} \mid B > \mid^2 \tag{3.10}$$

To evaluate the needed matrix element it's helpful to know the the $jj \rightarrow LS$ recoupling:

$$\mid 1s_{1/2}2p_{1/2}, J=1 > \;=\; \sqrt{2/3} \mid 1s\,2p\ {}^3P_1> \;+\; \sqrt{1/3} \mid 1s\,2p\ {}^1P_1> \tag{3.11}$$

The result is

---

[3] I. P. Grant, J. Phys. B12, 1458 (1974).

$$A^{M1}{}_{^3P_0\to{}^3P_1}=\frac{4}{9}\alpha\frac{k^3}{c^2} \qquad 3.12$$

A complete calculation using Dirac wavefunctions and incorporating the effects of the finite wavelength of the radiation would produce this formula with the typical extra factor Ω^2 where $\Omega \to 1$ for $(Z\alpha) \to 0$, where $\Omega < 1$, and where I guess Ω would be in the range ~ 0.7 — 0.9 for Z near 92. Using the value from Table 1.3 for the $1s\,2p_{1/2}{}^3P_0$ — $1s\,2p_{1/2}{}^3P_1$ energy difference,

$$k_{^3P_0\to{}^3P_1}=114\ ev \qquad 3.13$$

One gets

$$A^{M1}{}_{^3P_0\to{}^3P_1}= 2.77\bullet10^7 \bullet \Omega^2\ s^{-1} \qquad 3.14$$

This rate represents only $\sim 10^{-3}$ of the total decay rate for the $1s\,2p_{1/2}{}^3P_0$ state.

The two-photon decay rate $1s\,2p_{1/2}{}^3P_0\to 1s^2\,{}^1S_0$.

The $1s\,2p_{1/2}{}^3P_0$ state can decay by the simultaneous emission of two or more photons to the ground $1s^2\,{}^1S_0$ state. Because the $1s\,2p_{1/2}{}^3P_0$ state is parity odd and the $1s^2\,{}^1S_0$ state parity even, decay by the emission of two electric dipole (E1) photons is forbidden and the most probable decay is by the emission of a magnetic dipole and an electric dipole photon (E1M1). In the non-relativistic limit, to all orders in 1/Z (in the Coulomb repulsion between the bound electrons), *all* multiphoton decays of the $1s\,2p_{1/2}{}^3P_0$ state involving only magnetic dipole and electric dipole photons are forbidden. This follows because Schrodinger two-electron wavefunctions are exact eigenstates $^{2S+1}L_J$, and the electric and magnetic dipole matrix elements which connect atomic states,

$$< {}^{2S+1}L_J \mid \vec{r}_1+\vec{r}_2 \mid {}^{2S'+1}L'_{J'} > \qquad 3.15$$

$$< {}^{2S+1}L_J \mid \vec{L}+2\vec{S} \mid {}^{2S'+1}L'_{J'} > \qquad 3.16$$

do not connect states where $S\neq S'$ — there is no chain of intermediate states to connect the $1s\,2p_{1/2}{}^3P_0$ to the $1s^2\,{}^1S_0$. The mixture of spin triplet and singlet states by the Breit interaction, and the relativistic and finite wavelength corrections to the dipole transition

operators, contribute to a non-zero term $\sim (Z\alpha)^2$ in the dipole matrix elements which allows the decays to occur[4]. The two-photon E1M1 decay rate scales as $\alpha^2(Z\alpha)^{12}$; the rate for the emission of *three* photons (all electric dipole) scales as $\alpha^3(Z\alpha)^{12}$ and can be neglected.

The two-photon decay rate $1s\,2p_{1/2}{}^3P_0 \rightarrow 1s^2\,{}^1S_0$ has been calculated by Drake.[5] The expected discrete lines from the decay chains $1s\,2p_{1/2}{}^3P_0 \rightarrow 1s\,2s\,{}^3S_1 \rightarrow 1s^2\,{}^1S_0$ and $1s\,2p_{1/2}{}^3P_0 \rightarrow 1s\,2p_{1/2}{}^3P_1 \rightarrow 1s^2\,{}^1S_0$ appear as resonances embedded in a two-photon continuum. The line shapes are asymmetric because the amplitudes for the production of an E1 and M1 photon by the paths, for example, $1s\,2p_{1/2}{}^3P_0 \rightarrow 1s\,2s\,{}^3S_1 \rightarrow 1s^2\,{}^1S_0$ and $1s\,2p_{1/2}{}^3P_0 \rightarrow$ *any other intermediate state* $\rightarrow 1s^2\,{}^1S_0$, interfere. Once the contribution of the resonances is subtracted the remainder, which I define as the two-photon decay rate proper, $A^{\pi\pi}$, is insensitive to small changes in the binding energies of any states and in particular to the shifts due to self-energy and vacuum polarization. Drake's result for the two-photon decay rate,

$$A^{\pi\pi}=0.564(5)\bullet 10^{10}\ s^{-1} \qquad 3.17$$

is the sum of the calculated E1M1 rate and a contribution of $0.0025\bullet 10^{10} s^{-1}$ from the higher multipole transition E2M2. The error of $0.005\bullet 10^{10} s^{-1}$ is his estimate of the effect of uncluded terms in the electron-electron interaction, which one would indeed expect to enter at $\sim 1/Z \sim 0.01$ times the rate. As mentioned in Chapter 2 the total decay rate of the $1s\,2p_{1/2}{}^3P_0$ state is the sum

$$A_{^3P_0} = A^{\pi\pi} + A^{M1}{}_{^3P_0\rightarrow{}^3P_1} + A^{E1}{}_{^3P_0\rightarrow{}^3S_1} \qquad 3.18$$

I have shown that the M1 decay rate is only $\sim 10^{-3}$ of the total rate and can be dropped. Using the formula for the $1s\,2p_{1/2}{}^3P_0 \rightarrow 1s\,2s\,{}^3S_1$ E1 decay rate (Eq. 3.2), the value of $A^{\pi\pi}$ (Eq. 3.17), and the value of the $1s\,2p_{1/2}{}^3P_0 - 1s\,2s\,{}^3S_1$ dipole matrix element (Eqs. 3.6,3.7), for any experimental value for the total decay rate of the $1s\,2p_{1/2}{}^3P_0$ state Eq. 3.18 can be solved for the $1s\,2p_{1/2}{}^3P_0 - 1s\,2s\,{}^3S_1$ splitting:

---

[4]G.W.F Drake, Nucl. Instrum. Methods in Phys. Research B9, 465 (1985).

[5]G.W.F Drake, Nucl. Instrum. Methods in Phys. Research B9, 465 (1985).

$$k_{^3P_0-^3S_1} = \left[\frac{h}{2\pi mc^2}\left(A_{^3P_0}[s^{-1}]-0.564\bullet10^{10}[s^{-1}]\right)\left(\frac{1}{0.80014}\right)^2\right]^{1/3} mc^2 \qquad 3.19$$

This inversion is subject to the theoretical ambiguities discussed in Chapter 2. The effect of uncalculated terms $\sim Z^{-1}$ in the two-photon rate $A^{2\gamma}$ and of terms $\sim Z^{-1}(Z\alpha)^2$ in the dipole matrix element introduces an uncertainty in k of $\sim 0.3\%$, or for k $\sim$ 250 ev, an uncertainty of $\pm \sim 1$ ev. Equation 3.19 is the master equation I use to interpret the measurement of the $1s\,2p_{1/2}\,^3P_0$ lifetime.

Decays of the $1s\,2p_{3/2}\,^3P_2$ state: The electric dipole rate $1s\,2p_{3/2}\,^3P_2 \rightarrow 1s\,2s\,^3S_1$.

The calculation of this rate is very similar to the calculation of the electric dipole rate $1s\,2p_{1/2}\,^3P_0 \rightarrow 1s\,2s\,^3S_1$. The dipole length formula Eq. 3.1 yields Eq. 3.2 with the same correlation coefficient b but a different radial integral Ω:

$$\Omega_{^3P_2\rightarrow^3S_1} = \frac{(Z\alpha)}{3\sqrt{3}}\int_0^\infty [g_{2s_{1/2}}(x)\, g_{2p_{3/2}}(x) + f_{2s_{1/2}}(x)\, f_{2p_{3/2}}(x)]\, x^3 dx \qquad 3.20$$

This integral I have also evaluated analytically but the formula is cumbersome and I do not quote it here. The value of the integral for Z = 92 is

$$\Omega_{^3P_2\rightarrow^3S_1} = .90538 \qquad 3.21$$

From Table 1.3 the $1s\,2p_{3/2}\,^3P_2$ -- $1s\,2s\,^3S_1$ energy difference is

$$k_{^3P_2-^3S_1} = 4511\ ev \qquad 3.22$$

and substituting into Eq. 3.2 gives the decay rate

$$A^{E1}{}_{^3P_2\rightarrow^3S_1} = 8.6611\bullet10^{13}\ s^{-1} \qquad 3.23$$

The unincluded term in the matrix element from the relativistic correction to the correlation, $\sim Z^{-1}(Z\alpha)^2$, and the unincluded term from the finite wavelength of the emitted radiation, $\sim (Z\alpha)^2 < kx >$, would contribute $\sim 1\%$ and $\sim 0.6\%$ respectively. The error in k is a negligible $\sim 0.1\%$, so the error in the decay rate Eq. 3.23 is $\sim 1\%$.

The magnetic quadrupole decay rate $1s\,2p_{3/2}\,^3P_2 \rightarrow 1s^2\,^1S_0$.

To complete the calculation of the decay rate of the $1s\,2p_{3/2}{}^3P_2$ state I must calculate the magnetic quadrupole (M2) decay $1s\,2p_{3/2}{}^3P_2 \rightarrow 1s^2\,{}^1S_0$. The rate is given in the non-relativistic limit by the formula[6]

$$A_{M2} = \alpha k^5 \frac{2^{15}}{5^1 \bullet 3^{10}} (Z\alpha)^{-2} \left[\left\{ 1 - 0.640\,(Z\alpha)^2 - \cdots \right\} + \frac{0.245}{Z} \right]^2 \qquad 3.24$$

Here the sum {...} is the same matrix element which appears in the one-electron $2p_{3/2} \rightarrow 1s_{1/2}$ magnetic quadrupole decay. For Z in the range 1 to 60 the element may be found in Hillery and Mohr[7]. The term $0.640\,(Z\alpha)^2$ is just the first correction in powers of $(Z\alpha)^2$ from the combined effects of the relativistic contraction of the wavefunctions and of the finite wavelength of the emitted radiation. For accurate results for Z = 92 this expression {...} must be replaced by the complete integral

$$M(k,Z) \equiv$$

$$-\frac{(Z\alpha)^2}{2}\left[\frac{3}{2}\right]^{\frac{11}{2}} \int_0^\infty \left[f_{1s_{1/2}}(x) g_{2p_{3/2}}(x) + g_{1s_{1/2}}(x) f_{2p_{3/2}}(x)\right] \frac{j_2(kx)}{k^2} x^2\,dx \qquad 3.25$$

where $j_2(x)$ is the spherical Bessel function. Using

$$k_{2^3P_2 - 1^1S_0} = \frac{3}{8}(Z\alpha)^2 + \sim(Z\alpha)^4 + \cdots \qquad 3.26$$

the integral $M(k,Z)$ may be checked to have the explicit expansion

$$M \sim 1 - \left[\frac{287}{480} + \frac{5}{4}ln\,2 - \frac{3}{4}ln\,3\right](Z\alpha)^2 + \cdots = 1 - .64039\,(Z\alpha)^2 + \cdots \qquad 3.27$$

For Z = 92 and for a $1s\,2p_{3/2}{}^3P_2 - 1s^2\,{}^1S_0$ energy of $1.0052 \bullet 10^5$ ev, the exact value of M is[8]

$$M = .77698 \qquad 3.28$$

and the $1s\,2p_{3/2}{}^3P_2 \rightarrow 1s^2\,{}^1S_0$ M2 decay rate is[9]

---

[6]R. Marrus and P.J. Mohr, in *Advances in Atomic and Molecular Physics*, Vol. 14, p 181 Academic Press, (1978).

[7]M. Hillery and P. J. Mohr, Phys. Rev. A21, 24 (1980).

[8]The routine which evaluates the required integral reproduces the value of Hillery and Mohr for the integral evaluated at for Z = 60, accurate to the 5 digit precision derivable from their graph of the quantity F4.

[9]The rate reproduced by the formula for Z = 90 is slower by 4% than the rate quoted by W.R. Johnson and C.D. Lin, Phys Rev A14,565, (1976), and by Lin, Johnson and Dalgarno, Phys. Rev. A 15, 154 (1977), calculated us-

$$A^{M2}{}_{2\,^3P_2\rightarrow 1\,^1S_0} = 2.0481\bullet 10^{14}\ s^{-1} \qquad 3.29$$

The photon's finite wavelength has been incorporated exactly. The first missing term in the matrix element is the relativistic correction to the correlation, $\sim Z^{-1}(Z\,\alpha)^2$, which again with a coefficient taken to be 1.0 would make a $\simeq 0.5\%$ correction to the matrix element, and so a $\simeq 1\%$ correction to the rate. The total decay rate for the $1s\,2p_{3/2}{}^3P_2$ state is the sum

$$A^{E1}{}_{^3P_2\rightarrow ^3S_1} + A^{M2}{}_{2\,^3P_2\rightarrow 1\,^1S_0} = 2.9142\bullet 10^{14}\ s^{-1} \qquad 3.30$$

In Chapter 4 I need the branching ratios for the decays of the $1s\,2p_{3/2}{}^3P_2$ state to set limits to the contamination of the experiment by cascades; these ratios are

$$E1:\ {}^3P_2\rightarrow 2\,{}^3S_1 = .297 \qquad 3.31$$

$$M2:\ {}^3P_2\rightarrow 1\,{}^1S_0 = .703 \qquad 3.32$$

Nuclear spin and the hyperfine-induced decay rate $1s\,2p_{1/2}{}^3P_0\rightarrow 1s^2\,{}^1S_0$.

Finally consider the phenomenon of the hyperfine quenching of the metastable $1s\,2p_{1/2}{}^3P_0$ state. The single photon decay $1s\,2p_{1/2}{}^3P_0 \rightarrow 1s^2\,{}^1S_0$ is forbidden only because the $1s\,2p_{1/2}{}^3P_0$ state is pure $J=0$. If the nucleus has non-zero spin, and therefore a non-zero magnetic moment, the magnetic hyperfine interaction will mix the $1s\,2p_{1/2}{}^3P_0$ state with nearby $J=1$ states (principally with the $1s\,2p_{1/2}{}^3P_1$, which is closest in energy) and open an electric dipole decay to the ground $1s^2\,{}^1S_0$ state. The phenomenon was first observed for the $1s\,2p_{1/2}{}^3P_0$ state of heliumlike ions by Gould, Marrus, and Mohr[10] in heliumlike vanadium, and since in a number of heliumlike ions[11]. A calculation of the effect for Z in the range 9 to 29 has been done by Mohr[12].

---

ing the Relativistic Random Phase Approximation. 2% of the discrepancy is accounted for if one uses a $1s\,2p_{3/2}{}^3P_2 - 1s^2\,{}^1S_0$ energy which includes the Lamb shift instead of the RRPA energy.

[10]H. Gould, R. Marrus, and P. J. Mohr, Phys. Rev. Lett. 33, 676 (1974).

[11]See, for example, A.E. Livingston and S.J. Hinterlong, Nuclear Instruments and Methods in Physics Research 202, 103 (1982). [Phosphorus, Z = 15]; Engstrom *et al*, J. Phys. B 13, L143 (1980) [Fluorine, Z = 9]; Denne *et al*, Phys. Scr. 22, 45 (1980) [Aluminum, Z = 13].

[12]P. J. Mohr, in *Beam-Foil Spectroscopy*, eds. I. A. Sellin and D. J. Pegg, Plenum Press, New York, 1976, p. 97.

A non-zero uranium nuclear spin can appear in two ways. First, while natural uranium is 99.275% the spin-zero isotope ^{238}U, the rest of the natural abundance[13] is made up mostly of the 0.720% fraction ^{235}U, whose ground state is spin 7/2. It is also possible that the ^{238}U nucleus may by a close nuclear collision in the target be Coulomb excited from its $J^{\pi}=0^{+}$ ground state into long-lived $J^{\pi}=2^{+},4^{+},6^{+},8^{+}\cdots$ states in its first rotational band. Consider the first excited state of ^{238}U, the 2^{+}, at 44.91 kev. In neutral uranium this decays with a half-life[14] of 0.21 ns, primarily by ejection of atomic electrons with a calculated internal conversion coefficient[15] of $5.57\bullet10^{2}$. From this one can determine that the electric quadrupole decay rate of a bare ^{238}U nucleus in the 2^{+} state is $5.9\bullet10^{6}\ s^{-1}$. Scaling the E2 decay rate by $\sim k^{5}$ for the more energetic transitions, and using the tables of Rosel[15] *et al* for the internal conversion coefficients for the $2p_{1/2}$ and $1s_{1/2}$ states in neutral uranium to estimate the coefficients for the same states in heliumlike uranium, one can show, for example, that the ^{238}U 8^{+} state at 517.8 kev both lives long enough to perturb the $1s\,2p_{1/2}{}^{3}P_{0}$ state and does not destroy it outright by internal conversion.

I have calculated[16] the quenching of the metastable $1s\,2p_{1/2}{}^{3}P_{0}$ state by the magnetic hyperfine interaction along the isoelectronic sequence Z = 20 to 104. For Z = 92 the modified $1s\,2p_{1/2}{}^{3}P_{0}$ total decay rate, Γ^{Q}, is given accurately enough for my purposes here by the Bethe-Lamb formula and by considering only mixing of the $1s\,2p_{1/2}{}^{3}P_{0}$ state with the nearby $1s\,2p_{1/2}{}^{3}P_{1}$:

$$\Gamma^{Q} = \Gamma_{^{3}P_{0}} + \frac{|<{}^{3}P_{0} \mid H_{HFS} \mid {}^{3}P_{1}>|^{2}}{\left[E_{^{3}P_{0}} - E_{^{3}P_{1}}\right]^{2} + \left[\frac{1}{2}\Gamma_{^{3}P_{1}}\right]^{2}} \bullet \Gamma_{^{3}P_{1}} \qquad 3.33$$

---

[13]The sources used at the injector to the Hilac are probably made of depleted uranium, in which case the ^{235}U fraction will be reduced below its natural level. Also the Bevatron is a synchro-cyclotron and may be unable to accelerate *e.g.*, $^{238}U^{39+}$ and $^{235}U^{38+}$ simultaneously because of their different charge-to-mass ratios. The aim of the argument here is to set a limit to the effect which is independent of the details of the operation of the accelerator.

[14] *Table of Isotopes, Seventh Edition*, eds. C. M Lederer and V. S. Shirley, John Wiley & Sons, Inc. 1978.

[15]F. Rosel, H.M. Fries, K. Alder, and H.C. Pauli, Atomic Data and Nuclear Data Tables 21,91, 1978.

[16] C. T. Munger, manuscript in preparation.

The magnetic hyperfine Hamiltonian for Dirac electrons is well known [17, 18] and the required matrix element is[19]:

$$| < {}^3P_0 \mid H_{HFS} \mid {}^3P_1 > | \; = \; \sqrt{I(I+1)}\, g \frac{m_e}{m_P} \frac{2\alpha}{3} (Z\alpha)^3 \left[F_{1s\,1/2} - \frac{1}{24} F_{2p\,1/2} \right] \quad 3.34$$

Here I is the nuclear spin in units of $h/2\pi$, g is the nuclear g factor, m_e and m_P are the electron and proton masses, and H_{HFS} is the magnetic hyperfine Hamiltonian for electrons bound to a point magnetic moment. The numbers F involve integrals over the radial wavefunctions for the $1s$ and $2p_{1/2}$ states. The numbers F go to +1 in the non-relativistic limit $(Z\alpha) \rightarrow 0$, and increase as Z increases because the relativistic contraction of the Dirac wavefunctions toward the origin increases the strength of the hyperfine interaction. Using the $1s$ wavefunction for a point nuclear charge, F_{1s} takes a value $\simeq 2.5$ for Z = 92. Using a $1s$ wavefunction for the distributed nuclear charge of ^{238}U reduces F_{1s} by[20] $\simeq 20\%$ (This is the Rosenthal-Breit effect[21]). I have included this correction in F_{1s} and F_{2p}. Using a magnetic hyperfine Hamiltonian which takes account of the distributed magnetic moment of ^{238}U would further diminish this corrected value by by $\sim$ 10% (This is the Bohr-Weiskopf effect[22]). The magnitude of this correction depends on the unknown distribution of magnetic moment within a uranium nucleus and I have not included it in F_{1s} or F_{2p}. Substituting from Table 1.3

$$E_{^3P_0} - E_{^3P_1} = 114 \; ev \quad 3.35$$

and from Eq. 3.9, 3.17, and 3.18

$$\Gamma_{^3P_0} \; = \; A^{\pi\pi} + A^{E1}{}_{^3P_0 \rightarrow {}^3S_1} \; = \; 1.766 \bullet 10^{10} \; s^{-1} \quad 3.36$$

---

[17] C Schwartz, Phys. Rev. 97, 380, 1955.

[18] L. Armstrong, Jr. *Theory of the Hyperfine Structure of Free Atoms*, John Wiley & Sons, Inc. 1971.

[19] The matrix element is real but its absolute sign depends on a choice of phase conventions too complicated to detail here. Since I need only the square of the element I report here only its absolute value.

[20] H. J. Rosenberg and H. H. Stroke, Phys. Rev. A 5, 1992, 1972.

[21] E. Rosenthal and G. Breit, Phys. Rev. 41, 459 (1932).

[22] A. Bohr and V.F. Weiskopf, Phys. Rev. 77, 94 (1950).

And the value for the $1s\,2p_{1/2}{}^3P_1 \rightarrow 1s^2\,{}^1S_0$ decay rate[23]

$$\Gamma_{^3P_1} = 3.004 \bullet 10^{16}\ s^{-1} \qquad 3.37$$

one has the formula

$$\Gamma_Q = \left[1.766 \bullet 10^{10} + \quad 1.70 \bullet 10^{12}\ I(I+1)g^2\ \right] s^{-1} \qquad 3.38$$

The g-factor of the $^{238}U^*(2^+)$ state has been calculated by Nilsson and Prior[24] to be 0.24, based on a rigid-rotor model of the ^{238}U nucleus. The g-factor of the ^{235}U ground state is[25] 0.100(3) The $1s\,2p_{1/2}{}^3P_0$ decay rates for the $^{238}U^*(2^+)$ state and for the ground state of ^{235}U are respectively 34 and 16 times faster than the decay rate for a nucleus with no magnetic moment. Any population of the $1s\,2p_{1/2}{}^3P_0$ state formed at the target around such states will be attenuated by factors of $\sim 1 \bullet 10^{-8}$ and $\sim 2 \bullet 10^{-4}$ in the time it takes the beam to travel the minimum 0.625 cm to appear in front of our detector. States higher in the rotational band than the 2^+ will have larger magnetic moments[26] and so even faster quenched decay rates than the 2^+. I conclude that there can be no change in our measured ^{238}U $1s\,2p_{1/2}{}^3P_0$ lifetime from the presence of uranium nuclei with spin.

---

[23] G.W.F. Drake, Phys. Rev. A19, 1387 (1979).

[24] S.G. Nilsson and O. Prior, Danske Videnskabernes Selskab. Mathematisk-Fysiske Meddelelser, 32, 61 (1961); see also R.D. Meeker, G.M. Kalvins, B.D. Dunlap, S.L. Ruby and D. Cohen, Nuclear Physics A 224, 429 (1974).

[25] *Table of Isotopes, Seventh Edition,* eds. C. M. Lederer and V. S. Shirley, John Wiley & Sons, Inc. 1978. The magnetic moment of ^{235}U is negative; I give here for the value of g the *absolute value* of the ratio of the magnetic moment to the nuclear spin.

[26] Picturing the uranium nucleus as a rigid ellipsoid of charge one would expect the magnetic moment to scale as $|\vec{I}|$ and so the quenched decay rate to scale as $|\vec{I}|^2$.

Chapter 4

The Theory Supporting the Correction Made for Cascades

An electron falling from a long-lived initial state of high principal quantum number n can repopulate the $n=2$ states downstream of the target and past the point where I begin to record the exponential decay of the $1s\,2p_{1/2}{}^3P_0$ state. Such an electron may add to the $1s\,2p_{1/2}{}^3P_0$ population, or if it falls into another $n=2$ state, produce an $n=2\rightarrow1$ x ray which blends with the $1s\,2s\,{}^3S_1\rightarrow1s^2\,{}^1S_0$ x ray which I use to detect the decay $1s\,2p_{1/2}{}^3P_0\rightarrow1s\,2s\,{}^3S_1$. In this chapter I prove the absence of a *single* 84.4 kev fluorescence line in our spectra limits the presence of cascade feeding of *all* the key $n=2$ states, though I assume nothing about how collisions in the target populate highly excited states.

The argument which shows the change in the value of the $1s\,2p_{1/2}{}^3P_0$ lifetime due to cascades is long. The easiest path is to assert, and then prove at length, a series of propositions. In this chapter I use throughout units where $\hbar/2\pi = m = c = 1$.

Only cascades from initial $1snl$ states of heliumlike uranium with principal quantum number $n>22$ and large orbital angular momentum l reach the $n=2$ states after I start recording the $1s\,2p_{1/2}{}^3P_0$ decay curve.

As a first approximation examine two-electron uranium using Schrodinger wavefunctions and energies and ignoring the small ($\sim 1/Z$) effect of the two electrons mutual Coulomb interaction. For given n the longest lived state is the yrast state of maximum possible l, equal to $n-1$. Each yrast state decays only to the next yrast state with n reduced by 1, and so of cascades from any initial state nl it is the cascade starting from the yrast state which takes the longest to reach the $1s^2\,{}^1S_0$ ground state. The rate for the yrast decay $[n, l=n-1]\rightarrow[(n-1), l=(n-2)]$ is[1]

[1]The electric dipole radial integral needed to derive this formula may be found in H. A. Bethe and E. E. Salpeter, *Quantum Mechanics of One- and Two-Electron Atoms*, Springer-Verlag, 1957.

$$A^{yrast}{}_n = \frac{2\alpha(Z\alpha)^4}{3n^5} \bullet \frac{n(2n-1)}{2(n-1)^2} \bullet \left[\frac{(2n-1)^2-1}{(2n-1)^2}\right]^{2n} \qquad 4.1$$

The time required for a cascade from an initial yrast state with $n=N$ to reach ground is roughly

$$T(N) \sim \sum_{n=2}^{N} \left[A^{yrast}{}_n\right]^{-1} \qquad 4.2$$

$T(N)$ equals the proper time for the beam to fly the minimum 0.67 cm from the target to the first point on our decay curve for $N \simeq 22$; states of lower initial n cannot perturb our measurement. Consider how the time for a cascade to reach the $n=2$ states varies with the l of the initial state. The lifetime[2] of a Schrodinger nl state for $l \neq 0$ is given by[3]

$$T(nl) = \alpha^{-1}(Z\alpha)^{-4}\frac{3^8}{2^{12}} c_{nl}\, n^3\, l^2 \qquad 4.3$$

where c_{nl} is a very slowly varying coefficient of n and l, approaching a constant ≈ 1 for each n, l as $n, l \to \infty$. Taking c_{nl} to be simply 1 reproduces the lifetimes of all states with $n \leq 25$ and $l \neq 0$ to within a factor of 2. A cascade starting from an initial nl state of small l reaches the ground state quickly because the l^2 dependence of $T(nl)$ makes the small l intermediate states short-lived. Furthermore such a cascade typically leaps many units of n per transition, so there are few such intermediate states. For ns states the simple formula in Eq. 4.3 for $T(nl)$ does not apply. Omidvar's calculations[4] show that the ratio of the lifetime of the ns state to that of the np state decreases with increasing n, reaching a value ~ 10 for $n=10$. This factor is not big enough to give cascades starting from ns states any special importance. If the cascade from a yrast state with $l=n-1$ with $n \geq 22$ could affect our measurement, a cascade from a state with $l \sim 2$ would have to start with n greater than ~ 100. Such states will be only faintly populated, because the total population in all states of given n are predicted[5] to fall off as $1/n^3$.

---

[2]The time for an initial population of 1 to fall to $1/e$.

[3]This formula is adapted from the work of K. Omidvar, Atomic Data and Nuclear Data Tables 28, 1 (1983).

[4]K. Omidvar, Atomic Data and Nuclear Data Tables 28, 1 (1983).

[5]The dominant mechanism for producing the high-n states of heliumlike uranium by electron capture on to hydrogenlike uranium is, certainly at $\sim$ 200 Mev/amu, non-radiative, rather than radiative, capture. The prediction

Cascades from states of $n > 22$ and large l feed into the chain of yrast states and must pass through the $1s\,2p$ states, not the $1s\,2s$ states.

Any state with quantum numbers n, l with $n > l+1$ has electric dipole decays which change l by $\pm$ 1 but diminish n by more than 1, so that a sequence of electric dipole decays tends to enter a (yrast) state where $n = l+1$. Cascades from a yrast state must pass through the sequence of states ... $\rightarrow 5g \rightarrow 4f \rightarrow 3d$ to reach the $2p$ state, not the $2s$. The higher the original n and the higher the original l the larger the fraction of the initial population which enters the yrast sequence, and the higher the fraction of the population which enters the $2p$ state instead of the $2s$.

Table 4.1 shows for a Schrodinger electron Omidvar's calculations[4] of the fraction of the initial population of a state with $n = 15$ and arbitrary l which reaches the 2s and the 2p states. Only for initial s and p states is the ratio of the fraction of the initial population which enters the 2s state to the fraction which enters the 2p state greater than 10^{-1}. The ratio of the fractions averaged over l (weighting each l by the statistical factor $(2l+1)$) for $n = 15$ is only $\sim 6 \bullet 10^{-3}$. This ratio will be still smaller for $n > 22$, and the initial n must be this large for a cascade to affect my measurement. Furthermore the cascades from states of small l, which enter the $2s$ state, are fast; the cascades from states of large l, which enter the $2p$ state, are slow. What $n = 2$ state population appears *after the* $\sim$ *26 ps delay when* I begin to collect the $1s\,2p_{1/2}\,^3P_0$ decay curve will be in the $2p$ state; the $2s$ population will be essentially zero.

The highly excited $1snl$ states of heliumlike uranium are jj coupled product states of Dirac one-electron wavefunctions.

---

for an approximate $\sim 1/n^3$ dependence in non-radiative capture in relativistic heavy-ion collisions may be found in *Atomic Collisions with relativistic heavy ions. III. Electron capture,* W.E. Meyerhof, R. Anholt, J. Eichler, H. Gould, Ch. Munger, J. Alonso, P. Thieberger, and H.E. Wegner, Phys. Rev. A 32, 3291 (1985).

Table 4.1.
The probability that an n ,l electron will cascade through the $2s$ and $2p$ states, for n =15

l	$2s$	$2p$	$2s$ /$2p$
0	8.45(-2)	3.18(-1)	2.66(-1)
1	1.18(-1)	7.55(-2)	1.56
2	5.32(-2)	5.65(-1)	9.42(-2)
3	2.57(-2)	7.87(-1)	3.27(-2)
4	1.36(-2)	8.86(-1)	1.53(-2)
5	7.75(-3)	9.35(-1)	8.29(-3)
6	4.66(-3)	9.61(-1)	4.85(-3)
Average over l , weighting by $2l+1$:			
-	5.70(-3)	9.53(-1)	5.98(-3)

This coupling would be automatic for heliumlike uranium in no external fields if the interaction between the inner $1s$ and outer nl electron were turned off. Because the $1s$ electron screens the nuclear charge the wavefunction and binding energy of the outer electron correspond[6] to a charge Z = 91 instead of Z = 92. For excited s states there is no difference between the possible couplings LS and jj. The four jj coupled states for $l \geq 1$ are the $|\, 1s_{1/2}\, nl_{j=l-1/2}, J=l-1>$, the $|\, 1s_{1/2}\, nl_{j=l-1/2}, J=1>$, the $|\, 1s_{1/2}\, nl_{j=l+1/2}, J=1>$ and the $|\, 1s_{1/2}\, nl_{j=l+1/2}, J=l+1>$. The two states of the same j are degenerate. The splitting between the pairs of states with $j = l \pm 1/2$ is, for n so large that $1/n$ can be neglected compared to 1,

$$\Delta E_{jj} = \frac{1}{2}\frac{(Z\alpha)^4}{n^3}\frac{1}{l(l+1)} \qquad 4.4$$

Photon exchange between the $1s$ and nl electrons mixes the $|\, 1s_{1/2}\, nl_{j=l-1/2}, J=1>$ and $|\, 1s_{1/2}\, nl_{j=l+1/2}, J=1>$ states and partially restores LS coupling. The size of the off-diagonal matrix element can be estimated by looking at the splitting of the $S=0$ and $S=1$ LS coupled states of a high-Z Schrodinger system, where the electrons' interaction is

[6]An excited ns wavefunction corresponding to a charge Z-1 is not orthogonal to a 1s wavefunction corresponding to a charge Z. While this problem can be dealt with I can restrict the discussion to excited nl electrons with $l \geq 1$, where the orthogonality is guaranteed by the two wavefunctions' different angular momenta.

just the simple Coulomb interaction e^2/r_{12}. Following Bethe and Salpeter[7], the binding energy of a $1s$ electron bound to a charge Z and an outer nl electron bound to the screened charge Z - 1 is

$$E = -\frac{1}{2}(Z\alpha)^2 - \frac{1}{2}\frac{(Z-1)^2\alpha^2}{n^2} + J \pm K \qquad 4.5$$

where the + sign corresponds to $S=0$ and the — sign to $S=1$. The direct and exchange integrals J and K are the first correction to the binding energy for the fact that the charge density of an electron in a $1s$ orbital is not a point but is distributed. These integrals[6] are

$$J = (Z\alpha)^2 \int_0^\infty r_2^2 dr_2 \, R_{nl}^2(r_2) \int_{r_2}^\infty r_1^2 dr_1 \left[\frac{1}{r_1} - \frac{1}{r_2}\right] R_{10}^2(r_1) \qquad 4.6$$

$$K = \frac{2(Z\alpha)^2}{l+1} \int_0^\infty r_2^{l+2} \, dr_2 R_{10}(r_2) R_{nl}(r_2) \int_{r_2}^\infty r_1^{-l+1} \, dr_1 \, R_{10}(r_1) R_{nl}(r_1) \qquad 4.7$$

where R_{nl} is the Schrodinger radial wavefunction. For n so large that $1/n$ can be neglected compared to 1, I have evaluated the integrals J and K:

$$J = (-1)\frac{(Z\alpha)^2}{Z}\left(\frac{Z-1}{Z}\right)^{2l+3} \frac{1}{n^3}\frac{(l+1)}{(2l+1)!}\left[\frac{1}{n^{2l+1}}\frac{(n+l)!}{(n-l-1)!}\right] \qquad 4.8$$

$$K = (+1)\frac{(Z\alpha)^2}{Z}\left(\frac{Z-1}{Z}\right)^{2l+3} \frac{1}{n^3}\frac{4(l+1)}{(2l+1)!}\left[\frac{1}{n^{2l+1}}\frac{(n+l)!}{(n-l-1)!}\right] \qquad 4.9$$

The quantity in brackets [...] goes to 1 as $n \to \infty$, so like the fine structure splitting ΔE_{jj} both J and K fall as n^{-3} for fixed l. Both J and K decrease very rapidly with increasing l. The rapid decrease comes about because the radial wavefunction for the outermost nl electron varies as r^l near the origin and so its overlap with the $1s$ wavefunction decreases with increasing l. The splitting between the $S=0$ and $S=1$ states is

$$\Delta E_{SS} = 2K \qquad 4.10$$

The $1snl$ states for large n must be jj instead of LS coupled if the ratio

$$R_l \equiv \frac{\Delta E_{SS}}{\Delta E_{jj}} \sim \frac{1}{Z(Z\alpha)^2}\left[\frac{Z-1}{Z}\right]^{2l+3} \frac{8l(l+1)^2}{(2l+1)!} \qquad 4.11$$

---

[7]H.A. Bethe and E.E. Salpeter, *Quantum Mechanics of One- and Two- Electron Atoms*, Springer-Verlag, 1957.

is much less than one[8]. The first few values of R_l for Z = 92 are shown in Table 4.2. Only for $l \leq 3$ is there any appreciable departure of the states of high nl from jj coupling. Cascades through states of small l reach the $1s^2\,{}^1S_0$ ground state before we begin our measurement. For studying the way cascades fall through the states of high l, jj coupling can be treated as exact.

The populations of the four jj coupled states -- the $|1s_{1/2}\,nl_{j=l-1/2}, J=l-1>$, $|1s_{1/2}\,nl_{j=l-1/2}, J=1>$, $|1s_{1/2}\,nl_{j=l+1/2}, J=1>$, and $|1s_{1/2}\,nl_{j=l+1/2}, J=l+1>$ --are not redistributed in the cascades, but reach the corresponding $1s\,2p$ states.

I. P. Grant[9] has calculated the rates for one-photon transitions between Dirac one-electron states. I have adapted Grant's formalism to calculate the electric dipole decay rates of heliumlike uranium. In the approximation that the wavefunctions of heliumlike uranium are jj coupled product states of two Dirac one-electron wavefunctions for a nucleus of charge Z = 92, the electric dipole decay rate between an initial state $|1s_{1/2}\,nl_{j_B}, J_B>$ to a final state $|1s_{1/2}\,nl_{j_A}, J_A>$ is

$$\Gamma_{B\to A} = \frac{4}{3}\alpha\, k^3{}_{BA}\,(2j_A+1)(2j_B+1)(2J_A+1)\begin{pmatrix} j_B & 1 & j_A \\ \frac{1}{2} & 0 & -\frac{1}{2}\end{pmatrix}^2 \begin{Bmatrix} j_B & 1 & j_A \\ J_A & \frac{1}{2} & J_B\end{Bmatrix}^2 Q^2_{BA} \quad 4.12$$

Here the quantities in large parentheses (...) and curly braces {...} are 3J and 6J symbols[10]

Table 4.2. Values of the ratio R_l for small l.

l	R_l
1	$6.67 \bullet 10^{-1}$
2	$1.50 \bullet 10^{-1}$
3	$9.52 \bullet 10^{-3}$
4	$2.76 \bullet 10^{-4}$
5	$4.06 \bullet 10^{-6}$

[8]There is no strong dependence on l in the coefficients of the $jj \to LS$ recoupling matrix, which become $\pm 2^{1/2}$ as $l \to \infty$).

[9]I.P. Grant, J. Phys. B 7, 1458, (1974).

[10]A. R. Edmonds, *Angular Momentum in Quantum Mechanics*, Princeton University Press, 1960.

which keep track of the coupling of the various angular momenta, and Q_{BA} is an integral over the radial components of the Dirac wavefunctions. For the sake of completeness I give here the form of Q_{BA} written in the notation of Grant,

$$Q_{BA} = \frac{3}{\omega} J_1 + \frac{3}{2\omega}\left[(\kappa_\alpha - \kappa_\beta)\, I_2^+ + 2I_2^- \right] \qquad 4.13$$

though for my purposes here it is sufficient to note that Q_{BA} reduces, in the non-relativistic and long-wavelength limits appropriate for transitions between states with large n and large l, to the ordinary electric dipole integral[11] over Schrodinger radial wavefunctions R_{nl}:

$$Q_{BA} \rightarrow \int_0^\infty R_{n_A l_A}(r)\, R_{n_B l_B}(r)\, r^3 dr \qquad 4.14$$

Using Eq. 4.12 consider the set of electric dipole transitions $1sn_B l_B \rightarrow 1sn_A l_A$. The rates for transitions for which $|\Delta j| > 1$ or $|\Delta J| > 1$ vanish because a dipole photon carries off only one unit of angular momentum. A rule which lacks a motivation that is similarly obvious is that *the rates for transitions with* $\Delta j = 0$ *or* $\Delta J = 1$ *are weaker than the rates for other allowed* $l_B \rightarrow l_A$ *transitions by a factor which for large* l_B *diminishes as* $1/(2l_B^2)$. (Transitions for which both $\Delta j = 0$ and $\Delta J = 1$ are weaker by a factor $1/(2l_B^2)^2$) This rule arises solely from the the angular momentum coupling buried in the 3J and 6J symbols, not from the radial integrals Q_{BA}. As a consequence $\Delta j = 0$ and $\Delta J = 1$ transitions are suppressed for large l_B, and there are essentially no electric dipole decays which connect any one of the four possible jj coupled states -- the $|1s_{1/2}\, nl_{j=l-1/2}, J = l-1>$, $|1s_{1/2}\, nl_{j=l-1/2}, J = l>$, $|1s_{1/2}\, nl_{j=l+1/2}, J = l+1>$, and the $|1s_{1/2}\, nl_{j=l+1/2}, J = l>$ states -- to any of the others. If the rates for transitions with $\Delta j = 0$ and $\Delta J = 1$ *vanished* for all l_B, a chain of cascades starting from any one of the $1snl$ jj coupled states could empty into only one of the $1s\,2p$ states:

[11]Since I will be concerned mostly with branching ratios it is sufficient for my purposes that e.g., the dipole integrals $3d_{3/2}$-$2p_{1/2}$, $3d_{3/2}$-$2p_{3/2}$, $3d_{5/2}$-$2p_{3/2}$ diminish by the same factor because of relativistic contraction and the effects of finite wavelength.

$$
\begin{array}{lcll}
|\,1s_{1/2}\,nl_{j=l\,-1/2},J=l-1> & \rightarrow & |\,1s_{1/2}\,2p_{1/2},J=0> & \text{(nominally the } 1s\,2p_{1/2}{}^3P_0) \\
|\,1s_{1/2}\,nl_{j=l\,-1/2},J=\ 1\ > & \rightarrow & |\,1s_{1/2}\,2p_{1/2},J=1> & \text{(nominally the } 1s\,2p_{1/2}{}^3P_1) \\
|\,1s_{1/2}\,nl_{j=l\,+1/2},J=\ 1\ > & \rightarrow & |\,1s_{1/2}\,2p_{3/2},J=1> & \text{(nominally the } 1s\,2p_{3/2}{}^1P_1) \\
|\,1s_{1/2}\,nl_{j=l\,+1/2},J=l+1> & \rightarrow & |\,1s_{1/2}\,2p_{3/2},J=2> & \text{(nominally the } 1s\,2p_{3/2}{}^3P_2)
\end{array}
\qquad 4.15
$$

For small l_B one must allow for the small number of branches between the $1snl\ jj$ states which occur the last few steps of the yrast chain, from $l \simeq 5$ to $l=2$. If the initial populations of the four jj coupled states for each n,l are equal for large n, then the populations entering the $1s\,2p$ states are in the definite ratios

$$
\begin{array}{lcl}
|\,1s_{1/2}\,2p_{1/2},J=0> & = & 0.48 \\
|\,1s_{1/2}\,2p_{1/2},J=1> & = & 1.19 \\
|\,1s_{1/2}\,2p_{3/2},J=1> & = & 0.97 \\
|\,1s_{1/2}\,2p_{3/2},J=2> & = & 1.36
\end{array}
\qquad 4.16
$$

independent of the cascade's initial state. There is a 5% uncertainty in these ratios, which enters from two sources. First, I have not used the exact Dirac transition rates to calculate the branching ratios for the steps $l=5$ to $l=2$ but have used simply the Dirac transition energies and the Schrodinger matrix elements, thus accounting for most but not all the effects of relativity. Second, some of the cascade population which reaches the $2p$ states will not yet have entered the yrast sequence by $l=5$. I do not need to know the ratios better than to $\sim$ 5% to set a limit to the effect of cascade feeding on the $1s\,2p_{1/2}{}^3P_0$ lifetime and I have not explored these uncertainties further.

The rate for a dipole transition from a state n,l to any different state n',l' is the same no matter of the four jj-coupled states it starts from, except for relativistic differences in the wavefunctions and energies which are insignificant for large n. The time taken for a cascade to fall through any series of states must also then be the same. Therefore the rate at which cascades feed the four $1s\,2p$ states must be *instantaneously* in the ratios in Eq. 4.16.

A cascade which at some instant reaches the $1s\,2p$ states can have one of three effects on the experiment. It can of course add to the $1s\,2p_{1/2}{}^3P_0$ state population; or it can produce an x ray which blends with the $1s\,2p_{1/2}{}^3P_0$ -fed $1s\,2s\,{}^3S_1 \rightarrow 1s^2\,{}^1S_0$ signal; or it can produce a separate x ray which I can use to measure the number of cascades entering the $1s\,2p$ states. The $1s\,2p_{3/2}{}^1P_1$ state decays to the ground $1s^2\,{}^1S_0$ state by emitting a 100.5 kev x ray. The $1s\,2p_{3/2}{}^3P_2$ state decays 70% of the time[12] to the $1s^2\,{}^1S_0$ state by emitting a 100.6 kev x ray. These x rays would appear in our spectra as an isolated peak Doppler shifted to 81.4 kev. The $1s\,2p_{3/2}{}^3P_2$ state decays 30% of the time to the $1s\,2s\,{}^3S_1$ state by emitting a 4.5 kev photon, which does not appear in our spectra because we set a high threshold on the discriminator of our germanium detector to reduce the count rate from the large number of low-energy events. The subsequent $1s\,2s\,{}^3S_1 \rightarrow 1s^2\,{}^1S_0$ x ray is of course indistinguishable $1s\,2s\,{}^3S_1 \rightarrow 1s^2\,{}^1S_0$ x ray produced by a decay of the $1s\,2p_{1/2}{}^3P_0$ state. The $1s\,2p_{1/2}{}^3P_1$ state decays to the $1s^2\,{}^1S_0$ state by emitting a 96.16 kev x ray which is only 0.15 kev higher than the $1s\,2s\,{}^3S_1 \rightarrow 1s^2\,{}^1S_0$ x ray at 96.01 kev. The separation of these peaks in our spectra is only a tenth of the 1.5 kev peak width (full-width-at-half-maximum) caused by the Doppler shift of the beam and the finite acceptance angle of our detector, and by the 0.8 kev instrumental width. The two peaks are indistinguishable.

Suppose a cascade reaches the $1s\,2p$ states at some point in space downstream of the target. I define both a "cascade" and a "blend" precisely to mean the production of an x ray which is both at that point in space and aimed to enter the detector. I define a "feed" to mean the production of a $1s\,2p_{1/2}{}^3P_0$ state whose subsequent $1s\,2s\,{}^3S_1 \rightarrow 1s^2\,{}^1S_0$ x ray would be aimed to enter the detector if the detector were set to look at some point further downstream of the target. From the ratios of the instantaneous rates at which cascades populate the different $1s\,2p$ states (Eq. 4.16), and the from the different modes of decay of the $1s\,2p$ states, the ratio of cascades to blends to feeds is[13]:

---

[12]This branching ratio is derived in Chapter 3.

[13] To establish these ratios I assume that the radiation from the $n = 2$ states due to cascades is isotropic in

$$cascades : blends : feeds = 1.000 : 0.714 : 0.247 \quad (4.17)$$

The significance of Eq. 4.17, which is the key result of this chapter, is that the absence of the one "cascade" line at 81.4 kev limits *all* the deleterious effects of cascades on our measurement of the $1s\,2p_{1/2}\,^3P_0$ lifetime. It is useful that there are *fewer* blends and feeds than counts in the cascade line, instead of more. A perfect experiment would have, corresponding to Eq. 4.17, a set of ratios 1.000 : 0.000 : 0.000.

The pure jj coupling of the $1snl$ states makes the effect of cascades on our measurement larger than if the coupling had been mixed LS and jj. For a mixed coupling transitions with $\Delta j = 0$ would not be suppressed, and cascades would populate only the $1s\,2p_{3/2}\,^3P_2$ and $1s\,2p_{3/2}\,^1P_1$ states (a result discussed later when I examine the effect of an applied electric field on the cascade chains). There would be no feeding of the $1s\,2p_{1/2}\,^3P_0$ state and no blends from the $1s\,2p_{1/2}\,^3P_1$ state. The ratio of cascades to blends to feeds (Eq. 4.17), would improve to

$$cascades : blends : feeds = 1.000 : 0.176 : 0.000 \quad (4.18)$$

Nature has unfortunately not been so obliging.

Cascades in hydrogenlike uranium

The beam exiting our target is calculated[14] to be made up of $\sim$ 3.6% lithiumlike uranium, $\sim$ 24% heliumlike uranium, $\sim$ 69% hydrogenlike uranium, and $\sim$ 2.4% bare uranium[15]. Cascades feeding the $n = 2$ states of the hydrogenlike fraction of the beam can also produce x rays which blend with our $1s\,2s\,^3S_1 \rightarrow 1s^2\,^1S_0$ signal. Parallel arguments to those given for the way cascades populate the $n = 2$ states of heliumlike uranium show that in hydrogenlike uranium no cascade populates the $2s_{1/2}$ state, and that cascades populate the $2p_{3/2}$ and $2p_{1/2}$ states equally. Doppler broadening blends in our spectra the $2p_{3/2} \rightarrow 1s_{1/2}$

---

the rest frame of the uranium ion. Any initial alignment or polarization would be lost in a sequence of electric dipole decays.

[14]H. Gould, private communication.

[15]The calculation of this distribution of charge states is discussed in Chapter 5.

transition with the 81.4 kev cascade peak and the $2p_{1/2} \rightarrow 1s_{1/2}$ transition with the signal transition $1s\,2s\,{}^3S_1 \rightarrow 1s^2\,{}^1S_0$. If cascades occurred only in the hydrogenlike instead of the heliumlike fraction of our beam, the ratio of cascades to blends to feeds (Eq. 4.17) would be replaced by the ratio

$$cascades : blends : feeds = 1.000 : 1.000 : 0.000 \qquad 4.19$$

This is not an important change. In the analysis of the influence of cascades on the actual data I found that the net effect of cascades on the $1s\,2p_{1/2}\,{}^3P_0$ lifetime would decrease. I found it difficult to produce excited states of heliumlike uranium by direct excitation in a target, and therefore I expect to produce in the same way only a negligible number of excited states of hydrogenlike uranium. Accordingly I have used the ratios in Eq. 4.17 to set the experimental limit to the effect of cascades.

The effect of laboratory fields on the cascade chains

In our experiment the heliumlike uranium is not in the zero field so far assumed. We apply a $\sim$ 2400 gauss magnetic field along the beam direction to hold electrons ejected from the target away from the walls of the vacuum chamber. In the rest frame of the uranium ion there is also then a magnetic field $\sim$ 2400 gauss. There is also a motional electric field which is typically $\sim$ 20 statvolts-cm^{-1}. The electric field arises from a possible misalignment of the beam and the applied axial magnetic field by $\sim$ 5 milliradians, from the angular divergence of the beam, and from the $\sim$ 1 centimeter diameter of the beam spot which puts some of the uranium ions off the symmetry axis of our magnet and so into regions where our magnetic field has a radial component perpendicular to the beam.

Consider first the effect on the cascade chains of the electric field, which can mix the one-electron states of opposite parity whose Dirac energies are degenerate -- for example, the $4f_{5/2}$ and $4d_{5/2}$. Since both states have the same j, j remains a good quantum number until the electric field perturbation is strong enough to overcome the fine structure splitting and mix, for example, the $4d_{5/2}$ and the $4p_{3/2}$. The states of maximum total angular

momentum for a given value of n, for example, the $4f_{7/2}$, have no accompanying degenerate state of opposite parity and are to first order unaffected by the electric field.

In hydrogenlike uranium in zero electric field the states of maximum angular momentum j for a given n form a (yrast) cascade chain which feeds the $2p_{3/2}$ state. The states with the same parity, and with angular momentum j one unit less, form a second cascade chain which feeds the the $2p_{1/2}$ state. The rates for transitions which might branch from the second chain to the first, like the transition $4f_{5/2} \rightarrow 3d_{5/2}$, are suppressed by the characteristic factor $1/2l^2$. In an electric field the first cascade chain is unaffected, but states on the second chain now have strong decays to states on the first. For example, the original $4f_{5/2}$ state mixes with the degenerate $4d_{5/2}$ state and decays to the $2p_{3/2}$. The effect is that cascades from the highly excited states will populate only the $2p_{3/2}$ state instead of populating equally the $2p_{3/2}$ state and the $2p_{1/2}$. In heliumlike uranium a similar argument shows that of the four $1s\,2p$ states only the $|\,1s_{1/2}\,2p_{3/2},J=1>$ and the $|\,1s_{1/2}\,2p_{3/2},J=2>$ states will be populated. These two states will still however be populated equally because j and J remain good quantum numbers to first order in the applied field. The rates for transitions for which $\Delta J = 1$ therefore remain suppressed, and so there is no transfer of population between the chain that feeds the $|\,1s_{1/2}\,2p_{3/2},J=1>$ state and the chain that feeds the $|\,1s_{1/2}\,2p_{3/2},J=2>$. (The separate chains are indicated in Eq. 4.15) The net effect of the mixing of states by an electric field is to improve the ratio of cascades to blends to feeds from 1.000 : 0.714 : 0.247 (Eq 4.17) to the ratio

$$cascades\ :\ blends\ :\ feeds\ =\ 1.000 : 0.176 : 0.000 \qquad 4.20$$

Unfortunately the electric field in my experiment is too weak to mix the states enough.

To show the electric field is too weak examine Stark mixing of one-electron states for Z=92, using simple Schrodinger wavefunctions. The Stark matrix element coupling the degenerate $|\,nl_j> = |\,n\,,(l-1)_{j=l-\frac{1}{2}}>$ and $|\,n\,,l_{j=l-\frac{1}{2}}>$ states is[16]

[16]The required radial integral is evaluated analytically in H.A. Bethe and E.E. Salpeter, *Quantum Mechanics of One- and Two- Electron Atoms*, Springer-Verlag, 1957.

$$< \mid Stark \mid > \; = \; <n,(l-1)_{j=l-\frac{1}{2}} \mid eE_z\, z \mid nl_{j=l-\frac{1}{2}}>$$

$$= \; -\frac{\alpha}{(Z\alpha)} E_z \; \frac{3mn\;(n^2-l^2)^{\frac{1}{2}}}{(2l-1)(2l+1)} \qquad 4.21$$

where E_z is the electric field in units of $e/(\lambda_c/2\pi)^2$, where λ_c is the electron Compton wavelength, and where m is the eigenvalue of j_z (the two states must have the same m or the matrix element vanishes). The degree to which the two states mix is limited by their finite linewidth; a simple estimate is that the two states will mix if the ratio

$$R_{Stark} \equiv \frac{\mid < \mid Stark \mid > \mid}{\frac{1}{2}\Gamma} \qquad 4.22$$

is close to 1, where Γ is the linewidth of the shortest lived state. Using the expression for $T(nl)$ from Eq. 4.3 to estimate Γ one finds that for the l,m state which mixes most for a given n that

$$R_{Stark}^{Max} = \frac{3^9}{2^{14}}(Z\alpha)^{-3}\, E_z \;\; n^6 \qquad 4.23$$

The rapid scaling $\sim n^6$ occurs not only because states of high n are long-lived and so have narrow linewidths, but also because the Stark matrix elements increase with n because the size of the ion increases. Numerically $R_{Stark}^{Max} \simeq 1$ for $n = 42$. This particularly sensitive state has a lifetime of roughly 90 ps -- already longer than the $1s\,2p_{1/2}{}^3P_0$ lifetime -- and since it has l approx30 a cascade starting from this state must pass through ≈ 29 lower states before it can reach the $2p$ state. Even though states of this n and higher are mixed by the motional electric field, cascades from them can reach the $2p$ state only after our measurement is over. Therefore the unimproved ratios in Eq 4.17, not the improved ratios in Eq. 4.20, must be used to measure the sensitivity of our measurement of the $1s\,2p_{1/2}{}^3P_0$ lifetime to cascade feeding. It is however good to know that a motional electric field acts to decrease, instead of increase, the sensitivity of the measurement to cascades.

Finally consider the effect on the cascade chains of the 2400 gauss magnetic field. In the non-relativistic limit, and ignoring the departure of the electron g-factor from the value 2, the Zeeman Hamiltonian is

$$H_{Zeeman} = \mu_0 B_z \ (L_z + 2S_z) \qquad 4.24$$

where μ_0 is the Bohr magneton and B_z is the applied magnetic field assumed to be in the z direction. This Hamiltonian can mix the two nearly degenerate[17] states of different J in heliumlike uranium -- the states $|1s_{1/2}nl_j, J=j\pm\frac{1}{2}>$ -- and make J no longer a good quantum number. For n, l such that J is only approximately a good quantum number the transitions which change the nominal J by ±1 will no longer be suppressed by the factor $1/2l^2$. As a cascade chain proceeds from mixed states of large n and l to unmixed states of small n and l, there is however no preferential focusing of population into one of the particular cascades shown in Eq. 4.15. In a magnetic field there is, for example, no shift of population from the $|1s_{1/2}2p_{3/2}, J=2>$ state to the $|1s_{1/2}2p_{3/2}, J=1>$, or from the $|1s_{1/2}2p_{1/2}, J=1>$ to the $|1s_{1/2}2p_{3/2}, J=1>$, analogous to the shift of population in an electric field from the $2p_{1/2}$ state to the $2p_{3/2}$. The mixing of the high-n states by a magnetic field can therefore have no effect on the way the $1s\,2p$ states are populated by cascades, at least until the strength of the Zeeman perturbation is strong enough to overcome the fine-structure splitting and mix, for example, the $|1s_{1/2}3d_{3/2}, J=2>$ with the $|1s_{1/2}3d_{5/2}, J=2>$.

Calculate the effect of a magnetic field on the nearly degenerate states, using simple Schrodinger wavefunctions. In the two-by-two basis of states $|1s_{1/2}nl_{j=(l+\frac{1}{2})}, J=l, M>$ and $|1s_{1/2}nl_{j=(l+\frac{1}{2})}, J=l+1, M>$ (the first and second column of the matrix, respectively) the matrix for the Zeeman Hamiltonian is

$$B_z \frac{\alpha}{4} \begin{bmatrix} \frac{2(L^2+L+1)}{(L+1)(2L+1)}M & \frac{2L}{2L+1}\left[1-\frac{M^2}{(L+1)^2}\right]^{\frac{1}{2}} \\ \frac{2L}{2L+1}\left[1-\frac{M^2}{(L+1)^2}\right]^{\frac{1}{2}} & \frac{L+2}{L+1}2M \end{bmatrix} \qquad 4.25$$

where the magnetic field B_z is measured in terms of $e/(\lambda_c/2\pi)^2$, and where λ_c is the electron Compton wavelength. Similarly in the two-by-two basis of states $|1s_{1/2}nl_{j=(l-\frac{1}{2})}, J=l-1, M>$ and $|1s_{1/2}nl_{j=(l-\frac{1}{2})}, J=l, M>$ (the first and second column of

[17]The states of different J are split by the Coulomb interaction. The splitting is $\sim$ 2K, where K is the exchange integral evaluated in Eq. 4.7. The splitting falls with n as $1/n^3$ and diminishes very rapidly with l.

the matix, respectively) the matrix of the Zeeman Hamiltonian is

$$B_z \frac{\alpha}{4} \begin{bmatrix} \frac{2(L^2+L+1)}{(L+1)(2L+1)} M & (-1)\frac{2L+2}{2L+1}\left[1-\frac{M^2}{L^2}\right]^{1/2} \\ (-1)\frac{2L+2}{2L+1}\left[1-\frac{M^2}{L^2}\right]^{1/2} & \frac{L-1}{L} 2M \end{bmatrix} \tag{4.26}$$

The mixing of states of different J is largest when $M=0$, because the diagonal elements are zero and the off-diagonal at its maximum value. For large L the this off-diagonal element has the value

$$| < | \, Zeeman \, | > | = B_z \frac{\alpha}{4} \tag{4.27}$$

The degree to which these states mix is limited by their finite linewidth; a simple estimate is that the two states will mix if the ratio

$$R_{Zeeman} \equiv \frac{| < | \, Zeeman \, | > |}{\frac{1}{2}\Gamma} \tag{4.28}$$

is close to 1, where Γ is the linewidth of the shortest lived state. Using the expression for $T(nl)$ in Eq. 4.3 to evaluate Γ one finds for the state which mixes most for a given n

$$R_{Zeeman}^{Max} = \frac{3^8}{2^{13}} (Z\alpha)^{-4} B_z \; n^5 \tag{4.29}$$

For $B_z \simeq 2400$ gauss, R_{Zeeman}^{Max} has the value 1 for $n \simeq 32$. Thus the applied magnetic field mixes the excited states of heliumlike uranium at a lower value of n than does the motional electric field.

The analysis presented here of the effects of the applied fields on the cascades in heliumlike uranium holds until the strength of the Stark or Zeeman perturbation overcomes the fine structure splitting. The ratio of the half-width of a highly excited one-electron state, to the fine structure splitting approaches a constant for large n and l. From Eqs. 4.3 and 4.4,

$$\frac{\Gamma/2}{\Delta E_{jj}} = \frac{2^{13}}{3^8}\alpha = \frac{1}{219.5} \tag{4.30}$$

For the applied electric and magnetic fields of $\sim$ 2400 gauss and $\sim$ 20 gauss, respectively, the Stark and Zeeman perturbations will both overcome the fine-structure splitting for $n \sim$

100. The states beyond $n=100$ are both too long-lived and too sparsely populated to be of any consequence. Therefore the applied electric and magnetic fields have no effect on the way the cascades populate the $1s\,2p$ states, and the ratios in Eq. 4.17 correctly account for the way cascades affect the measurement of the $1s\,2p_{1/2}{}^3P_0$ lifetime.

A calculation of the population of the high- n states indicate the populations fall as $1/n^3$ and that there should be too little population to matter.

Non-radiative electron capture dominates radiative electron capture for a 218 Mev/amu uranium beam passing through palladium, at least for capture into states with small n and perhaps for all n. Anholt and Eichler[18], and Eichler[18], derive a formula using the eikonal approximation for the non-radiative capture of a target $1s$ electron into a projectile $1s$ state. They also propose a scaling rule with which one can estimate the average cross section for capture from any given n-shell of the target to any given n-shell of the projectile. Precisely, this estimate is for the capture cross section averaged over l in both the target and projectile. From their formula and scaling rule I calculate that for a 218 Mev/amu uranium beam passing through palladium that the cross section for non-radiative capture into a state with principal quantum number n is

$$\sigma_{capture} \sim \frac{1}{n^3} \bullet 10^6 \ \ barns \qquad 4.31$$

This formula reproduces the results of the actual scaling formula to within 20% for $3 \leq n \leq 100$. The approximate $1/n^3$ dependence is a direct prediction of the proposed scaling formula. For $n=2$ the scaling formula gives a cross section of $3 \bullet 10^4$ barns. Summing Eq. 4.31 shows that the initial population of the states with $n \geq 22$, some of which live long enough to perturb my time-of-flight measurement, should then be only 3% of the initial population of the $n=2$ states. Unfortunately there is no information about how this population should be distributed among the different angular momentum states for a given n so I cannot

[18]R. Anholt and J. Eichler, Phys. Rev. A 31, 3505 (1985).

[19]J. Eichler, Phys. Rev. A 32, 112 (1985).

calculate the cascade repopulation of the $n=2$ states *ab initio*. Nor do I know whether radiative instead of non-radiative capture better populates the states of $n \geq 22$. Because of these uncertainties I use the absence of the 81.4 kev cascade line and the ratios in Eq. 4.17 to set an experimental limit to the effect of cascade feeding, instead of calculating that the effect must be negligible. I can conclude however that what theory yet exists of the population of the high-n states does not predict enough population to have an effect on my measurement.

Chapter 5

Apparatus Design and the Method of Collecting Data

The technique of measuring atomic lifetimes by beam-foil time-of-flight spectroscopy is an old and successful one, and one of the reasons for its success is the high signal-to-noise ratios obtainable with simple apparatus. Extending the technique to measure the $1s\,2p_{1/2}{}^3P_0$ lifetime in heliumlike uranium required the design of an elaborate apparatus to suppress fierce backgrounds from atomic and nuclear processes whose effects are negligible in experiments on ions of less nuclear charge and with less energetic beams. After I give a general overview of the apparatus I will survey the physical processes which cause trouble, describe the features of our apparatus which deal with them, and finish with a critique of how the apparatus performed in practice.

A schematic diagram of our apparatus is shown in Figure 5.1. A 224 Mev/amu U^{39+} beam from the Lawrence Berkeley Laboratory Bevalac passes through a 25 mg/cm^2 tantalum target and then a 34 mg/cm^2 aluminum target to produce a 218 Mev/amu uranium beam which is about 29% U^{91+}. We separate the U^{91+} magnetically and pass it through a 0.9 mg/cm^2 palladium foil, where 0.7% converts by electron capture to U^{90+} -- heliumlike uranium -- in the metastable $1s\,2p_{1/2}{}^3P_0$ state.

The $1s\,2p_{1/2}{}^3P_0$ state decays in flight downstream of the target with a $1/e$ decay length of 1.2 cm. A germanium x-ray detector collimated to view emission perpendicular to the beam records the 96.01 kev x ray, Doppler-shifted to 77.8 kev, from the fed $1s\,2s\,{}^3S_1 \rightarrow 1s^2\,{}^1S_0$ transition. The collimating plates are aligned using a pentagonal prism and a transit to be perpendicular to a line drawn between the centers of of (retractable) wire chambers upstream and downstream of the apparatus. The wire chambers locate the center of the $\sim$ 1 cm diameter beam spot to $\pm \sim$ 0.5mm. The entire apparatus (Figure 5.2) is held on a rigid three-legged table which can be pushed, jacked and shimmed by hand to align the apparatus with the beam (the Bevalac Beam-40 line has too few steering magnets to guaran-

tee that we could simply adjust the beam to meet the apparatus). The (transverse) Doppler shift determines the beam velocity. Downstream of the target the beam passes through a kapton window, a wire chamber which monitors the beam position, and an ionization chamber which collects a charge proportional to the integrated beam current.

We move the target upstream to trace the exponential decay in space of the $1s\,2p_{1/2}\,^3P_0$ state. The target is mounted on a retractable shaft connected to a remote drive so that the target can be pulled from 0 to 6 cm upstream of the detector. The target-detector separation is reproducible to $\pm$ 0.005 cm; the absolute separation is not so well determined but we don't need it to be. During the 63 hours over which we collected our decay curve we made no change to the apparatus or to the electronics except to move the target and to refill the liquid nitrogen dewar on the detector. To minimize the shift of our measured decay length due to some slow drift in the beam position or in the calibration of our electronics we took two separate decay curves, on each taking every other point on the decay curve as we pulled the target upstream and filling in the missing points as we pushed it back. To confirm that the decay was truly exponential we traced the decay for a full 2.7 decay lengths, and counted longer far out on the the decay curve where the signal was weak. Once an hour we recorded the image of the beam spot on the wire chamber downstream of the target to keep track of any long-term drifts of the beam. From the measured $1/e$ decay length and the beam velocity we determine the $1s\,2p_{1/2}\,^3P_0$ lifetime.

The schematic diagram (Figure 5.1) also shows some features of the apparatus designed to reduce backgrounds. The germanium detector is shielded with lead and an extra crescent-shaped lead shield inside the beam pipe screens the detector from the x rays generated in the target. The target and detector sit between the pole tips of an electromagnet whose axial magnetic field holds electrons ejected from the target away from the beam pipe walls. A thin mylar window opposite the detector reduces the number of target x rays which scatter and enter the detector. A set of scintillators generates a signal to veto counts in the germanium

detector caused by nuclear fragments from the target. There are four key problems we built the apparatus to overcome:

Our signal rate is low.

The Bevalac provided a one-second pulse of $\sim 2 \bullet 10^6$ U^{91+} ions every six seconds. Our ultimate achievement was to collect 2300 $1s\,2p_{1/2}{}^3P_0$ -fed $1s\,2s\,{}^3S_1 \rightarrow 1s^2\,{}^1S_0$ x rays, distributed over a decay curve spanning 2.7 mean lives, over 63 hours of continuous running. This signal rate amounts to one signal count every minute and a half, and it was sufficient to determine the $1s\,2p_{1/2}{}^3P_0$ lifetime to a statistical precision of 5.8%. We needed an apparatus with a large solid angle for collecting photons, and so an apparatus built tightly around the beam.

Electrons in the target accelerated in the moving Coulomb field of the uranium nucleus are ejected into the vacuum chamber downstream of the target.

Our detector must be collimated to view a section of beam downstream of the target, and inevitably views both the material in the window in the vacuum chamber through which it looks and the material which forms the vacuum chamber's far wall. The uranium charge is 92 so the cross section for scattering electrons is large; the targets we require to prepare the $1s\,2p_{1/2}{}^3P_0$ state are thick ($\sim 1\ mg/cm^2$); and the scattered electrons can possess a kinetic energy greater than the $\sim$ 78 kev possessed by our signal x ray. The bremsstrahlung continuum recorded in our 78 $\pm$ 1.5 kev signal band, were these electrons allowed to strike the window or a part of the chamber wall within the view of the detector, would be 10 times brighter than our signal.

Bremsstrahlung is generated in the target both by electrons accelerated in the moving coulomb field of the uranium nucleus (primary bremsstrahlung) and by elastically scattered electrons which collide with atoms in the target (secondary bremsstrahlung).

The theoretical and experimental studies of the primary and secondary bremsstrahlung generated by relativistic beams have been reviewed by Anholt and Gould[1]. The endpoint energy of each of the two continua follows simply from the kinematics of the collision of a uranium ion with a target electron at rest with respect to the lab (neglecting the orbital velocity of a target electron bound to a nucleus). In the rest frame of the uranium ion the maximum energy of a primary bremsstrahlung photon is just the kinetic energy of the target electrons, $(\gamma-1)mc^2$. In the lab frame this photon's maximum energy is

$$K_{primary} = \frac{\gamma-1}{\gamma}\,\frac{1}{1-\beta}\,mc^2 \qquad 5.1$$

The maximum kinetic energy in the lab frame of an elastically scattered electron is

$$K_{e^-} = 2\beta^2\gamma^2\,mc^2 \qquad 5.2$$

The maximum lab energy of a photon from secondary bremsstrahlung is just the same,

$$K_{secondary} = K_{e^-} = 2\beta^2\gamma^2\,mc^2 \qquad 5.3$$

We ran the experiment with a beam energy on target of 218 Mev/amu for which the maximum energy for primary bremsstrahlung is 234 kev, and the maximum energy of a scattered electron and secondary bremsstrahlung is 535 kev.

When this apparatus was first designed we did not know enough about the electron capture and loss cross sections in the target to know if we could create heliumlike uranium in the $1s\,2p_{1/2}\,^3P_0$ state using a 218 Mev/amu uranium beam. A 400 Mev/amu beam we knew could strip most of the beam to make hydrogenlike uranium, and if it could excite a tightly-bound $1s$ electron into the continuum we supposed it could also excite a $1s$ electron into a low-lying bound state. The apparatus was therefore designed to function at 400 Mev/amu, where the endpoint energies for primary and secondary bremsstrahlung are respectively 538 and 1067 kev and so where there is more background to obscure the signal than at 218 Mev/amu. A model calculation showed that a beam pulse of 10^6 uranium ions passing

[1]R. Anholt and H. Gould, *Relativistic Heavy-Atom-Ion Collisions*, in *Advances in Atomic and Molecular Physics 22*, Academic Press, 1986, p. 315; see also R. Anholt, Ch. Stoller, J.D. Molitoris, D.W. Spooner, E. Morenzoni, S.A. Andriamonje, W.E. Meyerhof, H. Bowman, J.-S. Xu, Z.-Z. Xu, J.O. Rassmussen, D.H.H. Hoffman, Phys. Rev. A 33, 2270 (1986) [Paper VI].

through a $\sim$ 1 mg/cm Palladium target would generate $\sim 10^6$ scattered electrons, and $\sim 10^5$ photons, with energies greater than 50 kev; and that we could hope to see only $\sim$ 1 photon from a $1s\,2p_{1/2}\,^3P_0$ -fed $1s\,2s\,^3S_1 \rightarrow 1s^2\,^1S_0$ transition.

The x-ray continua are protean in the range of problems they may cause. The x rays may Compton scatter, Rayleigh scatter, or be photoabsorbed in any part of the apparatus. It is difficult, given the tight geometry imposed by our low signal rate, to find space for enough shielding, and any material introduced for shielding becomes itself a new center for scattering. There are three key problems. The x rays with energies above $\sim$ 180 kev can Compton scatter in the germanium elements can mimic our signal by depositing $\sim$ 78 kev in a recoil electron. X rays may Rayleigh or Compton scatter in any material with a line of sight to our germanium elements and send a spurious 78 kev x ray into an element. Particularly noxious places for this scattering to occur are in the vacuum chamber walls opposite the detector; in the collimating plates on the face of the detector; or within the shielded detector itself, in any part of framework which is near the elements. Lastly the x rays photoionize everything, which means that every material in the apparatus glows with its characteristic K_α and K_β x-ray doublets, complicating our spectra and (possibly) overlapping our signal.

A typical nuclear event in the target involving a $\sim$ 200 Mev/amu uranium nucleus scatters neutrons and protons of $\sim$ 200 Mev through wide angles to intersect the detector.

Data taken at the Bevalac by the Plastic Ball[2] collaboration on 200 Mev/amu Au on Au collisions show that a typical nuclear event produces $\sim$ 30 free protons of $> \sim$ 200 Mev mean energy in a cone extending a mean $\sim$ 45 degrees out from the beam direction, with some protons appearing at angles as large as $\sim$ 75 degrees[3]. Presumably the same number of

[2] Arthur Poskanzer, Plastic Ball Collaboration, private communication.

[3] This is a very crude and qualitative description of the kinematics of the products of a heavy ion collision at these energies, fortunately sufficient for my purposes. I do not know of a summary of the information likely to be of most use to the design of future beam-foil atomic physics experiments, namely the kind of particles produced and their lab frame angular and energy distributions averaged over the impact parameter of the incident heavy ion.

free neutrons are produced with the same kinematics, though to these the Plastic Ball detector[4] was not sensitive. The total cross section for a nuclear event is roughly that estimated from the geometric overlap of the two nuclei. Protons and neutrons produced in our target pass through the germanium elements in our detector, depositing energy both by ionization and by inelastic nuclear collisions. Certain evidence for this is the appearance in our x-ray spectra of lines corresponding to the nuclear excited states of germanium isotopes, which appear as the target is pulled upstream and as more of the cone of protons and neutrons intercepts our elements (See Figure 7.1). Also our continuum background is reduced by a factor of two when the signal from a set of scintillators designed to catch nuclear fragments is used to veto counts from the detector. The discrete lines are only an annoyance; however I believe counts generated by nuclear fragments still contribute at least 80% and possibly all of the our continuum background in our ultimate apparatus.

To reduce our background we designed a beam-foil time-of-flight apparatus with several novel features. The choices made to set small details of the apparatus' ultimate design represent many optimizations within constraints both too complicated and too obscure to detail here. I mention only major features of the design which might be relevant to the design of future experiments. In no particular order:

Minimum Beam energy.

The backgrounds associated the scattered electrons and the bremsstrahlung continua from the target increase rapidly with the beam energy, as is suggested by the the equations for the endpoint energies Eq. 5.1 - 5.3. My model calculations predict that the contribution to the total continuum background recorded by our detector would increase by an order of

These distributions would comprise the raw data taken by the Plastic Ball at the Bevalac at Lawrence Berkeley Laboratory. I suggest the interested reader contact the Plastic Ball detector group currently [1987] working at CERN.

[4]The Plastic Ball detector is described in A. Baden, H.H. Gutbrod, H. Lohner, M.R. Maier, A.M. Poskanzer, T. Renner, H. Riedesel, H.G. Ritter, H. Spieler, A. Warwick, F. Welk, and H. Wieman, Nucl. Instrum. and Methods Phys. Res. 203, 189 (1982).

magnitude if the beam energy were increased from 218 to 400 Mev/amu. Most of this increase would come from x rays from the target which would penetrate the lead shielding around the detector and Compton scatter in the germanium elements. I have not figured out how the background from nuclear fragments would change but it is most unlikely it would go down. We were fortunate that for a beam energy of as low as 218 Mev/amu we were able to attain a yield of the $1s\,2p_{1/2}{}^3P_0$ state equal to 0.7% of the available U^{91+} beam.

Restriction on allowed materials.

Because our $1s\,2p_{1/2}{}^3P_0$ -fed $1s\,2s\,{}^3S_1 \rightarrow 1s^2\,{}^1S_0$ signal is feeble we incorporated no material into the germanium detector or the apparatus whose inevitable K_α and K_β fluorescence would overlay our signal. Large quantities of lead must be present to shield the detector, we chose the beam energy of 218 Mev/amu to Doppler shift our signal x ray into the gap between the lead K_α and K_β lines. The other important materials in our apparatus are: tantalum, used to the collimating plates for the detector; palladium, used as our target; and dysprosium, used as shielding inside our detector.

Magnet.

We applied a 2400 gauss magnetic field along the beam direction. Electrons ejected from the target spiral down the beam direction and cannot strike those parts of the beam pipe which are viewed by the detector. Because we need a hole through the pole tips to accommodate the beam pipe and a wide gap between the tips to accommodate our detector the magnetic field could not be made uniform, and so the electron orbits are not simple. The field configuration was modeled by Dr. Klaus Halbach and Dr. David Humphries of LBL, and Dr. Harvey Gould and I studied the electron orbits analytically and numerically to show that no electron ejected from our target could reach the critical parts of the beam pipe wall which are within the collimated view of the detector. I did not judge it necessary to transport the electrons to a special shielded dump; they just strike the beam pipe wall a few inches down-

stream of our detector where the confining magnetic field weakens and diverges.

Detectors.

We had special germanium x-ray detectors designed and built by the x-ray detector group at LBL. Each detector contained two independently wired germanium elements, the two angled at 120 degrees to subtend the maximum solid angle around the beam. The active volume of each element was 5 cm high by 0.7 cm wide by 0.3 cm thick. The thickness of the active germanium was made as small as possible -- .3 cm is just sufficient to stop $\sim$ 78% of our $\sim$ 78 kev signal x rays -- to minimize the probability of a deposit of energy from nuclear fragments and from the Compton scatter of high-energy x rays. The detectors provide 800 ev energy resolution (full-width-at-half-maximum) at 78 kev. Each germanium element is backed by a 2.5mm photoabsorptive plate. The plate absorbs 78 kev x rays not coming from the beam direction, and also absorbs x rays of $\sim$ 105 kev coming from the beam direction which has passed undisturbed through the germanium element. This radiation could otherwise Compton scatter, reversing its direction and lowering its energy, and reenter the germanium element at $\sim$ 78 kev to overlay our signal. The plate is made of dysprosium, which is the most photoabsorbtive convenient material, other than lead, whose K_α and K_β x rays could not confuse our $1s\,2p_{1/2}\,^3P_0$ -fed $1s\,2s\,^3S_1 \rightarrow 1s^2\,^1S_0$ x ray whether it was Doppler shifted for a beam energy of 218 or for 400 Mev/amu. We did not use lead because we sought to limit the strength of the lead K_α and K_β lines near our signal.

A photograph of one of our detectors is shown in Figure 5.3. The shape of the head allows allows it to be inserted between the pole tips of our magnet and still accommodate 1/2" of lead shielding over 4π steradians. The 120 degree angle in the head increases our collection efficiency by allowing the germanium elements to angle around the beam pipe.

Shielding.

Our germanium detectors fit inside a box made of 1/2" thick lead plates and an interior 1/8" brass frame. Besides the 0.5" slots which fit around the tantalum collimating plates the only opening in the lead shielding was a small annulus about the copper coldfinger connected to the liquid nitrogen dewar. The tantalum plates were 0.006" thick, 0.5" high, and separated by 0.012". A photon which did not pass between the plates would have to pass through a minimum .095" of tantalum to enter a detector. A crescent-shaped lead shield within the beam pipe provided an additional 0" - 1.5" of lead between the target and the detector, the exact amount depending on how far upstream of the detector the target was pulled. The shielding box around the detector itself fit snugly between the pole tips of our magnet, whose iron bulk provided more protection against x rays or particles flying from far up-beam or returning from far down-beam. Candidates for the latter, rather unusual, sort are the x rays from the electrons spiraled downstream by the magnet and eventually brought to rest, or radiation from the passage of the uranium ions through the equipment downstream used to monitor the beam's position and intensity. Shown in Figure 5.4 is a photograph of the detector with the tantalum collimating plates, inside its lead shielding, and inserted between the pole tips of the magnet.

Minimal mass of material in the view of the detector.

To prevent the Compton or Rayleigh scatter of x rays into our detector we adopted as a principle of our design that no material which was illuminated by the direct x rays from the target could also be in the direct view of our detector. Accordingly we discarded the plausible idea of doubling our feeble signal rate by building two detectors facing each other, for fear that the x rays scattering off the face of the first detector would inundate the signal counted by the second, and vice versa. A crescent-shaped lead shield inside the beam pipe prevented x rays from the target from striking the tantalum collimating plates mounted to the face of the detector. *Some* material, however, must be left in the beam pipe in the view of the detector to hold a vacuum, and it proved impossible to screen this material from the direct x rays

from the target without merely making the problem now the screen instead of the wall. To minimize the mass we cut large holes in the beam pipe and made a vacuum seal with a flexible 10 mil mylar window. The part of the beam pipe in the view of the detector was on average 99.9% transparent any x ray coming from the target. The cutouts in the beam pipe opposite the detector and the mylar window can be seen in Figure 5.4. The x rays hitting the window simply dispersed into the room. Our apparatus was located on a table well away from any wall; the nearest surface the target x rays could strike to be redirected into the detector was the floor, some 3 1/2 feet away.

Scintillators to veto counts from nuclear fragments.

Three scintillators attached to photomultipliers were set to intersect the cone of protons generated by a typical nuclear event in the target and to generate a time signal for a veto. We used the trigger signal from the fast amplifier of the germanium detector as a time signal. This could pin the time of arrival of a $\sim$ 78 kev deposit of energy in the germanium detector to within 50 ns, though in practice we set a generous time window of $\sim$ 500 ns. The scintillators are shown in Figure 5.5.

Production of the heliumlike uranium $1s\,2p_{1/2}{}^3P_0$ state by electron capture onto a charge-separated beam of hydrogenlike uranium.

We have been unable to observe heliumlike uranium in the metastable $1s\,2p_{1/2}{}^3P_0$ state except by capturing a second electron onto hydrogenlike uranium (U^{91+}). For both the detailed theory and experiment concerning collisions of relativistic heavy ions and atoms the

---

[5] *Atomic collisions with relativistic heavy ions, I-VIII:*

R. Anholt, W.E. Meyerhof, Ch. Stoller, E. Morenzoni, S.A. Andriamonje, J.D. Molitoris, O.K. Baker, D.H.H. Hoffman, H. Bowman, J.-S. Xu, Z.-Z. Xu, K. Frankel, D. Murphy, K. Crowe, J.O. Rassmussen, Phys. Rev. A 30, 2234 (1984) [Paper I].

R. Anholt, Phys. Rev. A 31, 3579 (1985) [Paper II].

W.E. Meyerhof, R. Anholt, J. Eichler, H. Gould, Ch. Munger, J. Alonso, P. Thieberger, H.E. Wegner, Phys. Rev. A 32, 3291 (1985). [Paper III].

R. Anholt, W.E. Meyerhof, H. Gould, Ch. Munger, J. Alonso, P. Thieberger, H.E. Wegner, Phys. Rev. A 32, 3302 (1985) [Paper IV].

reader is referred to a series of articles by Anholt, Meyerhof, and others[5]. Our 224 Mev/amu beam of U^{39+} passes through a 25 mg/cm^2 tungsten ($Z_t = 74$) target[6] which strips all but the K and some of the L electrons, and then through a 34 mg/cm^2 aluminum (Z_t =13) target which finishes the stripping. This preliminary stripping is done with less energy loss and less dispersion of the beam in tantalum instead of aluminum: the beam loses 1.6 and 4.5 Mev/amu of kinetic energy in the tungsten and aluminum targets, respectively[7]. Aluminum produces about the largest U^{91+} charge state fraction possible for a final beam energy of 218 Mev/amu.

Appreciable hydrogenlike uranium can be made only if after stripping the uranium L electrons the collisions in the target crack the tightly bound K-shell and do not swiftly fill the resulting K-vacancy. A K-electron strips by being excited into a continuum state by the pulse of electric field from a close Coulomb collision with particles in the target. This cross section scales as the square of the particle charge; for a nucleus of charge $+Z_t\,e$ with Z_t bound electrons of charge $-e$ the net stripping cross section per target atom scales roughly[8] as $Z_t^2 + Z_t$. A projectile K-vacancy can fill in two ways. The first way is by non-radiative electron capture, which is a double-scattering process. Pictured classically the projectile nucleus first collides with a target electron. The electron scatters off the target nucleus acquiring a velocity and direction matching the motion of the projectile nucleus, whereupon the

---

R. Anholt, W.E. Meyerhof, Phys. Rev. A 33, 1556 (1986) [Paper V].

R. Anholt, Ch. Stoller, J.D. Molitoris, D.W. Spooner, E. Morenzoni, S.A. Andriamonje, W.E. Meyerhof, H. Bowman, J.-S. Xu, Z.-Z. Xu, J.O. Rassmussen, D.H.H. Hoffman, Phys. Rev. A 33, 2270 (1986) [Paper VI].

R. Anholt, W.E. Meyerhof, manuscript in preparation [Paper VII].

R. Anholt, W.E. Meyerhof, X.-Y. Xu, H. Gould, B. Feinberg, R.J. MacDonald, H.E. Wegner, P. Thieberger, manuscript in preparation, LBL Report #22699 [Paper VIII].

See also:

R. Anholt and H. Gould, *Relativistic Heavy-Atom-Ion Collisions*, in *Advances in Atomic and Molecular Physics 22*, Academic Press, 1986, p. 315.

H. Gould, D. Greiner, P. Lindstrom, T.J.M. Symons, and H. Crawford, Phys. Rev. Lett. 52, 180 (1984) (Errata, 52, 1654 (1984)).

[6]Here and in the following discussion Z_t refers to the atomic number of the target material.

[7]The dE/dx in these materials for a $\sim$ 220 Mev/amu uranium beam is interpolated from J.F. Ziegler, *Handbook of Stopping Cross-Sections for Energetic Ions in All Elements*, (Volume 5 of *The Stopping and Ranges of Atoms in Matter*), Pergamon Press.

[8]There are, for some projectile ions, targets and incident energies, screening corrections which modify the simple $Z_t^2 + Z_t$ dependence.

electron is captured. This non-radiative capture cross section rises as a high power of Z_t, speaking very crudely, as $\sim Z_t{}^{\sim 4}$, and falls with increasing projectile energy. The second way a K-vacancy can fill is by radiative electron capture, which is the inverse of the photo-electric effect. Seen the the rest frame of the projectile a free (continuum) electron from the target falls into the K shell and the transition energy is emitted as a photon. The radiative capture cross section per target atom increases with the number of electrons on the target atom, or just proportional to Z_t, and falls with increasing projectile energy, though less rapidly than the cross section for non-radiative capture. For uranium projectiles at low energies, where non-radiative capture is dominant, a low-Z target makes the most K-vacancies, because the capture cross section scales as $\sim Z_t{}^{\sim 4}$ and the stripping only as $\sim Z_t{}^2$. For uranium projectiles at high energies, where radiative electron capture dominates, a high-Z target makes the most k-vacancies, because the the capture cross section now scales only as Z_t. For intermediate energies the most effective Z_t represents a balance and for a 218 Mev/amu uranium beam an aluminum target ($Z_t = 13$) makes the most k vacancies, and so the most hydrogenlike uranium. The (equilibrium) charge state distribution on exit from our 34 mg/cm^2 aluminum target is calculated[9] to be 13% U^{89+}, 51% U^{90+}, 29% U^{91+}, and 6% U^{92+}.

The useful 29% of the beam that is hydrogenlike we separate magnetically and pass through a 0.9 mg/cm^2 palladium target. Discarding the useless 71% of the beam made up of other charge states improves our signal-to-noise by about a factor of 3. The beam is calculated to be on exit from the palladium target roughly 3.6% U^{89+}, 24% U^{90+}, 69% U^{91+}, and 2.4% U^{92+}. We observe that 0.7% of the U^{91+} beam passing the palladium target converts to heliumlike uranium in the metastable $1s\,2p_{1/2}{}^3P_0$ state.

Critique of the design in the light of experience.

---

[9]H. Gould, private communication

With our minimum detector-target separation we achieved in our x-ray detector spectra a ratio of the peak height to the height of the continuum underneath of 1 : 1. (Figure 1.2) Using magnets to hold the electrons ejected from the target away from the walls proved crucial – the continuum background increased by more than a factor of 10 when we turned off the magnets. The veto of nuclear events using the scintillators to catch the cone of protons reduced the background by a factor of 2. Removing all but the U^{91+} charge state from the incident beam did indeed reduce our background by a factor of 3. Minimizing our detector active volume was also crucial. Our limiting background is due to the deposit of energy in the detector by nuclear fragments, and this rate increases linearly with the active volume.

Using dysprosium to make the shield inside the detector was an error. We chose dysprosium over the more photoabsorbtive lead to limit the brightness of the lead K_α and K_β lines. However we found these lines not only to be harmless, but that the fluorescence from the shield inside the detector was no greater than the fluorescence from the masses of lead shielding outside the detector. Not only do the dysprosium K_α and K_β lines unnecessarily complicate our spectra, but many lines in the range 0 to 100 kev could potentially appear in our spectra from the many low-energy *nuclear* excited states of the dysprosium isotopes, a systematic problem I discuss in chapter 6. Were I to repeat the experiment I would replace the dysprosium with lead, or, to match the material the of which the collimating plates are made, with tantalum.

The wings of the Bevalac beam spot of $\sim$ 1 cm diameter run into the inner edge of the crescent-shaped lead shield within the beam pipe, and into the 3/32" thick circular aluminum rim (7/16" inner diameter) which supports the palladium target[10]. Because we need less lead shielding between the target and the detector at 218 Mev/amu, instead of at an energy of 400 Mev/amu for which the shield was designed, we can afford to make the inner radius of the shield larger. Because we no longer need to explore what foil materials and thicknesses best

[10]The rim, target foil and target holder can be seen in Fig. 5.4.

produce the heliumlike uranium $1s\,2p_{1/2}{}^3P_0$ state, it is no longer necessary to have a foil-holder which allows swift exchange of different targets. For a single target we can easily make a holder gossamer-light to oppose no mass to the wings of the uranium beam.

Tests run during the experiment show that at least 80% of our remaining continuum background is not due to the x rays and electrons coming from the target. I believe this background is due to nuclear events, because we vetoed more and more noise as we adjusted the threshold on the photomultipliers which generated the veto signal right down into the electrical noise, so I believe we were losing valid vetos. I could improve the performance of the veto scintillators by seeing that more light from fragments crossing the scintillator actually reached the photomultiplier.

An elegant way to reduce the background from nuclear fragments as well as from a whole class of problems is to require a coincidence in time between a count generated in the x-ray detector and the arrival of an intact uranium ion downstream of the apparatus. If the uranium ions fly one by one down the beam pipe they arrive in our experiment at a rate of roughly one every 3000 ns. Since the arrival time of a $\sim$ 78 kev event in the detector can be determined to $\sim$ 50 ns, if a time signal of the same accuracy can be generated for the passage of an intact uranium ion, one could reduce the contribution from nuclear fragmentation by as much as a factor of 50 to 100. I tried to do this using a scintillator paddle to generate the uranium time signal, and I garnered the worst of all results possible in an experiment -- my scheme failed and I have no certain idea why. Our signal appeared to vanish along with the continuum background. Were I to repeat the experiment I would use an avalanche detector to generate the uranium time signal. Avalanche detectors I think would stand up better to the shock of energy deposited by a 218 Mev/amu uranium ion -- scintillator, I discovered, visibly blackens.

The cumulative result of these improvements should be, based in part on the pricking of my thumbs, a further reduction in background of about a factor of 10. Improvement by more

than this it is futile to forecast because there is too much scope for the play of the unknown. Even if this full factor of 10 were realized, with the current beam intensity of $\sim 2 \bullet 10^5$ U^{91+} ions per pulse, with 1 pulse every $\sim$ 6 seconds, the experimental precision in the $1s\,2p_{1/2}\,^3P_0$ lifetime would be limited by counting statistics with a final error only a factor of $\sim$ 2-3 smaller than what I have already achieved. The techniques discussed here may, however, be useful in reducing the background in other studies of highly ionized uranium.

Chapter 6

Data Analysis

The typical unit of data in our experiment is a pair of histogram x-ray spectra (one for each element of our x-ray detector) which correspond to a certain detector-target separation and integrated beam current. This chapter discusses how we identify our signal, and how we extract the two quantities we need to compute the $1s\,2p_{1/2}{}^3P_0$ lifetime: the beam velocity (and therefore also the time dilation), and the $1/e$ decay length.

Identification of the $1s\,2p_{1/2}{}^3P_0$ -fed $1s\,2s\,{}^3S_1 \rightarrow 1s^2\,{}^1S_0$ signal x ray.

Figure 6.1 shows for two of our x-ray spectra a section which includes lead K_α and K_β lines and the $1s\,2p_{1/2}{}^3P_0$ -fed $1s\,2s\,{}^3S_1 \rightarrow 1s^2\,{}^1S_0$ x ray. The 96.01 kev energy of the $1s\,2s\,{}^3S_1 \rightarrow 1s^2\,{}^1S_0$ transition appears as a peak correctly Doppler shifted to 77.8 and 80.8 kev for the two beam energies 218 Mev/amu and 175 Mev/amu These energies are determined from the operating conditions of the Bevalac, corrected for the energy loss in our target and stripping foils using the tables of J.F. Ziegler[1]. The width and triangular shape of the peaks match those calculated from folding the relativistic Doppler shift with angle with the different degree of collimation of the detector in the two runs. For both beam energies the peak amplitude decays exponentially with as the detector-target separation is increased (Figure 1.3, Figure 6.3). The same peak is observed for Au, Pd, and Ag targets, and disappears when a target foil is removed. There are no other long-lived, $n = 2$ states of hydrogenlike or heliumlike uranium capable of producing a $\sim$ 100 kev x ray besides the heliumlike $1s\,2p_{1/2}{}^3P_0$ state (Figures 3.1 and 1.1) There is no doubt whatever that we have observed the $1s\,2p_{1/2}{}^3P_0$ -fed $1s\,2s\,{}^3S_1 \rightarrow 1s^2\,{}^1S_0$ decay.

The peak's yield using foils of different Z and thickness matches our rough calculation. Non-radiative electron capture dominates radiative electron capture in palladium at 218

---

[1] J.F. Ziegler, *Handbook of Stopping Cross-sections for Energetic Ions in All Elements,* (Volume 5 of *The Stopping and Ranges of Atoms in Matter*), Pergamon Press.

Mev/amu. Eichler[2], and Anholt and Eichler[2], derive a formula using the eikonal approximation for the non-radiative capture of a target $1s$ electron into a projectile $1s$ state. They also propose a scaling rule with which one can estimate the average cross section for capture from any given n-shell of the target to any given n-shell of the projectile. Precisely, this estimate is for the capture cross section averaged over l in both the target and projectile. From their formula and scaling rule I estimate that for a 218 Mev/amu uranium beam passing through palladium that the cross section for non-radiative capture into the uranium $n=2$ shell is $\sim 3 \bullet 10^4$ barns. The scaling rule does not give any information about how the resulting population would be distributed among the sixteen $n=2$ states. If it is distributed statistically, so that the $1s\,2p_{1/2}{}^3P_0$ state acquires 1/16th of the population, then $\sim 0.7\%$ of a beam of U^{91+} should convert to U^{90+} in the $1s\,2p_{1/2}{}^3P_0$ state. That the agreement is so close between this crude estimate and the measured yield of 0.7% is accidental but even the rough match of the magnitudes confirms that our observed fluorescence is indeed due to the decay of the $1s\,2p_{1/2}{}^3P_0$ state.

Beam velocity (and time dilation).

Our $1s\,2p_{1/2}{}^3P_0$ -fed $1s\,2s\,{}^3S_1 \rightarrow 1s^2\,{}^1S_0$ signal peak has a roughly triangular shape given by the convolution of the angular acceptance of our collimating plates and the linear change with angle of the Doppler shift. The peak center I judge by eye (splitting the full width by a factor of 10) to lie at 77.758(.177) kev. Our value for the lab energy of the of the $1s\,2s\,{}^3S_1 \rightarrow 1s^2\,{}^1S_0$ radiation emitted at true right angles to the beam must include a $\pm$ 0.25 kev uncertainty from a possible misalignment of the collimating plates with respect to the normal to the beam. (The plates were aligned perpendicular to a line drawn between the centers of the upstream and downstream wire chambers to within $\pm$ 1 milliradian using a surveying transit and a pentagonal prism) Our value is 77.758(.306) kev. The theoretical value

---

[2]J. Eichler, Phys. Rev. A 32, 112 (1985).

[3]R. Anholt and J. Eichler, Phys. Rev. A 31, 3505 (1985).

for the rest energy of the $1s\,2s\,^3S_1 \rightarrow 1s^2\,^1S_0$ x ray is 96.01 kev[4], and the beam velocity determined from the transverse Doppler shift is $\beta = 0.5866(44)\ c$. This agrees with the value of $0.538(2)\ c$ of the beam velocity determined from the nominal accelerated charge state and the operating magnetic field of the Bevalac, corrected for the beam's energy loss of 1.6 Mev/amu, 4.5 Mev/amu, and 0.1 Mev/amu in our 25 mg/cm^2 tantalum, 35 mg/cm^2 aluminum and 0.9 mg/cm^2 palladium foils[5].

We choose to use the value of the beam velocity determined from the Doppler shift of the $1s\,2s\,^3S_1 \rightarrow 1s^2\,^1S_0$ line. There is no real difference, because the two values agree and the different errors are both lost in the total error for the $1s\,2p_{1/2}\,^3P_0$ lifetime, which is dominated by counting statistics. The difference is one of philosophy: determination by the Doppler shift is more direct, and the measurement is one for which we alone are responsible. I remark that velocities determined by the Bevalac magnetic rigidity, despite their apparent precision, can be wrong by a large jump if the staff operating the Bevalac happen to incorrectly note which uranium charge state they accelerate. I remark also that to determine the beam velocity by the Doppler shift we must assume something about the radiative shifts of the $1s_{1/2}$ level in order to calculate the $1s\,2s\,^3S_1 - 1s^2\,^1S_0$ splitting. The logic of our experiment is weakly circular: we take as given the radiative corrections for $n=1$ in order to measure the radiative corrections for $n=2$. However the $1s_{1/2}$ binding energy would have to shift $\pm$ 5.4 kev -- 15 times the ground state self-energy shift of 0.36 kev -- for our experimental value of 70.4(8.3) ev for the $2s_{1/2} - 2p_{1/2}$ splitting to be off systematically by as much as our quoted error.

Extraction of the $1/c$ decay length.

A typical histogram spectrum taken for our smallest detector-target separation (0.67 cm) is shown in Figure 1.2, and a spectrum for our largest separation (3.90 cm) is shown in

[4]See Table 1.3.

[5]The dE/dx in these materials for a $\sim$ 220 Mev/amu uranium beam is interpolated from J.F. Ziegler, *Handbook of Stopping Cross-Sections for Energetic Ions in All Elements,* (Volume 5 of *The Stopping and Ranges of Atoms in Matter),* Pergamon Press.

Figure 7.1. The problem is to fit and subtract the continuum background under the signal. The continuum background, except for identifiable x-ray fluorescence peaks, appears to be smooth and structureless from 59 kev to 105 kev. There is no reason *a priori* to suppose that the shape of the continuum is the same for both detector elements, nor for the shape to be independent of target position, and indeed the shape is found to vary; each histogram must be fit independently. All the properties of the background which I shall assume are contained in the following hypothesis:

Except for a small number of identified lines, the background in the energy range 59 to 105 kev is a smooth function which can be described adequately by a simple quadratic.

A typical spectrum showing such a fit, and showing the regions from 59 to 105 kev included in the fit and the curve fit to the background, is shown in Figure 6.2, for a detector-target separation of 2.04 cm. The reader may judge the plausibility of the hypothesis with his or her own eye. Further defense of this "structureless continuum" hypothesis I defer until Chapter 7. The rest of this chapter is devoted to the statistical and computational problem of how to make the fit.

The mean number of counts per histogram channel, μ, is small in our spectra. It makes a difference whether one correctly takes into account the Poisson distribution of the integer number N counts in a histogram channel with a small mean number μ, or incorrectly approximates the distribution as a gaussian with mean μ and standard deviation $\sigma \simeq \sqrt{\mu}$. Only for large μ is the latter approximation, and as a consequence the formulae for fitting by the method of least squares, possibly valid. Even so the integrated areas under curves fit by the method of least squares turn out to be low *systematically* by approximately one count per channel[6]; for the fits to my spectra the error accumulated in an integral over many channals

[6] See, for example, P. R. Bevington, *Data Reduction and Error Analysis for the Physical Sciences*, McGraw-Hill, 1969.

would be gross. The correct general technique for fitting is the Method of Maximum Likelihood[7], from which the method of least squares can be derived as a special case. The method of Maximum Likelihood in particular gives fits whose integrated areas are correct.

I wrote a computer program which would fit an Nth order polynomial to a continuum background with possible excised regions, using the method of Maximum Likelihood, and which would integrate under the fit curve between arbitrary limits. The method of Maximum Likelihood requires finding the absolute minimum of the so called negative-log-likelihood function, which is a function tailored to each particular problem. To perform the required search I used the single-precision version of the public domain program MINUITL[8], a program I found to be prone to infinite loops and inadequate convergence and which I would not choose again.[9] To guard my results against MINUITL's vagaries I treated each "best set" of polynomial coefficients found by MINUITL as merely a proposed best set. My own code checked that the set of coefficients corresponded at least to a point near a local, if possibly not the absolute, minimum in the negative-log-likelihood function, by using analytic formulas for the gradient vector and the matrix of second derivatives of the negative-log-likelihood function. My code also assessed the proximity of the proposed set to the true minimum and if necessary iterated a search until the convergence was adequate -- "adequate" meaning the error in each polynomial coefficient from lack of convergence of the program to the true minimum of the negative-log-likelihood function was less than 1/10th the error one would expect from a simple one-standard-deviation statistical fluctuation were a fit made to a different spectrum. My code also calculated the error matrix for the polynomial coefficients by formula, independent of the error matrix calculated by MINUITL. The two matrices agreed except when at irregular intervals the subroutine in MINUITL which calculated the

[7]See, for example, *Formulae and Methods in Experimental Data Evaluation, Volume 3,* R. K Bock, K. Bos, S. Brandt, J. Myrheim, and M. Regler, editors; published by the European Physical Society(Computational Physics Group), CERN Documentation Department, January, 1984.

[8]FORTRAN program MINUITL, amended version 20.6.1974, F. James and M. Roos, authors.

[9]To do justice to the program's authors, the origin of these troubles probably lies in some flaw in the way other people translated the code from its original machine to the VAX.

required second derivative fell into infinite loops. Once the coefficients of the polynomial and the error matrix were known I could calculate the integral of the background under the signal peak and the error in the integral.

A liability of the Maximum Likelihood method is that a particular negative-log-likelihood function can have spurious local minima as well as the desired absolute minimum, and any numerical minimization procedure may become trapped in a local minimum and give wrong results. I checked for this by using the Monte Carlo search routine of MINUITL to span the whole reasonable region of parameter space to look for local minima; none were found. This is not surprising. For the particular Maximum Likelihood problem of fitting a constant to a histogram spectrum one can prove analytically that the log-likelihood-function can have only one (global) minimum no matter how choppy a spectrum one chose to fit. To reduce the real, smoothly varying data it was necessary only to use a quadratic fit, which happens to have linear and quadratic coefficients which are small. While I was unable to show analytically that local minima were *impossible* for the fit of a quadratic, my work suggests that such minima would correspond to values of the polynomial coefficients very far from the true minimum. So far, in fact that the resulting incorrect fit to the background would be so peculiar and unreasonable that it could not escape my notice.

Once I had the sum of the counts in those channels which spanned the signal peak and the integral under the background I could subtract to get the number of counts in the peak, and fit the number with an exponential decay. Here again one runs into potential problem in choosing the correct fitting procedure. While for the integral of the background the distribution of the error is approximately gaussian[10], the sum of the counts in the channels comprising the peak is an integer selected from a Poisson distribution with some mean, and so has a more complicated distribution of the error. Fortunately *this* mean is large enough that *this* Poisson distribution *can* be well approximated by a gaussian, and one can fit an exponential

[10]This follows for a Maximum Likelihood fit if at the global minimum the third and higher derivatives of the negative-log-likelihood function are "small" compared to the second.

decay with distance Ae^{-Bz} by the simple method of nonlinear least squares (the method of least squares has has no hidden systematic errors applied to this problem as it does for determining the areas under curves). One cannot, however, justify the further approximations needed to determine the $1/e$ decay length by fitting a *straight line* to the *natural log* of the count rate, by the yet simpler method of linear least squares; we have too little signal.

A very human problem arises when one analyses complicated data with a computer. One naturally searches for bugs in the computer program, adjusts the form of the model functions one fits, and makes all sorts of plausible "corrections" only until one gets just the result originally expected -- then the experimenter stops. I was responsible for mastering the statistical theory and writing the programs which extracted from our histogram spectra the $1/e$ decay length. I wrote, debugged and ran data through these programs and adjusted the fit while deliberately remaining ignorant of just what experimental $1/e$ decay length would exactly match that predicted by theory. I debugged the programs exclusively with mock data simulated by random number generators; my co-worker and I agreed that if, after I pronounced the programs correct, I found a flaw while working with our real data that we would report that flaw, since any use of the data to correct the program diminished the reliability of our results. I adjusted the degree of the polynomial fit to the background and the regions to be excluded from the fit until I judged the fit reasonable; my co-worker and I also agreed to report any tailoring of the fit we made subsequently because we found the $1/e$ distance different from what we expected. We have nothing to report.

The decay of the $1s\,2p_{1/2}{}^3P_0$ state, and the Maximum Likelihood fit of an exponential to the data, is shown in Figure 1.3a. The error bars represent the $\pm$ one standard deviation statistical errors after the subtraction of the continuum background. The error bars shrink far out along the decay curve where the signal weakens because for these points we accumulated data for longer and longer periods, thus confirming the exponential character of the decay. The decay curve spans 2.7 decay lengths, and the reduced χ^2 for the nonlinear least-

squares fit of the exponential is 0.89. The $1/e$ decay length is 1.182(0.069)cm, and the 5.8% statistical error dominates our final error in the $1s\,2p_{1/2}{}^3P_0$ lifetime.

Our measurement of the $1s\,2p_{1/2}{}^3P_0$ decay length can be confused by repopulation of the $1s\,2p$ states from cascades from initial states of high principal quantum number n. As discussed at length in the chapter on cascades, the rate of the repopulation of the $1s\,2p_{1/2}{}^3P_0$ state and the rate of production of x-ray lines indistinguishable from our $1s\,2p_{1/2}{}^3P_0$ -fed $1s\,2s\,{}^3S_1 \rightarrow 1s^2\,{}^1S_0$ signal are both in proportion to the intensity of an isolated "cascade peak" which would appear in our spectra at 81.4 kev. The count rate in this supposed peak after the subtraction of the background is shown in Figure 1.3b. The horizontal line is a fit of a hypothetical constant count rate; the result is $\sim$ .75 standard deviations below, but consistent with, zero.

We do not know, of course, the true time dependence of the rate of cascade feeding in our beam. As I have derived in the chapter on the theory of cascades, for cascades in helium-like uranium the rate at which cascades feed transitions which produce an isolated 81.4 kev line, and the rate at which cascades feed transitions which produce a 77.8 kev line indistinguishable from our $1s\,2p_{1/2}{}^3P_0$ -fed $1s\,2s\,{}^3S_1 \rightarrow 1s^2\,{}^1S_0$ signal, and the rate at which cascades feed the $1s\,2p_{1/2}{}^3P_0$ state to make a $1s\,2s\,{}^3S_1 \rightarrow 1s^2\,{}^1S_0$ x ray we would subsequently detect, are always instantaneously in the ratios 1.000 : 0.714 : 0.247. The resulting shift of the measured $1s\,2p_{1/2}{}^3P_0$ decay length would be positive for a constant or slowly decreasing cascade rate and negative for a rapidly decreasing decay rate. The bounds set by the data, using the ratios derived in the chapter on cascades, are shifts of +3.2% and -1.4% respectively. These bounds are smaller than the simple 5.8% statistical error in the $1s\,2p_{1/2}{}^3P_0$ lifetime and we combine the uncertainties into a single error[11] of 2.3%, which we add in quadrature to the statistical error from the fit.

---

[11]As it happens, in calculating the lamb shift from the $1s\,2p_{1/2}{}^3P_0 \rightarrow 1s\,2s\,{}^3S_1$ E1 decay rate the asymmetry in the error due to cascades is mostly canceled by an asymmetry which comes from calculating the $1s\,2p_{1/2}{}^3P_0 - 1s\,2s\,{}^3S_1$ energy difference from the cube root of the decay rate.

Possible cascades in the hydrogenlike fraction of our beam feed the $2p_{3/2}$ and $2p_{1/2}$ states whose lines are unresolved from the corresponding lines in heliumlike uranium. From the theory developed in the chapter on cascades, the cascade-induced population of these two states must be equal. I find that if part of the cascades in our experiment came from hydrogenlike instead of heliumlike uranium that the net effect of cascades on the $1s\,2p_{1/2}\,^3P_0$ lifetime would decrease. We have found it difficult to produce the $1s\,2p_{1/2}\,^3P_0$ state of heliumlike uranium by direct excitation of a heliumlike uranium beam to high-n states (followed by cascades), and so we expect to produce only a negligible number of high-n states of hydrogenlike uranium by direct excitation of a hydrogenlike uranium beam.

We combine our extracted $1/e$ decay length and the beam velocity and time dilation determined from the Doppler shift of our $1s\,2s\,^3S_1 \rightarrow 1s^2\,^1S_0$ signal to obtain our experimental value for the $1s\,2p_{1/2}\,^3P_0$ lifetime of 54.4(3.4) ps The contributions to our total 6.3% error are: 1.2% from the determination of the beam velocity and time dilation using the transverse Doppler shift of the $1s\,2s\,^3S_1 \rightarrow 1s^2\,^1S_0$ transition; 2.3% from the experimental upper limit to contamination from cascade feeding; and 5.8% from simple statistical uncertainty. A discussion of other sources of error, all of negligible consequence, may be found in Chapter 8.

Figure 6.3 shows the decay curve taken using an earlier (and cruder) version of the experiment, with a beam energy of 175 Mev/amu and with a 2.28 mg/cm^2 Au target. The spectrum in the lower half of Figure 6.1 contributes to the point at 1.50 cm. The continuum background is high because the U^{91+} was provided only as an $\approx$ 30% charge state fraction of a beam exiting by a 1/32" Al target, and because this Al target was only $\sim$ 5 feet upstream of our detector and so showered the detector with nuclear fragments. We had no scintillators then to veto counts from fragments. The signal counts are few, the background is high, and because the cascade line is Doppler-shifted on top of the lead K_β peaks, there is no experimental limit to the presence of cascades. The quality of the data I feel does not justify any elaborate fitting. I subtracted the background simply by dividing the triangular signal peak

into four even bands and by subtracting the sum of the outer bands from the sum of the bands in the middle (the cost of the simplicity is that I sacrifice half the signal). The curve is a fit of a single exponential to the data; the 1/e decay length is 1.24(28) cm, and the reduced χ^2 for the fit is 1.3. The beam velocity determined from the Doppler shift of the signal is 0.540 c , and the resulting $1s\,2p_{1/2}{}^3P_0$ lifetime is 65(15) ps. Both the decay of the signal, and the lifetime extracted from the fit, are consistent with the exponential decay of the $1s\,2p_{1/2}{}^3P_0$ state lifetime of 54.4(3.4) ps, though the decay curve in Fig 6.3 is hardly convincing evidence that the measured decay is truly exponential. I chose not to include this data in our experimental value for the $1s\,2p_{1/2}{}^3P_0$ lifetime.

Chapter 7

Atomic and Nuclear X-Ray[1] Lines

The x-ray spectra recorded by our germanium x-ray detectors are complicated by lines of atomic and nuclear origin. A line which appears in that part of the continuum, 59 to 105 kev, which I have assumed to be smooth would have to be strong enough to be easily seen and therefore easily cut around if it is also to be strong enough to perturb my fit to the background. A line appearing under our $1s\,2p_{1/2}\,^3P_0$-fed $1s\,2s\,^3S_1 \rightarrow 1s^2\,^1S_0$ signal, however, cannot be seen, cannot be avoided and could easily distort our decay curve. The aim of this chapter is to show the origin of all the lines we see in our spectra, and to show that the mechanisms which produce these lines do not also produce a line hidden under our signal with enough intensity to matter.

Figure 7.1 shows one of the x-ray spectra taken with our largest detector-target separation. The separation is so great that little $1s\,2p_{1/2}\,^3P_0$ population remains, so we integrated for a full eight hours to see our signal; as a result this spectrum shows our background with the best statistics. The background is made of a continuum smoothly falling from 10 to 100 kev and a number of discrete fluorescence lines. Easiest to identify are the atomic K_α and K_β x-ray fluorescence patterns from the elements we use in the apparatus. A list of the atomic x-ray lines we see, and their energy and characteristic relative intensities, appears in Table 7.1. We see lines from lead and dysprosium, which we use for shielding; and tantalum, which we use to make our collimating plates. In spectra taken with a small detector-target separation (and so not in Figure 7.1) we also see lines from palladium, which we use for our target foil; a special systematic affect associated with these lines I discuss later in Chapter 8.

No other atomic line can appear in the range 59 to 105 kev, the range of energies included in our fit to the background, because the required elements make no part of our

[1]Photons emitted by transitions in nuclei are usually called γ rays instead of x rays. Since I care only about photons from nuclei which are in the range in the range 0-100 kev, the "x-ray region" of the spectrum, I will call the photons x rays instead of γ rays.

apparatus. The elements with K x rays which might possibly interfere are those with $Z \geq 67$. These are the rare earths Holmium, Erbium, Thulium, Ytterbium, and Lutetium; the elements Hafnium, Tantalum, Iridium, Platinum, Gold, Mercury, Thallium, Lead, Bismuth, and Polonium; and the natural radioactive isotopes. Besides those three elements deliberately incorporated in the apparatus only two of the others are accidentally present. Bismuth is present as a 0.03% contamination in the lead sheets and bricks we use to shield the detector. The Bismuth $K_{\alpha 1}$ line at 77.108 kev would merge with our signal line at 77.8 kev. The Bismuth $K_{\alpha 1}$ line must however be a factor $\sim 3 \bullet 10^{-4}$ weaker than our observed Lead $K_{\alpha 1}$ line and its contamination of our signal is negligible. Gold is present in the form of fine wires and thin electrical contacts inside the detector. The quantity is minute; however the Gold $K_{\beta 1}'$ line at 77.9 kev would also contaminate our signal. Any Gold $K_{\beta 1}'$ line at 77.9 kev merging with our signal must be 2.9 times weaker than a Gold $K_{\alpha 1}$ line at 68.804. This line we do not see, so I have an independent check that there is no contamination of our signal by Gold.

Table 7.1. Observed atomic x-ray fluorescence lines

Element	Line	Energy[kev]	Intensity Relative to $K_{\alpha 1}$
Palladium	$K_{\alpha 2}$	21.0201	52.9
Palladium	$K_{\alpha 1}$	21.1771	100
Palladium	$K_{\beta 1}'$	23.81	27.3
Palladium	$K_{\beta 2}'$	24.30	4.8
Dysprosium	$K_{\alpha 2}$	45.2078	56.0
Dysprosium	$K_{\alpha 1}$	45.9984	100
Dysprosium	$K_{\beta 1}'$	52.1	31.2
Dysprosium	$K_{\beta 2}'$	53.5	8.9
Tantalum	$K_{\alpha 2}$	56.277	56.0
Tantalum	$K_{\alpha 1}$	57.532	100
Tantalum	$K_{\beta 1}'$	66.2	33.7
Tantalum	$K_{\beta 2}'$	67.0	8.5
Lead	$K_{\alpha 2}$	72.804	59.3
Lead	$K_{\alpha 1}$	74.969	100
Lead	$K_{\beta 3}$	84.450	11.6
Lead	$K_{\beta 1}'$	84.936	22.2
Lead	$K_{\beta 2}'$	87.3	10.2

Also appearing in the spectrum shown in Figure 7.1 are three isolated lines at 13.3, 23.5, and 53.4 kev (The extra 53.4 kev line appears superimposed on the ordinarily weak 53.4 kev $K_{\beta 2}'$ line of dysprosium). These lines are due to the de-excitation of low-lying *nuclear* states of the germanium which makes up the detector element. The lines at 13.3 and 53.4 kev are from the de-excitation of levels in ^{73}Ge and the line at 23.5 from a level in ^{71}Ge. What is odd is that ^{71}Ge is not a naturally occurring isotope of germanium -- ^{71}Ge decays by electron capture to ^{71}Ga with a half-life of only 11.2 days.

The most likely origin of the ^{71}Ge is that it is formed by a p,pn or $n,2n$ collision involving ^{72}Ge and some of the protons and neutrons of $\sim$ 200 Mev kinetic energy which are liberated by the uranium nuclear collisions in the target. This origin is consistent with the observation that the germanium nuclear lines increase in intensity as the target is pulled upstream of the detector, because more of the cone of forward-directed fission fragments then pass through the detector elements. Though such a sleet of particles will create excited nuclei throughout the whole volume of any material in our apparatus, one would see lines 0 - 100 kev only from excited nuclei in the active volume of our detector elements. There are three reasons for this. First, many levels de-excite by the ejection of an atomic electron by internal conversion, instead of by emitting a photon. Any internal conversion in our detector automatically generates a count; any internal conversion elsewhere is automatically lost. Second, if a level outside our detector element emits a photon, that photon must be aimed to enter the germanium element to generate a count; for a level inside the detector element this is automatic. Finally the range of 0-100 kev photons in heavy materials, such as lead, dysprosium, and tantalum, is short, so only excited nuclei formed in a thin surface layer can generate counts; levels formed throughout the whole (active) volume of the detector element can generate counts. Our detector elements are made of ultrapure germanium. If the ^{71}Ge line is produced by fast nuclear fragments the list of lines which may appear in our detector is just the list of all the lines arising from any excited nucleus which a 200 Mev neutron or proton can produce by striking a germanium nucleus.

A second, more unlikely, possibility is that at least some of the ^{71}Ge is formed by the capture of a slow, thermalized neutron by ^{70}Ge. A gas of thermalized neutrons could be created in our experimental area, for example, by the moderation of fast neutrons liberated in our beam dump. The intensity of a nuclear line produced by an ambient neutron gas would be independent of the position of our target, however, so little of the intensity of the observed germanium nuclear lines can be be explained by the presence of such a gas. Unfortunately the presence of such a gas would make it possible to observe nuclear lines from dysprosium, alone of all elements found outside the active volume germanium of our detector (The dysprosium is present in an x-ray shield behind our detector elements). I postpone a discussion of what nuclear lines might be generated by such a gas until after I discuss the lines which might be produced by excited nuclei which are buried in the germanium of the elements.

Whether an excited level of a nucleus buried in our detector element can produce a line in our spectra depends on many things. Obviously the transition energy must lie between 0 and 100 kev, and the transition must represent a probable way for the excited level to decay. The germanium detector counts electron-hole pairs formed by the ionization along the track of any charged particle (usually an electron liberated from a germanium atom by photoionization or by Compton scattering). If a nuclear state decays by ejecting an atomic electron (by internal conversion), a count will always appear in the detector; if the upper state decays by emitting a photon the photon can escape and the count can be lost. The probability that a photon escapes depends on the details of our detector geometry but it can be roughly estimated as the probability that the photon could pass undisturbed through 0.3 cm of germanium, the full thickness of the active germanium in our elements.

Our detector sums into a single event any two events which occur within $\sim$ 250 ns of each other. Two nuclear decays occurring within 250 ns can thus produce a sum peak. Our detector also takes time to reset and so it vetos any second event which occurs between 250 ns and 10 microseconds after a first. Nuclear lines will be lost -- summed or vetoed -- if they

must occur within 10 microseconds of some other deposit of energy in the detector. For example, lines from the levels of a daughter nucleus produced by a nuclear β-decay of an unstable germanium isotope are typically lost, because the detector will trigger on the energy deposited by the β-electron, and because the lifetimes of the nuclear levels in the daughter are usually much less than 10 microseconds. Lines from levels in a nucleus produced by the collision of a fast charged particle (like a proton) with a germanium nucleus are typically lost because the detector will trigger on the ionization along the track of the incident particle. Lines from gallium isotopes produced by knocking a proton out of a germanium nucleus are typically lost because the detector will trigger on the ionization along the track of the ejected proton.

Finally any level which lives longer than $\sim$ 1 s will be formed when the beam is on but will mostly decay when the beam is off, when we do not collect data, so the intensity recorded in our spectra will be weak. Also, if an excited level is created by a nuclear fragment originating in the target, its contribution to our spectra will be partly vetoed by the signal from our scintillators unless the lifetime of the excited level exceeds the duration of the veto, which in our experiment was $\sim$ 500 ns.

With these many considerations in mind consider the lines which may occur from the isotopes of germanium ^{69}Ge through ^{76}Ge. I will mention all of the transitions possible in the range 0 to 100 kev, and some important lines which might appear from 100 to 200 kev. Except where noted the information on the nuclear structure is taken from the tables of Lederer *et al,* [2] and the needed internal conversion coefficients are interpolated from the tables of Rosel *et al.* [3] Photon ranges in matter are taken from the tables of McMaster *et al.* [4] All isotopes of germanium except ^{69}Ge, ^{71}Ge, ^{73}Ge and ^{75}Ge have no nuclear transitions in the range 0 to 100 kev.

---

[2]C. M. Lederer and V. S. Shirley, editors, *Table of Isotopes, Seventh Edition,* John Wiley and Sons, Inc. 1978.

[3]F. Rosel, H.M. Fries, K. Alder and H.C. Pauli, Atomic Data and Nuclear Data Tables 21, 91, 1978.

[4]W. H. McMaster, N. Kerr Del Grande, J. H. Mallett, and J. H. Hubbell, *Compilation of X-ray Cross Sections,* UCRL-50174 Sec. II, Rev. 1.

^{69}Ge -- natural abundance, 0; half-life 39.1 hours (Figure 7.2a).

This isotope does not occur naturally and must be formed by knocking a neutron out of ^{70}Ge (20.5% natural abundance). The $1/2^-$ state has a half-life of 5.1 microseconds. If the event which forms the nucleus deposits energy into the detector nonetheless $\sim$ 25% of the $1/2^-$ state will survive to decay after the detector has reset, so it is possible to see the 86.8 kev line. The $1/2^-$ state decays roughly half the time by emitting an electron (internal conversion coefficient $\sim$ 1.3), and an 86.8 kev photon will interact and will be absorbed, mostly by photoionization, 66% of the time in crossing .3 cm of germanium. Thus most of the decays of the $1/2^-$ state can generate an 86.8 kev line in our detector.

^{71}Ge -natural abundance, 0; half-life 11.2 days (Figure 7.2b).

Because ^{71}Ge does not occur naturally it must be formed either by neutron capture on ^{70}Ge (20.5% natural abundance) or by neutron knock-out from ^{72}Ge (27.4% natural abundance). If the event which forms the nucleus deposits energy into the detector nonetheless the long half-life of the $9/2^+$ state (22 ms) still guarantees that we will see its lines; however lines from the short-lived $5/2^+$ state (half-life 73 ns) will be lost. The $9/2^+$ state decays by internal conversion almost entirely (internal conversion coefficient $\sim$ 220), so the detector will always record the 23.5 kev transition energy. The transition feeds the $5/2^-$ state which decays with a half-life of only 73 ns. The resulting release of 174.9 kev will either be simply lost or it will sum or veto the 23.5 kev line; one can never see an isolated 174.9 kev line from feeding of the $5/2^-$ state by the 23.5 kev transition. Few decays of the $5/2^-$ state will however deposit any energy in our detector: only $\sim$ 10% of the decays of the $5/2^-$ state decay by emitting an electron, and a 174.9 kev photon could pass undisturbed through the .3 cm full thickness of our germanium element 75% of the time. Most of the 23.5 kev transitions, then, will not be summed or vetoed, so we can see a 23.5 kev line in the detector. After looking at the precise way our detector functions I estimate that about 23.5 kev one transition in 10 generates a sum peak at 198.4 kev.

^{73}Ge -- natural abundance 7.8% (Figure 7.2c).

Excited ^{73}Ge can be formed by neutron capture on ^{72}Ge (27.4% natural abundance), by direct excitation of ^{73}Ge (7.8% natural abundance), or by knocking a neutron out of ^{74}Ge (36.5% natural abundance). There are several possible lines from ^{73}Ge. One can record 13.26 kev from the $5/2^+ \rightarrow 9/2^+$ transition; 53.4 kev from the $1/2^- \rightarrow 5/2^+$ transition, and 68.75 kev from the $(7/2)^+ \rightarrow 9/2^+$ transition (The parenthesis around the spin (7/2) indicates that the nuclear spin of this level is somewhat uncertain). The 13.26, 53.4, and 68.75 kev transitions proceed mostly by internal conversion, so the probability of generating a count in the detector is high. The short half-life (1.6 ns) of the $(7/2)^+$ state guarantees that if the level is excited by some process which also deposits energy in the detector that the 68.75 kev line will be lost. The longer 2.95 μs half-life of the $5/2^+$ state guarantees that some initial population ($\sim$ 12%) would survive to make a detected 53.4 kev line. The 0.50 s half- life of the $1/2^-$ state guarantees that all the initial $1/2^-$ population would survive to make a 13.26 kev line.

The 53.4 kev transition from the $1/2^-$ state feeds the 13.26 kev transition from the $5/2^+$ state, so can in principle both sum lines or veto them entirely. The precise way our detector functions allows the decay of the $1/2^-$ state to make lines at 53.4 line, 13.26 kev , or at 66.73 kev from the sum of the two.

^{75}Ge -- natural abundance, 0; half-life 82.8 minutes (Figure 7.2d).

For the moment ignore in ^{75}Ge the weakly established $(1/2)^?$ level (The parentheses and question mark indicate a level of uncertain spin and unknown parity) at 61.9 kev above the ground state. The $7/2^+$ level has a half-life of 48 seconds. If the same event which excites the level also deposits energy in the detector the level nonetheless survives to make a 139.68 kev line in the detector. The level decays mostly by emitting an electron (internal conversion coefficient $\sim$ 2.2), so the decay of the $7/2^+$ level has a high probability of producing a 139.68 kev line in the detector.

What if the $(1/2)^g$ level does exist? It is now possible to have $7/2^+ \rightarrow (1/2)^g$ and $(1/2)^g \rightarrow 1/2^-$ transitions at 77.8 and 61.9 kev. The former, by malicious accident, is superimposed exactly on our $1s\,2p_{1/2}\,^3P_0$-fed $1s\,2s\,^3S_1 \rightarrow 1s^2\,^1S_0$ signal. This 77.8 kev line constitutes a grave danger, particularly since I know that the observed intensities of the germanium nuclear lines vary strongly with the separation of the detector and the target.

The most complete study of the decays of the $7/2^+$ state of ^{75}Ge, on which the tables of Lederer rely, is the work of Bhattacharyya *et al* [5]. They see a weak 77.8 kev line and a weak 61.9 kev line whose intensities both decay with the 48 second half-life characteristic of the $7/2^+$ state, which is the strongest evidence yet put forward for the existence of a 61.9 kev level in ^{75}Ge between the $7/2^+$ level and ground. They find the ratio of the probability that the $7/2^+$ state emits a 77.8 kev photon, to the probability that it emits a 139.7 kev photon, to be tiny: $8.0 \bullet 10^{-5}$. My detector can register a count from either an emitted photon or an ejected atomic electron. If I assume their provisional assignment of spin 1/2 to the 61.9 level is correct, the ratio of the number of counts in a line at 139.7 kev to the number of counts at 77.8 kev must be $\sim 1.4 \bullet 10^3$. If the spin proved to be 3/2 instead, the ratio would *increase* to $\sim 1.2 \bullet 10^4$. These ratios do not yet take into account that any 77.8 kev transition must feed a following 61.9 kev transition to ground which may sum with or veto any 77.8 kev line. Whether the spin is 1/2 or 3/2, the 61.9 kev transition to the ground $1/2^-$ state would be a dipole transition -- electric or magnetic depending on the unknown parity of the 61.9 kev level. The single-photon decay rate can be estimated from the Weisskopf estimates for the single-photon transition rates in nuclei[6]:

$$A_{E1}^{nuc} \sim 1.0 \bullet 10^{14}\, A^{2/3}\, E_\gamma^3 \quad [s^{-1}] \qquad 7.1$$

$$A_{M1}^{nuc} \sim 3.1 \bullet 10^{13}\, E_\gamma^3 \quad [s^{-1}] \qquad 7.2$$

---

[5] P. Bhattacharyya, R. K Chattopadhyay, B. Sethi, V. K. Tikku and S. K. Mukherjee, Il Nuovo Cimento 31A, 519 (1976).

[6] C. M. Lederer and V. S. Shirley, editors, *Table of Isotopes, Seventh Edition*, John Wiley and Sons, Inc. 1978, Appendix 24.

Here E_γ is the transition energy in Mev and A is the atomic number. Internal conversion is improbable for either dipole transition, and the Weisskopf estimate for the radiative transition rate of the 61.9 kev level gives a lifetime of $\sim$ 2.4 ps or 0.14 ns if the transition is E1 or an M1, respectively. Of course, most E1 transition rates well below the giant resonance in nuclei are retarded at least four orders of magnitude below the rates given by the Weisskopf estimate, so the E1 rate is more likely $>\sim$ 24 ns. Still, nothing can prevent the 60.9 kev transition from occurring within the $\sim$ 10 microseconds that it must in order to sum or veto the 77.8 kev line. A 61.9 kev E1 or M1 transition will occur by photoionization only $\sim$ 25% of the time; however a 61.9 kev photon will photoabsorb or Compton scatter in .3 cm of germanium 94% of the time, so few 61.9 kev transitions would fail to trigger the detector and to destroy the 77.8 kev line. I estimate that any potential 77.8 kev line will be reduced further in intensity by another factor of 20. The net result, despite the uncertain spin and parity of the 61.9 kev level, is that any 77.8 kev line in our spectra must be accompanied by a 139.7 kev line at least $\sim 2.8 \bullet 10^4$ times brighter. No 139.7 kev line is even visible in those spectra we recorded in the energy range 0 to 200 kev, so there can be no contamination of our signal from this 77.8 kev nuclear line.

To conclude the analysis of this isotope, I note that because the $(1/2)^g$ level is short-lived, if it were populated directly by some event which also deposited energy in the detector any 61.9 kev line would be lost.

Besides lines from the germanium isotopes themselves there are two other possible sources of lines from nuclei buried in the detector elements. Fortunately both possibilities can be eliminated swiftly. No line from any isotope of gallium (which might be formed by knocking a proton and zero or more neutrons from a germanium nucleus) can produce a line 0-100 kev in our detector, nor can such a line be produced from any nucleus produced in the chain of radioactive decay from any unstable gallium or germanium isotope. The possible nuclear transitions are all either at the wrong energy or are from states too short-lived to survive the

$\sim$ 10 μs for the detector to reset after the event which creates the nucleus. Our detector would trigger on the ionization from the track of the ejected proton from a created gallium nucleus, or on the electron emitted in nuclear β-decay. The few nuclei which decay by internal conversion, a process which does not trigger the detector, lack suitable levels.

The possible lines originating from excited nuclei embedded in the germanium elements are listed in Table 7.2. Those I have actually seen are noted. The cross sections for producing excited germanium nuclei by the impact of 200 Mev/amu neutrons and protons are not known, so I have not been able to find out if the pattern of observed lines is in fact consistent with production this mechanism. To summarize, with the exception of the 77.8 kev line in ^{75}Ge, all these lines not only miss our signal but also lie outside the parts of the spectrum assumed structureless in making the fit to the background[7]. The 77.8 kev in ^{75}Ge line lies directly under our signal; however its intensity is known to be $\sim 10^4$ times weaker than an accompanying 139.7 kev line which does not appear in our spectra. Therefore no nuclear line from nuclei buried in our detector elements can confuse either our signal or our fit to the

Table 7.2. List of all possible lines of nuclear origin
0 to 100 kev from Germanium isotopes
(and some of the lines possible from 100 to 200 kev)

Isotope	Abundance	Initial J^π	X-ray energy	$T\frac{1}{2}$	Production	Line Seen?
^{69}Ge	0.	$1/2^-$	86.8	5.1 μ s	n^-	no
^{69}Ge	0.	$3/2^-$	146.2	176 ps	n^-	no
^{71}Ge	0.	$9/2^+$	23.5	22 ms	n^+,n^-	yes
^{73}Ge	7.8%	$5/2^+$	13.26	2.95 μ s	$*,n^+$	yes
^{73}Ge	7.8%	$1/2^-$	53.47	0.50 s	$*,n^+$	yes
^{73}Ge	7.8%	-	66.73	-	(pileup)	no
^{75}Ge	0.	(1/2)	61.9	??	n^-,n^+	no
^{75}Ge	0.	$7/2^+$	77.8	48 s	n^-,n^+	no
^{75}Ge	0.	$7/2^+$	139.68	48 s	n^-,n^+	no
^{77}Ge	0.	$1/2^-$	159.7	53 s	n^+	no
^{77}Ge	0.	$1/2^-$	53 s	159.7	n^+	no

Legend for the possible ways to make the excited state	
$*$	Direct excitation
n^-	Neutron knockout
n^+	Neutron capture

[7]These regions are displayed in Figure 6.2.

background.

Finally consider the nuclear lines arising from the possible presence of a gas of slow neutrons. The capture cross section for neutrons in natural germanium is 2.2 barns; the capture cross section in natural dysprosium is extraordinarily large – 940 barns. Our .3 cm thick germanium elements are backed by a 2.5 mm dysprosium plate. A neutron moving at thermal velocities will be captured in our element only $\sim$ 10% of the time, to make (perhaps) a germanium nuclear line. It will pass through our detector elements 90% of the time to be captured within $\sim$ 0.034 cm of the surface of the dysprosium plate facing the element. The nucleus which captures the neutron relaxes by emitting mostly γ-rays of $\sim$ 1-6 Mev energy but also by emitting some x rays with energies $<\sim$ 100 kev. Enough such x rays can survive passage through merely 0.034 cm of dysprosium to enter the back of the germanium element (only a millimeter or so away) to make in our spectra the intensity of the dysprosium capture lines comparable to the intensity of the germanium capture lines. The dysprosium isotopes unfortunately have *scores* of nuclear transitions in the range 0-100 kev, instead of the few possessed by other elements. Only thermal neutron capture can one make the number the number of nuclear excitations in the outermost $\sim$ .03 cm layer of the dysprosium 10 times *greater* than the number of excitations in the .3 cm thickness of the germanium element. The number would be 10 times *smaller* if the dysprosium and the germanium were were excited by fission fragments, assuming the excitation cross sections for dysprosium and germanium to be roughly the same.

The cross sections for thermal neutron capture for the naturally occurring dysprosium isotopes are known[8]. Over 99.85% of the thermal neutron capture in natural dysprosium occurs in the isotopes ^{161}Dy, ^{162}Dy, ^{163}Dy, and ^{164}Dy for which the x-ray yields are known[9].

[8]S.F. Mughabghab, M. Divadeenan, and N.E. Holden, *Neutron Resonance Parameters and Thermal Neutron Cross Sections, Fourth Edition*, Academic Press, New York, 1981.

[9]L.V. Groshev, A. M. Demidov, V. I. Pelekhov, L.L. Sokolovskii, G. A. Bartholomew, A. Doveika, K. M. Eastwood, and S. Monaro, Nuclear Data Tables A3, 367(67); A5, 1(1968); A5, 243(1969).

For these four isotopes the energies of the nuclear x rays which are in the range 0-100 kev, and which are emitted more often than once in every 1000 neutron captures in natural dysprosium, are listed in Table 7.3. Also listed for each nuclear x ray is the corresponding $1/e$ attenuation length for the x ray in dysprosium[10]. The most troublesome potential line is the line at 77.5 kev which underlies our $1s\,2p_{1/2}\,^3P_0$-fed $1s\,2s\,^3S_1 \rightarrow 1s^2\,^1S_0$ signal. A line at 50.4 kev is however emitted $\sim$ 9 times more often, and moreover this photon has a greater range in dysprosium (because the energy is just below the dysprosium K-edge at 53.8 kev). Therefore for *any* possible geometry this 50.4 kev line must be at least 9 times brighter than the 77.5 kev line. This line at 50.4 kev cannot be seen in any of our spectra, and so there can be no contamination of our signal by the 77.5 kev line.

Table 7.3.
Nuclear x rays 0-110 kev from neutron capture in natural dysprosium which occur more than once in every thousand captures, and their $1/e$ attenuation length in dysprosium.

Energy [kev]	Excited nucleus	Photons per 1000 captures	$1/e$ length, [cm]
50.431	^{165}Dy	25.	$2.8 \bullet 10^{-2}$
72.766	^{165}Dy	3.7	$1.4 \bullet 10^{-2}$
73.392	^{164}Dy	9.3	$1.5 \bullet 10^{-2}$
73.440	^{163}Dy	1.0	$1.5 \bullet 10^{-2}$
77.521	^{165}Dy	2.9	$1.8 \bullet 10^{-2}$
80.660	^{162}Dy	15.	$2.0 \bullet 10^{-2}$
83.397	^{165}Dy	4.0	$2.2 \bullet 10^{-2}$
94.700	^{165}Dy	32.	$3.2 \bullet 10^{-2}$
108.160	^{165}Dy	20.	$2.0 \bullet 10^{-1}$

[10]W. H. McMaster, N. Kerr Del Grande, J. H. Mallett, and J. H. Hubbell, *Compilation of X-ray Cross Sections*, UCRL-50174 Sec. II, Rev. 1.

Chapter 8

Miscellaneous Systematic Effects

This chapter discusses and sets limits to the change in our measured $1s\,2p_{1/2}{}^3P_0$ lifetime from a number of small systematic effects. Besides the ± 2.3% error from the experimental upper limit to cascade feeding of the n =2 states the largest systematic error is an error of ± 0.4% which arises from slow horizontal drifts of the beam. Both are much less than the simple 5.8% statistical error in the $1s\,2p_{1/2}{}^3P_0$ lifetime.

The data which make up our final decay curve were acquired over 63 continuous hours. During this time no changes whatever were made in the apparatus except to scan the target position. We took two complete decay curves, each taken by counting at every other point on the decay curve as the detector-target separation was increased and filling in the gaps as the detector-target separation was decreased. This procedure makes the effect on our decay curve of any long-term electronic or geometrical drifts an increase of the scatter of the points instead of a distortion of the apparent decay length. I estimate, crudely, that any random error in each of the separate points on the decay curve of X% creates an error in the $1s\,2p_{1/2}{}^3P_0$ lifetime of roughly X%/2.

Error due to the apparatus deadtime.

The *device-busy* signals from the various components of the apparatus were fed into a logical OR whose output was used to gate off the integration of the beam current when the electronics was known to be incapable of accepting signal. I used corrected integrated current to construct the decay curve (Fig. 1.3). The fraction of the time the apparatus was dead (the "deadtime") never exceeded 1%; and the system we used to monitor the deadtime provided a correction good to $\sim$ 10%. This 10% error in the deadtime correction arises because there is an inevitable and often variable lag in time between the moment any device is actually triggered and the moment when it generates a busy signal. Each point on our decay curve may then require a further correction due to deadtime amounting to 0.1%. Since any *constant*

deadtime has no affect whatever on the measured lifetime only the *variations* as a function of target position of the remaining $\sim$ 0.1% correction have any effect. These *variations* are averaged over when the decay curve is fit; the net error in the $1s\,2p_{1/2}{}^3P_0$ lifetime due to uncorrected apparatus dead time is roughly 0.05%.

Fluctuations in the beam position.

Once an hour over the 63 hours we used to collect our decay curve the operators of the Bevalac recorded the image made by a single beam pulse in the wire chamber downstream of our apparatus. The separate records show that the center of the beam spot never wandered more than $\pm$ 2 mm from its mean position. The average position of the spot corresponding to any of the separate points on the decay curve (Fig. 1.3) never deviated by more than 1 mm from the mean position.

Our apparatus is almost symmetric about a horizontal (though not a vertical) plane through the center of the target (see Fig. 5.4), so there is only a small linear change in the collection efficiency for a vertical shift of the beam. For each point on the decay curve a $\pm$ 1 mm vertical shift would make only a $\pm \sim$ 0.2% change in the measured intensity of $1s\,2p_{1/2}{}^3P_0$ -fed $1s\,2s\,{}^3S_1 \rightarrow 1s^2\,{}^1S_0$ x rays. The effect of such a small shift per point on the apparent $1s\,2p_{1/2}{}^3P_0$ lifetime will be smaller because the shifts in the individual points are averaged; the net effect will be $\sim$ 0.1%. There is a larger linear change in the collection efficiency for a horizontal shift of the beam and a $\pm$ 1 mm horizontal shift would make to each point on the decay curve a $\pm \sim$ 1.7% change in the measured intensity. These shifts are calculated from the geometry of the collimating plates which select the x rays which enter the germanium detector. The wire chamber records show, however, that these large shifts in intensity because of the horizontal motion of the beam are distributed across the decay curve in a way which makes the resulting error in the $1s\,2p_{1/2}{}^3P_0$ lifetime only $\sim \pm$ 0.4%.

The effect of beam passing through the rim of the target.

Roughly once every 5 hours during our 63 hours of data collection we took a polaroid photograph of the beam by letting a single beam pulse pass through the apparatus into a standard package of polaroid film. The photographs showed the beam profile in far finer detail than could the readout from the downstream wire chamber because a spot appears on the film from the passage of each uranium ion. The photographs also showed the position of the beam with respect to the target since the holder that grasped the rim of the target cast a shadow. From these photographs I estimate that roughly 0.5% of the total beam passed through the circular aluminum rim supporting the Pd foil, and then through the foil glued to the rim, instead of passing through the Pd foil only. The lower half of this rim was 3/32" thick; the upper half had been milled to a thickness of 1/32" to reduce the backgrounds from the beam hitting the aluminum.

The first systematic effect is that a 218 Mev/amu uranium beam will lose $\sim$ 86 and $\sim$ 26 Mev/amu in passing through 3/32" and 1/32" of aluminum, respectively[1]. Any $1s\,2p_{1/2}{}^3P_0$ states in the beam which passes through the lower and upper half of the rim (and then the palladium foil) decay with a $1/e$ decay length respectively 24% and 7% shorter than the decay length for states in the beam which passes through the foil only. The lab energy of any $1s\,2p_{1/2}{}^3P_0$ -fed $1s\,2s\,{}^3S_1 \rightarrow 1s^2\,{}^1S_0$ x ray from the beam degraded by the lower half of the rim is increased by 6.3 kev, which is enough to move even the low energy edge of the Doppler-broadened peak out of our 77.8 $\pm$ 1.5 kev signal band. States made by beam hitting the lower half of the rim cannot contribute to our decay curve (Fig 1.3). The corresponding increase in the lab energy for the beam degraded by the thinner upper half of the rim is only 1.9 kev and some of these states can contribute. A $\sim$ 218 Mev/amu beam of 100% U^{90+} which passes through more than roughly 1/32" of aluminum will capture and lose electrons to produce an equilibrium distribution of charge states of roughly 1% U^{88+}, 13%

[1]The dE/dx in aluminum for a $\sim$ 220 Mev/amu uranium beam is interpolated from J.F. Ziegler, *Handbook of Stopping Cross-Sections for Energetic Ions in All Elements*, (Volume 5 of *The Stopping and Ranges of Atoms in Matter*), Pergamon Press.

U^{89+}, 51% U^{90+}, 29% U^{91+}, and 6% U^{92+} [2]. Our searches for signal with aluminum targets show that little U^{90+} in the $1s\,2p_{1/2}{}^3P_0$ state is formed by the passage of a U^{91+} beam through aluminum. Only the the $\sim$ 30% of the beam which is still U^{91+} when it exits the aluminum rim can produce the U^{90+} $1s\,2p_{1/2}{}^3P_0$ state, by capturing an electron from the attached Pd foil. Thus the 0.25% of the beam which passes through the upper rim of the target generates only 0.08% of the $1s\,2p_{1/2}{}^3P_0$ states. The change in the average the decay length due to a 0.15% contamination of states, with a decay length only 7.0% smaller than the average, is less than 0.01%.

The second systematic effect is that a U^{91+} ion which passes through the rim of the target and then the Pd foil produces roughly the same charge in our ionization chamber as the U^{91+} which goes through the foil only, though the probability the ion produces a U^{90+} $1s\,2p_{1/2}{}^3P_0$ state with a lab $1s\,2s\,{}^3S_1 \rightarrow 1s^2\,{}^1S_0$ energy within our signal band is very small ($<$0.1). As the beam drifts and the fraction of the beam which goes through the rim changes, so does the ratio change of the total number of produced $1s\,2p_{1/2}{}^3P_0$ states to the total integrated charge. Only a ***variation*** in this fraction can affect the measured $1s\,2p_{1/2}{}^3P_0$ decay length. The variations in this fraction over the time we collect our data are not well known, because the fraction can be estimated only from the extra detail shown in the polaroid photographs taken every $\sim$ 5 hours and not from the wire chamber records taken every hour. For each point on the decay curve I estimate that the fraction of the beam which goes through the rim of the target may vary by $\pm \sim$ 0.5% from the $\sim$ 0.5% that is the fraction averaged over all the points. For each point the corresponding change in the ratio of the total number of $1s\,2p_{1/2}{}^3P_0$ states produced to the total integrated charge is also $\pm \sim$ 0.5% The errors in the individual points are averaged in the fit, and the effect on the measured $1s\,2p_{1/2}{}^3P_0$ lifetime is $\sim$ 0.25%.

Scatter of n =2→1 x rays in the tantalum collimating plates.

---

[2] H. Gould, private communication.

In the spectra corresponding to the first points in the decay curve in Figure 1.3, those with the smallest detector-target separations, there appear both an x-ray line at 21.2 kev and a powerful fluorescence of the tantalum K_α and K_β x rays (see Fig. 1.2). For these small separations the tantalum collimating plates on the face of the detector are partly or wholly exposed to x rays coming directly from the target. For larger separations these x rays are blocked by the crescent shaped lead shield inside the beam pipe (to understand the geometry see Figure 5.4). The 21.2 kev line is due to target foil Pd $K_{\alpha 1}$ radiation which elastically scatters[3] in the surface of the tantalum collimating plates and then enters the detector. There are no gaps in the collimating assembly which would allow the radiation to enter the detector directly. Since the target is also a source of radiation from $n=2\rightarrow 1$ transitions in heliumlike and hydrogenlike uranium, it is possible that the part of the $n=2\rightarrow 1$ radiation which Doppler shifts to $\sim$ 77.8 kev may also scatter elastically in the tantalum and add counts to our $1s\,2p_{1/2}\,^3P_0$ -fed $1s\,2s\,^3S_1\rightarrow 1s^2\,^1S_0$ peak at 77.8 kev. There is no chance that 77.8 kev radiation could simply burn through the tantalum collimating plates. Any such radiation would have to pass through at least 0.095" of tantalum, and in this thickness a beam of 77.8 kev x rays would be attenuated -- photoabsorbed or scattered -- by a factor of $\sim 10^{13}$.

Examine the contribution for the point with the smallest detector-target separation, 0.625 cm. An x ray interacting with a material may either scatter elastically, Compton scatter with a change in energy, or be photoabsorbed. At this target position the radiation from the target can strike the tantalum collimating plates at an angle differing from grazing incidence by at most 13 degrees. The probability that a 21.2 or a 77.8 kev x ray incident at an angle of less than 13 degrees, will interact in a 6 mil tantalum plate is essentially 1. (The probability the more penetrating 77.8 kev x ray will pass through the plate at an angle of 13 degrees is $\sim 3 \bullet 10^{-4}$.) In tantalum the ratios of the elastic scattering cross section to the total cross section for 21.2 kev radiation and for 77.8 kev radiation are nearly identical:

[3]This scattering is often called Rayleigh or coherent scattering. Physically it represents a redistribution of the incident radiation by a classical oscillation of the electron cloud around an atom.

$3.5 \bullet 10^{-2}$ and $3.3 \bullet 10^{-2}$, respectively[4]. Because the amount of radiation scattered back from an illuminated surface depends only on this ratio, and not on the $1/e$ absorption length for the radiation in the material, a 21.2 kev x ray and a more penetrating 77.8 kev x ray will scatter in the same way through the set of collimating plates. The ratio of the number of counts in a 21.2 kev peak from scattered radiation, to the number of counts in a 77.8 kev peak, is just the ratio of the numbers of the photons of each energy which strike the tantalum collimating plates.

In our spectra taken looking at the Pd target the ratio of the yield of the 21.2 kev Pd $K_{\alpha 1}$ line, to the 77.8 kev line from $2s_{1/2}$, $2p_{1/2} \rightarrow 1s_{1/2}$ transitions in both heliumlike and hydrogenlike uranium, is approximatedly 16.5 : 1. For the spectra taken at a detector-target separation of 0.625 cm the change in the Doppler shift with angle spreads the $2s_{1/2}$, $2p_{1/2} \rightarrow 1s_{1/2}$ line in energy from 78 to 94 kev across the face of the stack of tantalum collimating plates. Only 7.5% of the radiation falls in our 77.8 ± 1.5 kev signal band, while all the scattered Pd $K_{\alpha 1}$ radiation from the target contributes to a single peak at 22.1 kev. The number of counts in the observed Pd peak is about 1.5 times the number of counts $1s\,2p_{1/2}{}^3P_0$ -fed $1s\,2s\,{}^3S_1 \rightarrow 1s^2\,{}^1S_0$ counts in the signal peak. Therefore only $\sim 0.7\%$ of the excess of counts over background in the signal peak may be due to scattered $n = 2 \rightarrow 1$ radiation from the target. The statistical error in the excess is 13 times larger, so I neglect the tiny contribution from scattered $n = 2 \rightarrow 1$ radiation from the target. For points on the decay curve with a larger detector-target separation than 0.625 cm the $n = 2 \rightarrow 1$ radiation from the target which strikes the tantalum collimating plates is Doppler shifted entirely above the signal and cannot contribute.

Zeeman beats.

---

[4]These numbers can be derived from the tables of x-ray cross sections found in W.H. McMaster, N. Kerr Del Grande, J.H. Mallet, and J.H. Hubbell, *Compilation of X-ray Cross Sections*, UCRL-50174 Sec II, Rev. 1. The near equality of this ratio for 21.2 and 77.8 kev in tantalum is an accidental consequence of the fact that the tantalum K-edge lies between the two energies.

In beam-foil time-of-flight spectroscopy any alignment or polarization of an excited state produced by the target will precess in an applied magnetic field. Because of this precession a detector records damped oscillations (Zeeman beats) in the photon intensity as a function of target position, instead of a simple exponential decay. We study decay of $1s\,2p_{\,1/2}\,^3P_0$ state and an alignment or polarization of a spin-0 state is impossible.

Chapter 9

Results and Conclusions

From our measured $1s\,2p_{1/2}{}^3P_0$ lifetime of 54.4 (3.4)ps and Drake's calculated E1M1 decay rate (Eq. 3.17) of $0.564(5)\bullet 10^{10}\ s^{-1}$, I obtain from Eq. 3.19 a value for k, the $1s\,2p_{1/2}{}^3P_0$ - $1s\,2s\,{}^3S_1$ splitting, of 260.0 (7.9) ev. Subtracting the calculated Coulomb contribution 330.4 ev yields an experimental Lamb shift of 70.4 (7.9) ev.

So far I have propagated only experimental uncertainty; theoretical uncertainty enters from the effect of small terms omitted from the calculations. I estimate a $Z^{-1}\,(Z\,\alpha)^2$ correction to the $1s\,2p_{1/2}{}^3P_0$ - $1s\,2s\,{}^3S_1$ E1 matrix element, and a 1/Z correction to the E1M1 decay rate, contribute a total of $\simeq$ 1 ev to our inferred $1s\,2p_{1/2}{}^3P_0$ - $1s\,2s\,{}^3S_1$ splitting; a term of $Z^{-2}\,(Z\,\alpha)^5$ or $Z^{-2}\,(Z\,\alpha)^6$ contributes $\simeq$ 2 ev to the 330.4 ev Coulomb splitting of the $1s\,2p_{1/2}{}^3P_0$ - $1s\,2s\,{}^3S_1$ states; and a 1/Z screening correction to the self energy, vacuum polarization and finite nuclear size contributes $\simeq$ 1 ev to the Lamb shift. These combine to give a separate theoretical error of of 2.4 ev in our value of the Lamb shift extracted from the $1s\,2p_{1/2}{}^3P_0$ lifetime. This theoretical error I add in quadrature to the experimental error of 7.9 ev to get an ultimate value for the Lamb shift of 70.4(8.3) ev.

For all Z, 1 to 92, the largest part of the Lamb shift is the contribution from the electron self-energy. The results of all other measurements of the Lamb shift in few-electron ions can be explained by an expansion of the exact Feynman diagram (Fig. 2.1b) for the self-energy Σ state as a series in powers of $(Z\,\alpha)$:

$$\Sigma = n^{-3}\,\frac{\alpha}{\pi}\,mc^2\left\{\left[A_{40} + A_{41}\ln(Z\,\alpha)^{-2}\right](Z\,\alpha)^4 + A_{50}(Z\,\alpha)^5 + \left[A_{60} + A_{61}(Z\,\alpha)^{-2} + A_{62}\ln^2(Z\,\alpha)^{-2}\right](Z\,\alpha)^6 + A_{70}(Z\,\alpha)^7 + \textit{higher order terms}\right\} \qquad 9.1$$

Here n is the principal quantum number of the bound state and the values of the coefficients[1] A_{40}—A_{70} depend on n, l, and j. The sum of the series Eq. 9.1 can be subtracted from the result of an exact numerical calculation of the self-energy by Mohr[2] to get the sum of the higher order terms.

The ratio of the sum of the higher order terms to the total self-energy for the $2s_{1/2}$ state is plotted in Fig. 9.1. These terms are invisible in experiments at low Z, but contribute almost the entire $2s_{1/2}$ self-energy for Z=92. Since the $2s_{1/2}$ self-energy of + 66.4 ev (Table 2.1) accounts for most of the $2s_{1/2} - 2p_{1/2}$ splitting at Z=92, agreement within ± 12% for the experimental and theoretical uranium Lamb shifts provides an important test of the correctness of QED for electrons bound in the strongest steady electric fields found in nature. In hydrogen (Z=1) the higher order terms contribute less than 0.1 ppm of the Lamb shift, compared to an experimental uncertainty of ~ 8 ppm[3] and an theoretical uncertainty due to the unknown structure of the proton of ~ 10 ppm[4]. In argon (Z=18) the higher order terms contribute a larger fraction, ~ 1%, of the Lamb shift. Present experiments[5] near Z=18 have, however, precisions which allow the contribution of the higher order terms to be at best barely observed but not measured.

When a 12% measurement of the Lamb shift is made obsolete, our measurement of the $1s\,2p_{1/2}{}^3P_0$ lifetime can be reinterpreted to check the either the calculated $1s\,2p_{1/2}{}^3P_0 - 1s\,2s\,{}^3S_1$ splitting or the calculated two-photon decay rate of the $1s\,2p_{1/2}{}^3P_0$ state. To check one one must confirm or grant the correctness of the other. Figure 9.2 shows a comparison

---

[1]Values for the $2s_{1/2}$ state are summarized and references to original work given in P.J. Mohr, Ann. Phys. (N.Y.)88,26 (1974); J. Sapirstein, Phys. Rev. Lett. 47, 1723 (1981). Analytic expressions for the values of the low-order coefficients for states of arbitrary n, l, and j are listed, with references to original work, in a review by G.W.F. Drake, *Quantum Electrodynamics Effects in Few-Electron Atomic Systems*, in *Advances in Atomic and Molecular Physics 18*, Academic Press, 1982.

[2]P.J. Mohr, Phys. Rev. A26, 2338 (1982).

[3]S.R. Lundeen and F.M. Pipkin, Phys. Rev. Lett. 46, 232 (1981).

[4]See, for example, S.R. Lundeen and F.M. Pipkin, Phys. Rev. Lett. 46, 232 (1981).

[5]See for example H. Gould and R. Marrus, Phys. Rev. A28, 2001 (1983); O.R. Wood II, C.K.N. Patel, D.E. Murnick, E.T. Nelson, M. Leventhal, H.W. Kugel, and Y. Niv, Phys. Rev. Lett. 48, 398 (1982); H.D. Strater, L. von Gerdtell, A.P. Georgiadis, D. Muller, P. von Brentano, J.C. Sens, and A. Pape, Phys. Rev. A29, 1596 (1984); P. Pellegrin, Y. El Masri, L. Palffy, and R. Priells, Phys. Rev. Lett. 49, 1762 (1982).

between theory and experiment made by Galvez[6] for the $1s\,2p_{1/2}{}^3P_0 - 1s\,2s\,{}^3S_1$ interval for lower Z. The value of 260.0(7.9) ev for Z=92 is derived from the measured $1s\,2p_{1/2}{}^3P_0$ lifetime and Eq. 3.23, assuming a value of $0.564(5)\bullet 10^{10}\ s^{-2}$ for the two-photon decay rate as calculated by Drake[7]. (The theoretical uncertainty in the energy due to missing terms $\sim Z^{-1}(Z\alpha)^2$ in the $1s\,2p_{1/2}{}^3P_0 - 3s\,1$ dipole matrix element amounts to only $\sim$ 1 ev and negligible). The agreement here adds really no new information; the terms of high order in $(Z\alpha)$ in the expansion analogous to Eq. 9.1 of the Feynman diagram for photon exchange (Fig 2.1b) are already confirmed in the experiments on ions of low-Z. Indeed it is this very fact which makes it possible to interpret our experiment as a test of higher-order terms in the electron self-energy, instead of as a test of a sum of higher-order terms in both self-energy and in photon-exchange.

Of more interest is the rate for the two-photon decay. No two-photon decay of an atomic state by two photons of opposite parity had hitherto been observed. If the $1s\,2p_{1/2}{}^3P_0 - 1s\,2s\,{}^3S_1$ interval of 260.0 ev is confirmed by spectroscopy on the $1s\,2p_{1/2}{}^3P_0 - 1s\,2s\,{}^3S_1$ transition, then Eq. 3.18 and 3.2 would yield a value for the two-photon decay rate, A^{π}, of $0.63(12)\bullet 10^{10} s^{-1}$ (18%). This is in agreement with Drake's value of $0.564(5)\bullet 10^{10} s^{-1}$. Since the two-photon decay rate vanishes in the non-relativistic limit, even an 18% measurement provides a useful test of relativistic and finite-wavelength corrections to multiphoton decay rates[8].

This work was supported by the Director, Office of Energy Research: Office of Basic Energy Sciences, Chemical Sciences Division; and in part by the Office of High Energy and Nuclear Physics, Nuclear Science Division, of the U.S. Department of Energy under Contract No. DE-AC-03-76SF00098.

---

[6]E.J. Galvez, private communication.

[7]G.W.F Drake, Nucl. Instrum. Methods in Phys. Research B9, 465 (1985).

[8]A departure of the rate for the 2 E1 decay rate of the $1s\,2s\,{}^1S_0$ state of heliumlike krypton (Z=36) from its non-relativistic value has been observed by R. Marrus, V. San Vicente, P. Charles, J.P. Briand, F. Bosch, D. Liesen and I. Varga, Phys. Rev. Lett. 56, 1683, 1986. For a comparison of theory and experiment for this relativistic correction see G.W.F. Drake, Phys. Rev. A 34, 2871 (1986).

Figure Captions

FIG. 1.1 Energy level diagram of the n=1 and n=2 states of heliumlike uranium. Decay rates, except for the $1s\,2p_{1/2}{}^3P_0$ state, are taken from ref. 1.9. Energies are taken from ref. 1.5,1.6,1.9. M1 and M2 decays are magnetic-dipole and magnetic-quadrupole decays, respectively, and decays without labels are electric-dipole decays. An approximate radiative width is indicated for the $^1P_1$ and $^3P_1$ states.

FIG. 1.2 Spectrum recorded by a Ge x-ray detector collimated to view emission perpendicular to the uranium beam at a point 0.67 cm downstream from the Pd foil. This spectrum represents 135 minutes of counting - about 10^8 uranium ions. The Doppler-shifted peak from the decay of $1s\,2p_{1/2}{}^3P_0 \rightarrow 1s\,2s\,{}^3S_1 \rightarrow 1s^2\,{}^1S_0$ is at 77.8 kev. Cascades from higher excited states would produce a peak at 81.4 kev. Peaks at 72.8 kev and 75.0 kev are Pb $K_{\alpha 2}$ and Pb $K_{\alpha 1}$ x rays, and those at 84.5 kev - 87.3 kev are Pb $K_{\beta 1-\beta 3}$ x rays. Peaks at 56.3 kev and 57.5 kev are Ta $K_{\alpha 2}$ and Ta $K_{\alpha 1}$ x rays, and those at 65.2 and 67.0 kev are Ta $K_{\beta 1}$ and $K_{\beta 2}$ x rays. Peaks at 45.2 kev - 46.0 kev are Dy $K_{\alpha 2-\alpha 1}$ x rays. Pb and Dy are used for shielding and Ta is used for x-ray detector collimators. The peak at 21.2 kev is scattered Pd $K_{\alpha 1}$ radiation from the Pd foil. Background is caused by bremsstrahlung of the foil electrons in the field of the uranium projectile; by bremsstrahlung of electrons scattered in and ejected from the Pd foil; and by fast nuclear fragments colliding with the Ge in the x-ray detector. Other sources of background may also exist. To reduce background we restricted the scatter of x rays into the detector, held electrons ejected from the foil away from the detector with a magnetic field, and vetoed background from nuclear fragments using scintillators.

FIG. 1.3 Linear plots of the intensity of x rays from (a) the transition $1s\,2s\,{}^3S_1 \rightarrow 1s^2\,{}^1S_0$, and (b) the sum of the transitions $1s\,2p_{1/2}{}^3P_1 \rightarrow 1s^2\,{}^1S_0$ and $1s\,2p_{3/2}{}^3P_2 \rightarrow$

$1s^2\,{}^1S_0$, as a function of distance downstream from the Pd foil. Each point is the sum of the spectra from two x-ray detectors. Error bars are one standard deviation statistical errors. The horizontal line in (b) is the fit of a hypothetical constant count rate to the data. The count rate is consistent with zero and sets a limit to the contamination of our signal by cascade feeding.

FIG. 2.1 The zeroth and first order Feynman diagrams in the Furry picture of QED for the binding energies of the states of heliumlike uranium. The characteristic coupling constant is 1/Z; different diagrams of the same order in 1/Z may have different leading powers of $(Z\,\alpha)$ which for large Z are all $\sim$ 1. A double line indicates an electron in a bound or continuum state of electrostatic potential of a ^{238}U nucleus, instead of the more familiar plane wave states appropriate for a free electron. Top: the diagram showing the zero-order state of two non-interacting Dirac electrons. Bottom: the contributions from the exchange of one photon, from vacuum polarization, and from electron self-energy, respectively.

FIG. 3.1 Energy level diagram of the n=1 and n=2 states of hydrogenlike uranium. Decays without labels are E1 decays. The state binding energies are the sum of the energies from the Sommerfeld formula, Eq. 2.1, and the finite size, vacuum polarization and self-energy corrections from Ref. 1.6. The transition rates are from Ref. 1.11.

FIG. 5.1 A schematic diagram of the time-of-flight apparatus. A beam of 218 Mev/amu U^{91+} from the Lawrence Berkeley Laboratory Bevalac passes through a movable 0.9 mg/cm^2 palladium target. 0.7% of the beam is converted to heliumlike uranium in the metastable $1s\,2p_{\,1/2}{}^3P_0$ state, which decays in flight downstream of the target with a $1/e$ distance of 1.2 cm. Using a germanium x-ray detector collimated to view emission perpendicular to the beam we count with several target positions photons from the 96.01 kev fed $1s\,2s\,{}^3S_1 \rightarrow 1s^2\,{}^1S_0$ transition, which are Doppler shifted to 77.8 kev. The count rate as a

function of position determines the $1/e$ decay length and the Doppler shift determines the beam velocity. Downstream of the target the beam passes through a wire chamber which monitors the beam position and an ionization chamber which generates a charge proportional to the integrated beam current.

To reduce backgrounds the detector is shielded with 1/2" of lead and the target is held behind a chunk of lead in the beam pipe. A thin mylar window replaces the beam pipe wall opposite the detector to reduce the scatter of x rays into the detector. A magnet supplying a $\sim$ 2400 gauss field prevents electrons ejected from the target from striking the window in the view of the detector. A set of scintillators vetos counts from nuclear events in the target.

FIG. 5.2 Overview of the entire apparatus. The apparatus is mounted on a rigid three-legged table which can be pushed, jacked and shimmed by hand to align the apparatus with the beam. The beam enters from the right. The beam passes first through a plungable wire chamber which marks its position upstream of our apparatus. It then passes through a vacuum chamber which contains a pressure gauge, and a retractable racks of collimators and another of extra targets. The pressure in the chamber was $2 \bullet 10^{-5}$ torr; the two racks were not used in the experiment. The chamber also contains the target translator, whose position readout is viewed by a television camera shielded against stray magnetic fields. The beam passes next through a spare magnet; then the magnet we use in the experiment; then the downstream wire chamber, an ionization chamber, and a scintillator paddle. The planar veto scintillator, and the fiber optic light guides leading to the cylindrical veto scintillator in the bore of the magnet, can also be seen. The x-ray detectors, and the cables supplying current to the magnets, have been draped in black cloth to make the foreground stand out in the photograph.

FIG. 5.3 Photograph of the germanium x-ray detector. Two independently wired germanium elements each with an active volume 5 cm high by 0.5 cm wide by 0.3 cm thick are

angled at 120 degrees so that the detector captures photons from the beam from a 120 degree azimuthal angle. The detectors provide a resolution of 800 ev full-width-at-half-maximum for a 78 kev photon. The detector slides into a box providing 1/2" of lead shielding over 4π steradians, and the box slides between the pole tips of our magnet. The tantalum collimating plates bolt to the face of the detector. The detector is shown in place on the beam line in FIG. 5.2 and FIG. 5.4.

FIG. 5.4 Close-up view of the shielded detector, tantalum collimating plates, target, the crescent-shaped lead shield inside the beam pipe, the cut-outs in the beam pipe opposite the detector, and the mylar window. The window is glued to two aluminum bracelets which seal against two "O" rings set in the beam pipe. (The second groove downstream of the target has no function). The window has been slipped like a sleeve along the beam pipe into the bore of the upstream pole tip of the magnet, as if we were about to change a target. The beam pipe is 3.0 inches in diameter. The planar scintillator (See FIG. 5.5) has been removed to make this photograph.

FIG. 5.5 Photograph showing the planar and cylindrical scintillators used to veto counts from nuclear events in the target. The cylindrical scintillator is made of two half-cylinders which are connected to their phototubes by acrylic optical fiber light guides. The cylindrical scintillator extends up to the face of the downstream pole tip of the magnet. A 1/32" layer of lead between the beam pipe and the cylindrical scintillator reduces the amplitude of counts from x rays from electrons which strike the beam pipe near the scintillator as the confining magnetic field diverges and weakens.

FIG. 6.1 X-ray spectra 70 to 95 kev showing the Doppler shift of the $1s\,2p_{\,1/2}\,^3P_0$-fed $1s\,2s\,^3S_1 \rightarrow 1s^2\,^1S_0$ x ray, observed downstream of the target and at right angles to the beam, for the two beam energies of 218 (upper spectrum) and 175 (lower spectrum) Mev/amu. These energies are determined from the nominal energy of the Bevalac corrected for the

energy loss in our targets. To aid the eye the inserts show in black the lead K_α and K_β x rays, with their characteristic relative amplitudes and with the 800 ev full-width-half-maximum resolution of our germanium detector. A white peak shows the calculated location and width (though not the height) of the $1s\,2s\,^3S_1 \rightarrow 1s^2\,^1S_0$ line for the two beam energies. The $1s\,2s\,^3S_1 \rightarrow 1s^2\,^1S_0$ peak is roughly twice as broad in the 175 Mev/amu spectrum because for this spectrum we doubled the angular acceptance of the detector. The upper spectrum was taken with a 0.9 mg/cm^2 palladium target and the lower spectrum taken with 2.28 mg/cm^2 gold target. The decay curve for the palladium target is shown in FIG. 1.3 and the curve for the gold target is shown in FIG. 6.3.

FIG. 6.2 A typical signal spectrum (here for a detector-target separation of 2.04 cm) showing the quadratic fit to the background. The regions labeled F are the regions the curve is constrained to fit. These regions lie, in order, between the Dy K_β and the Ta K_α lines, between the Ta K_β lines and the Pb K_α lines, and above the Pb K_β lines. The region S is the range of energy spanned by our Doppler-broadened $1s\,2s\,^3S_1 \rightarrow 1s^2\,^1S_0$ signal peak at 77.8 kev, and the region C that spanned by the the cascade peak at 84.1 kev.

FIG. 6.3 A decay curve, similar to FIG. 1.3, collected during a the run of an earlier and cruder version of the experiment, when we first observed a $1s\,2s\,^3S_1 \rightarrow 1s^2\,^1S_0$ signal for a beam energy of 175 Mev/amu using a 2.28 mg/cm^2 gold target. Part of a spectrum contributing to the point at 1.5 cm is shown in the lower half of FIG. 6.1. The curve is a nonlinear least-squares fit of an exponential to the data, which gives a $1/e$ distance of 1.24(.28) cm (23%). The reduced χ^2 for the fit is 1.3. There is no plot of the intensity of the cascade peak because for this beam energy the peak is Doppler-shifted on top of the prominent Pb K_β fluorescence lines.

FIG. 7.1 A spectrum taken at our largest detector-target separation of 3.90 cm. Superimposed on a continuum background falling smoothly from 10 to 100 kev are the atomic

K_α and K_β lines of dysprosium, tantalum, and lead. At 13.3 and 53.5 kev appear lines from excited nuclear levels of ^{73}Ge , and at 23.5 a line from an exited nuclear level of ^{71}Ge . The line at 53.5 kev is superimposed on the ordinarily weak $K_{\beta_2'}$ line of dysprosium.

FIG. 7.2 The energies, lifetimes and principal transitions of the lowest-lying levels of ^{69}Ge , ^{71}Ge , ^{73}Ge , and ^{75}Ge , which are the only isotopes of germanium with low-lying nuclear transitions with energies less than 100 kev. The data are from ref. 7.1.

FIG. 9.1 Ratio for the $2s_{1/2}$ state of the higher order terms in the electron self-energy to the total self-energy obtained by comparing the sum of the series through the term $A_{70}(Z\alpha)^7$ with a numerical calculation which includes terms to all orders in $(Z\alpha)$.

FIG. 9.2 Comparison between theory and experiment across the isoelectronic sequence for the $1s\,2p_{1/2}\,^3P_0$--$1s\,2s\,^3S_1$ interval. With the exception of the new points at Z=92 this figure is the work of Dr. E.J. Galvez[1]. The references for the individual points for Z $\leq$ 30 are listed in FIG. 9.3. For Z $\neq$ 92 the horizontal line which give the zero for the figure is the calculation of Goldman and Drake[2]. The upper and lower bounds show the effect of the largest uncalculated term in the energy difference which they estimate to be $\sim 0.2\ Z^{-2}(Z\alpha)^6 mc^2$. The dot-dash line shows a calculation of Deserio *et al*[3], and the dotted line shows a calculation by Hata and Grant[4]. The point (a) shows the agreement between our experimental value of 270.0(7.9) ev and Drake's[5] theoretical value of 258.63 ev, the theoretical error in which I have extrapolated from ref. 2. The point (b) shows the agreement between our experimental value and the theoretical $1s\,2p_{1/2}\,^3P_0$--$1s\,2s\,^3S_1$ interval of 255.1 ev derived in Chapter 2.

---

[1]E.J. Galvez, private communication.

[2]S. P. Goldman and G.W.F. Drake, J. Phys. B 17, L197-L202 (1984); G.W.F. Drake, private communication.

[3]R. Deserio, H.G. Berry, R.L. Brooks, J. Hardis, A.E. Livingston, and S.J. Hinterlong, Phys. Rev. A 24, 1872 (1981).

[4]J. Hata and I.P. Grant, J Phys. B 16, 507 (1983); J Phys. B 16, 523(1983); J Phys. B 16, L369 (1983); J Phys. B 17, 931 (1984).

[5]G.W.F. Drake, Nucl. Instum. Methods in Phys. Research B9, 465 (1985).

FIG 9.3. List of references for the points in FIG. 9.2, in order left to right across the figure.

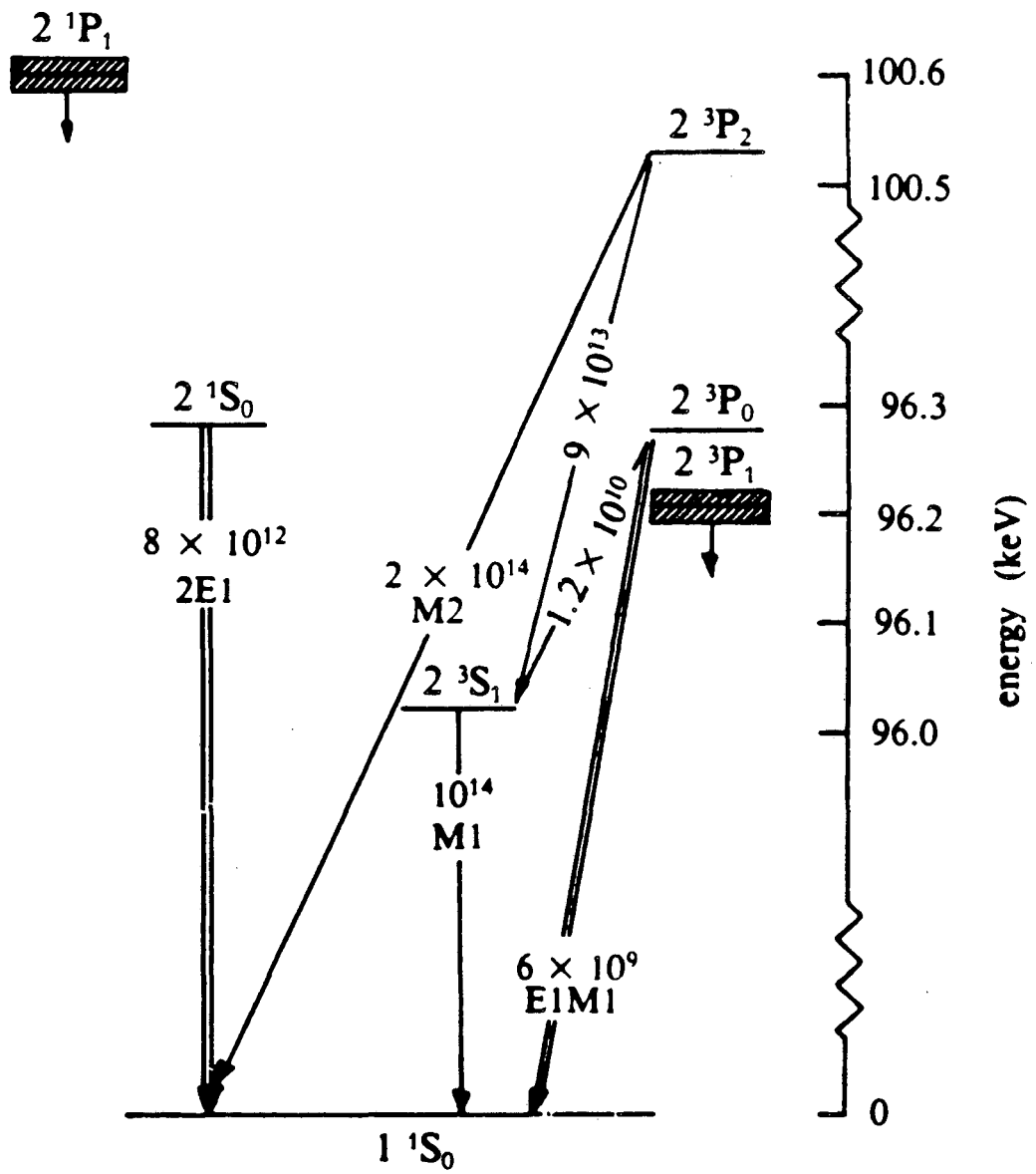
Heliumlike Uranium
2 ¹P₁
2 ³P₂
2 ¹S₀
2 ³P₀
2 ³P₁
2 ³S₁
1 ¹S₀
8 × 10¹²
2E1
2 × 10¹⁴
M2
9 × 10¹³
1.2 × 10¹⁰
10¹⁴
M1
6 × 10⁹
E1M1
100.6
100.5
96.3
96.2
96.1
96.0
0
energy (keV)
XBL 868-2977

Figure 1.1

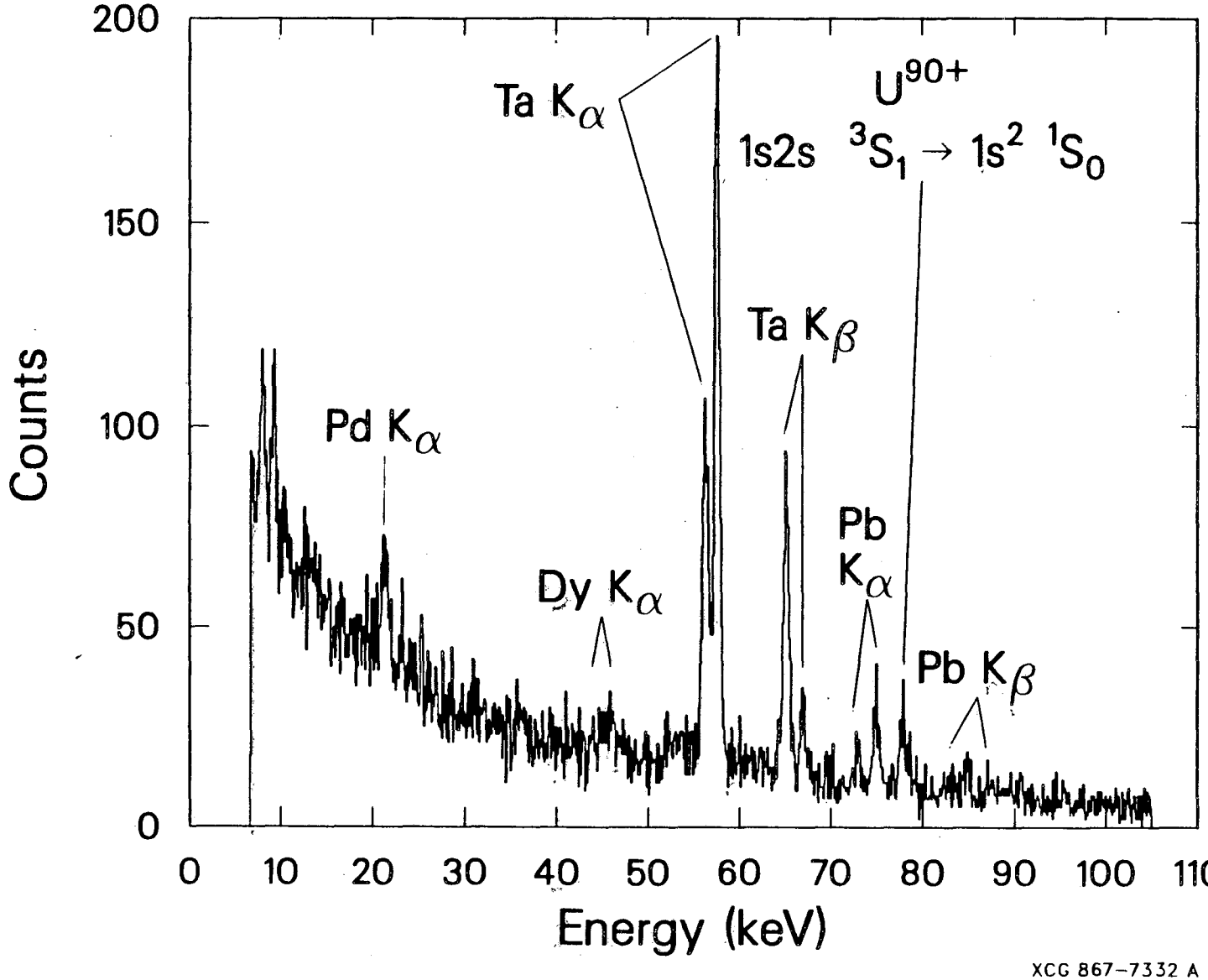
200
150
100
50
0
Counts
Ta K_α
U^{90+}
1s2s $^3S_1 \rightarrow 1s^2\ ^1S_0$
Ta K_β
Pd K_α
Dy K_α
Pb K_α
Pb K_β
0 10 20 30 40 50 60 70 80 90 100 110
Energy (keV)
XCG 867-7332 A

Figure 1.2

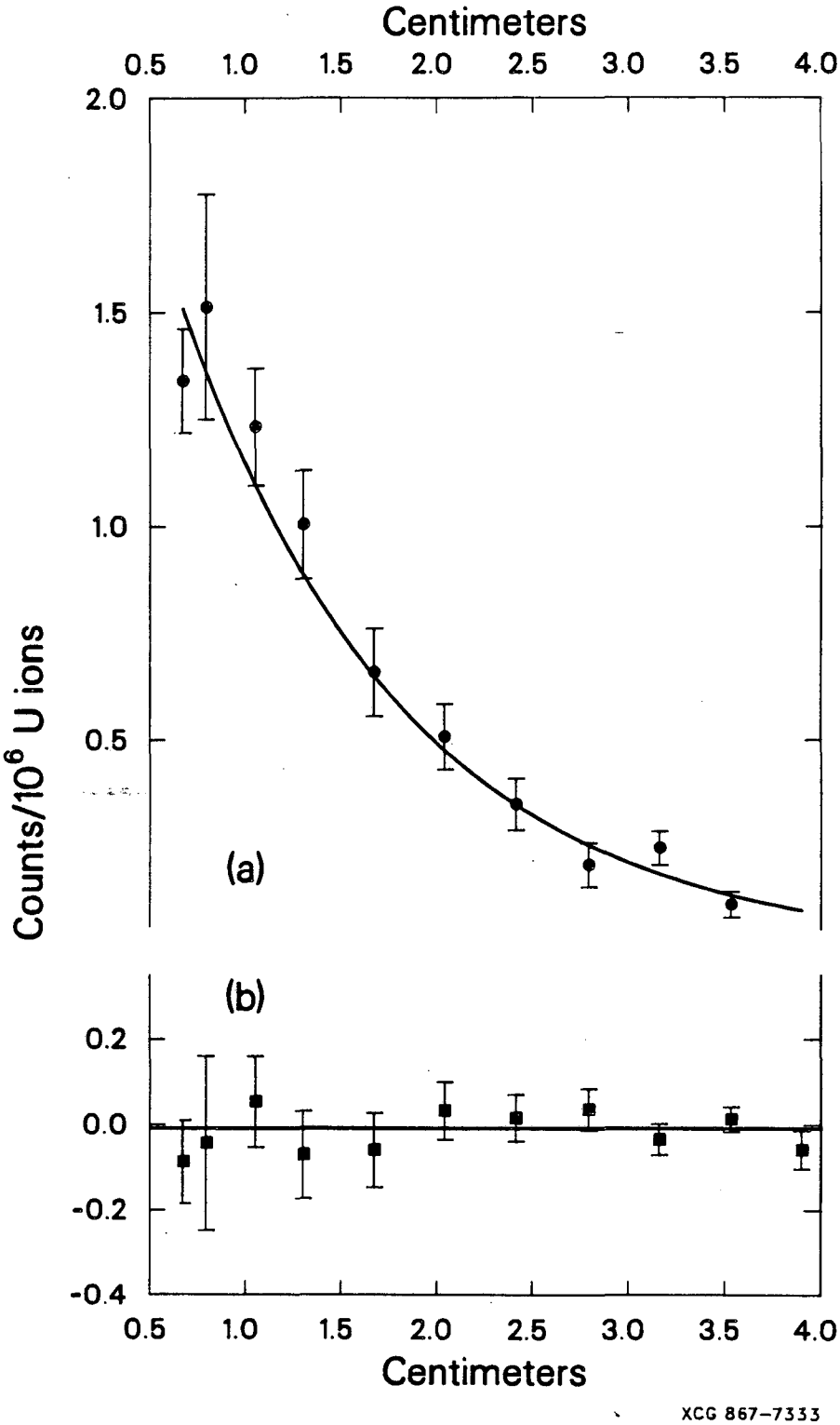
Centimeters
0.5
1.0
1.5
2.0
2.5
3.0
3.5
4.0
2.0
1.5
1.0
0.5
Counts/10^6 U ions
(a)
(b)
0.2
0.0
-0.2
-0.4
0.5
1.0
1.5
2.0
2.5
3.0
3.5
4.0
Centimeters
XCG 867-7333

Figure 1.3

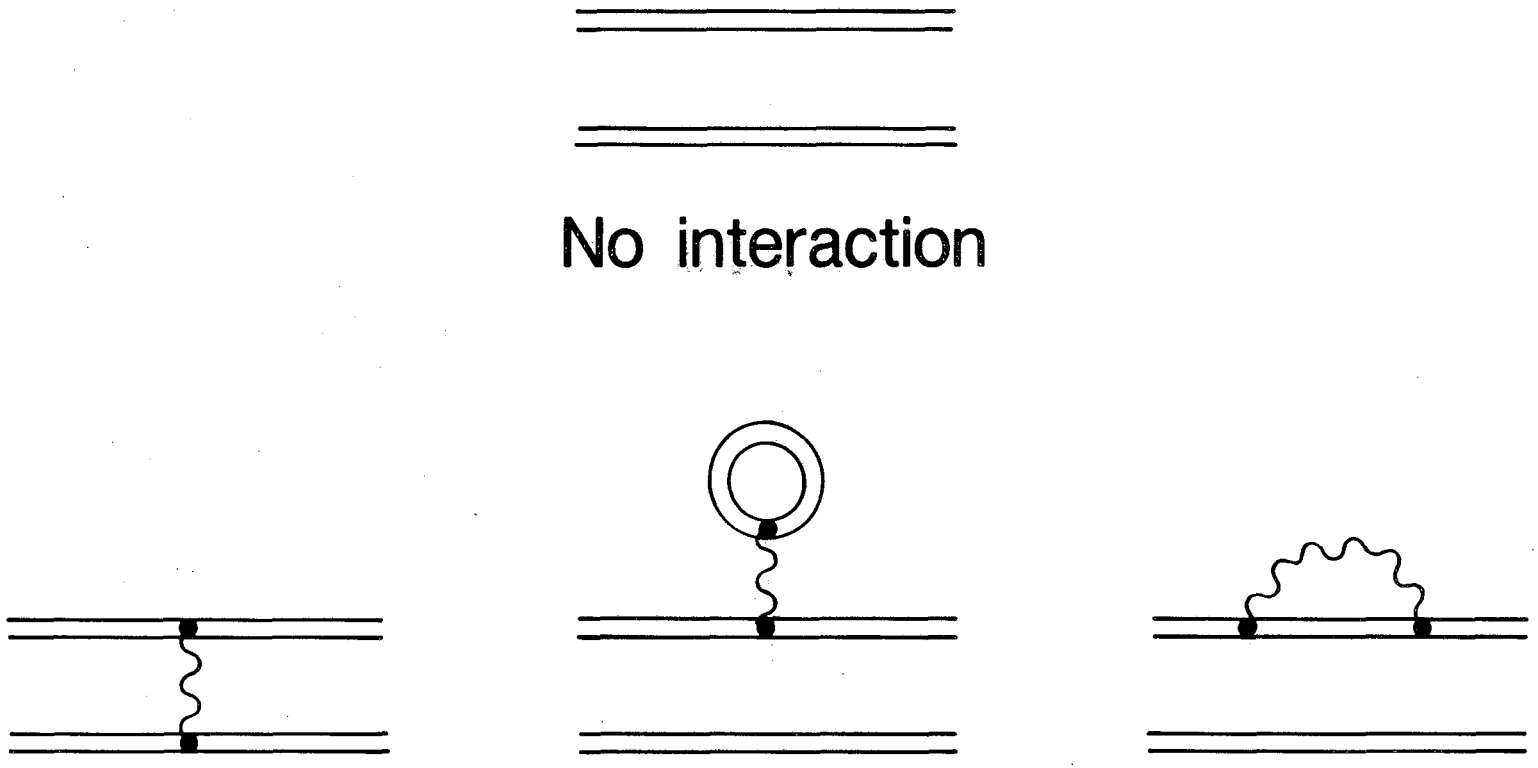

XBL 8612-5017

Figure 2.1

Hydrogenlike Uranium

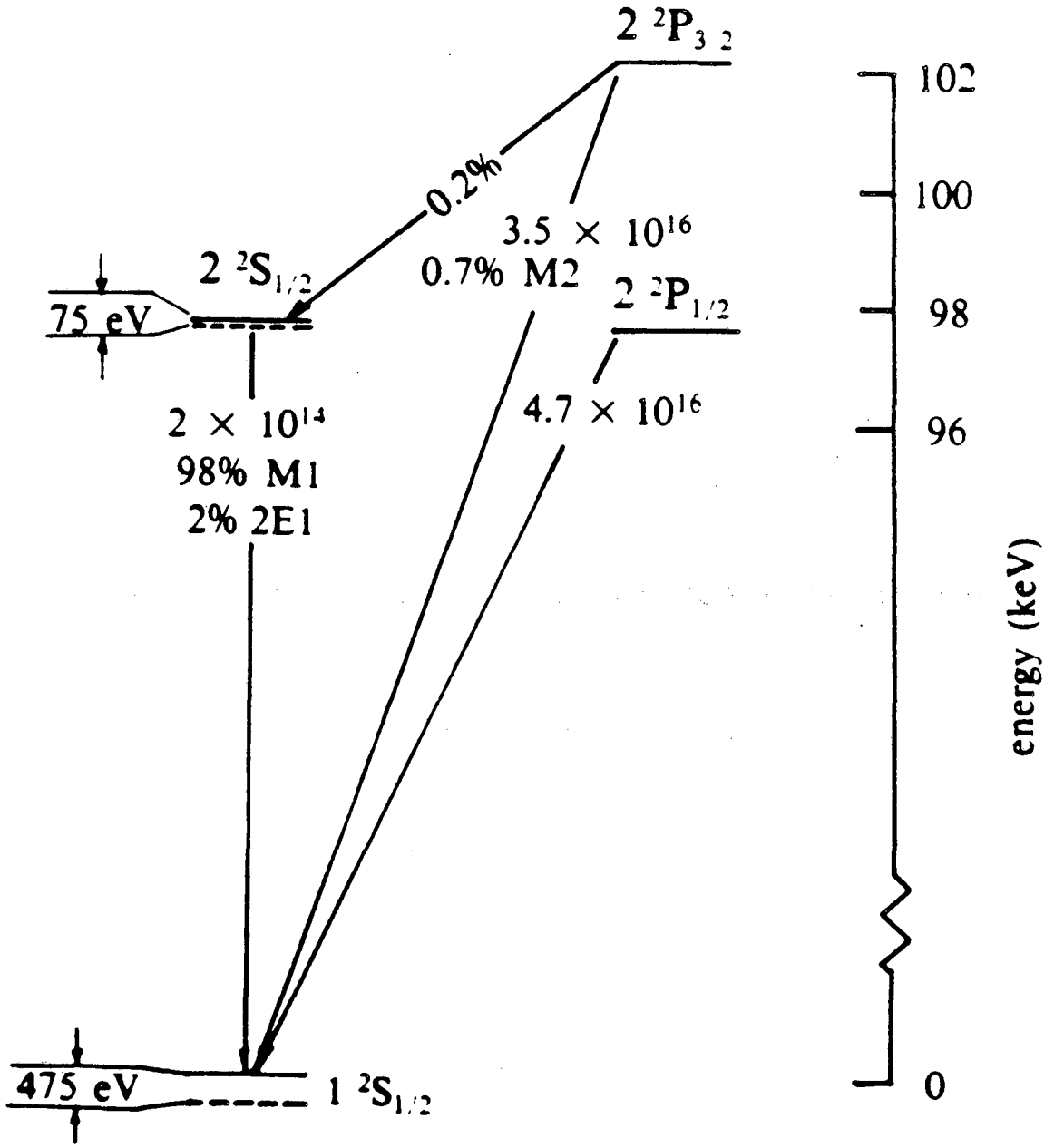

XBL 848-8592

Figure 3.1

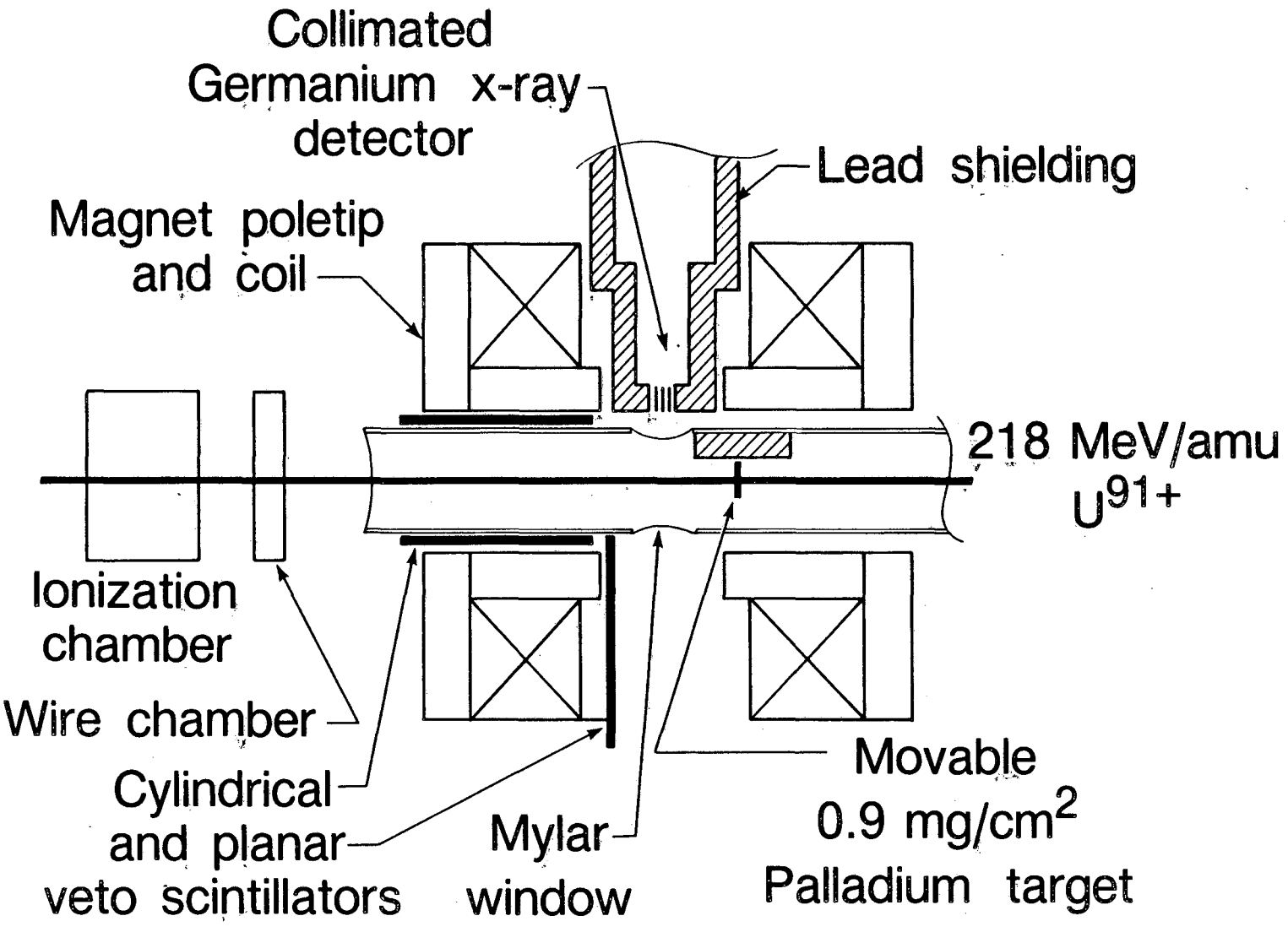

XBL 8612-5018

Figure 5.1

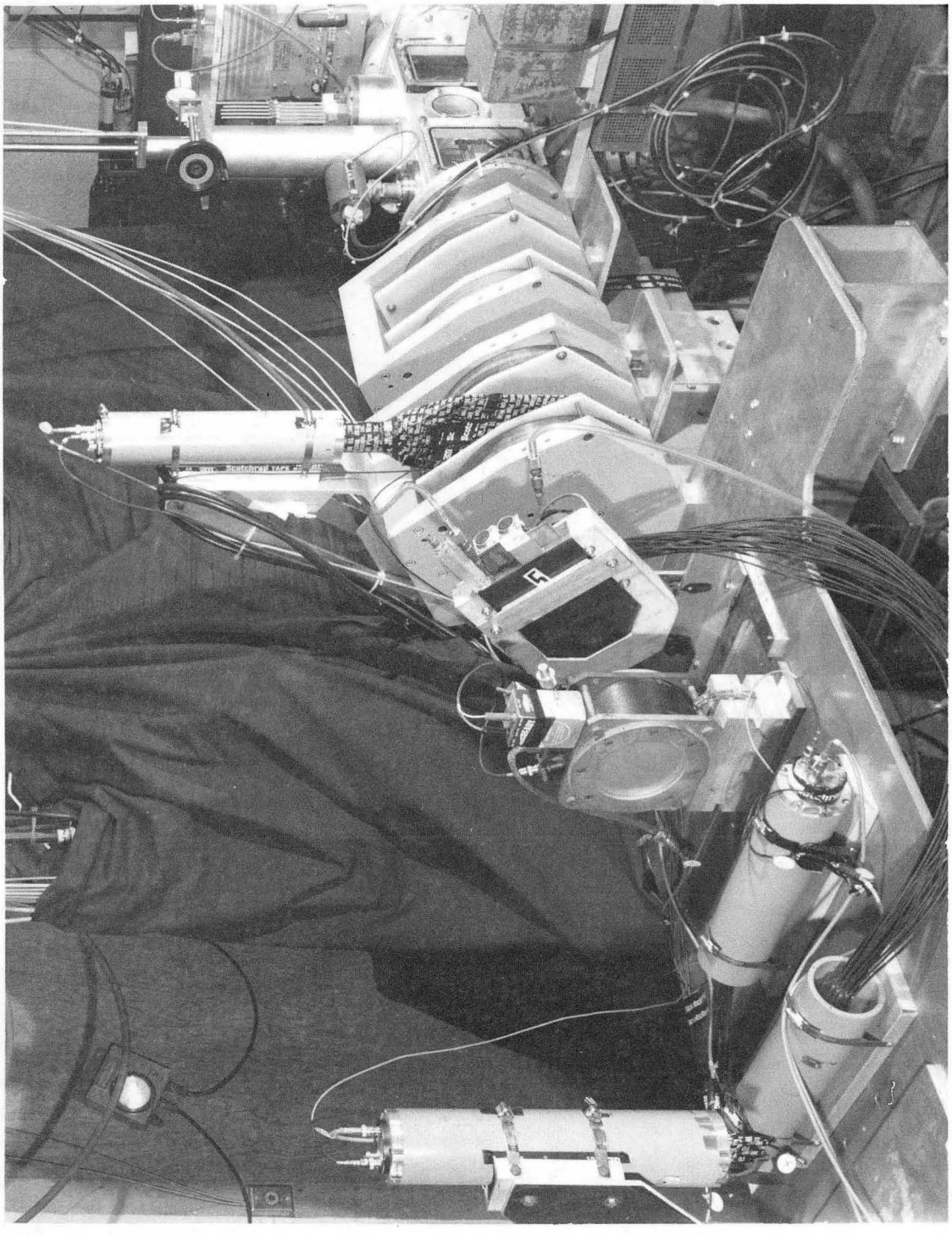

CBB 861-321

Figure 5.2

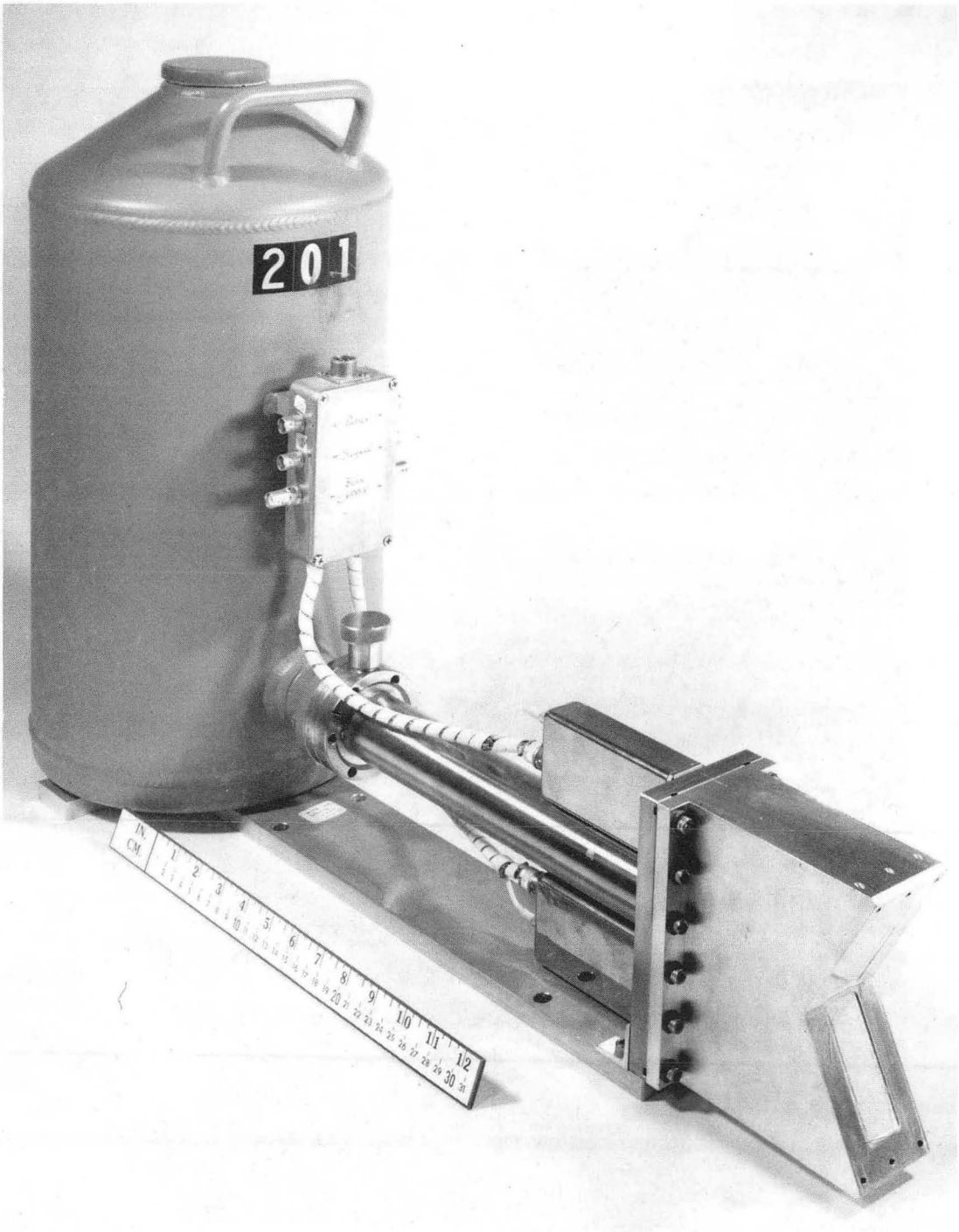

CBB 860-9541

Figure 5.3

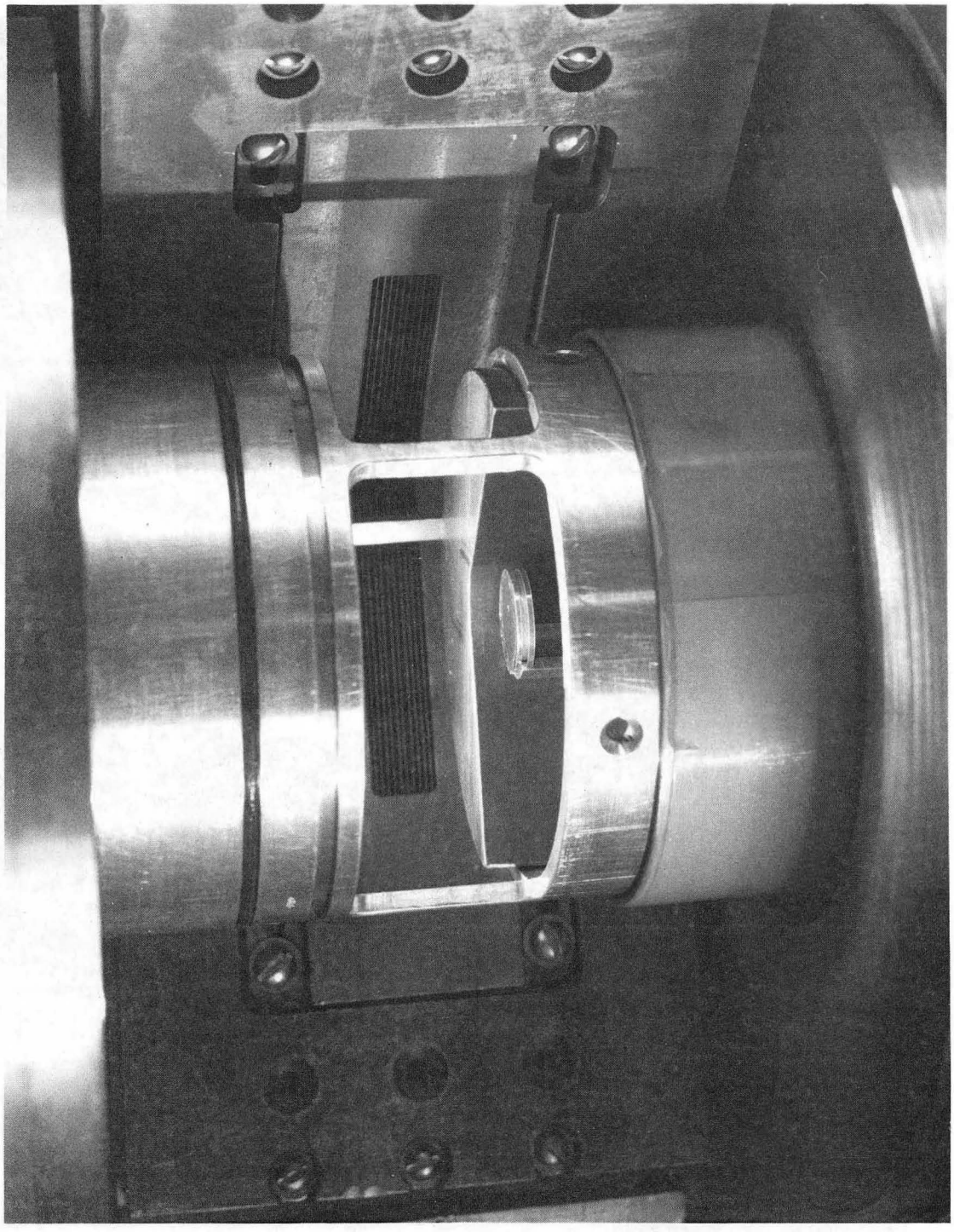

CBB 855-3743

Figure 5.4

CBB 861-325

Figure 5.5

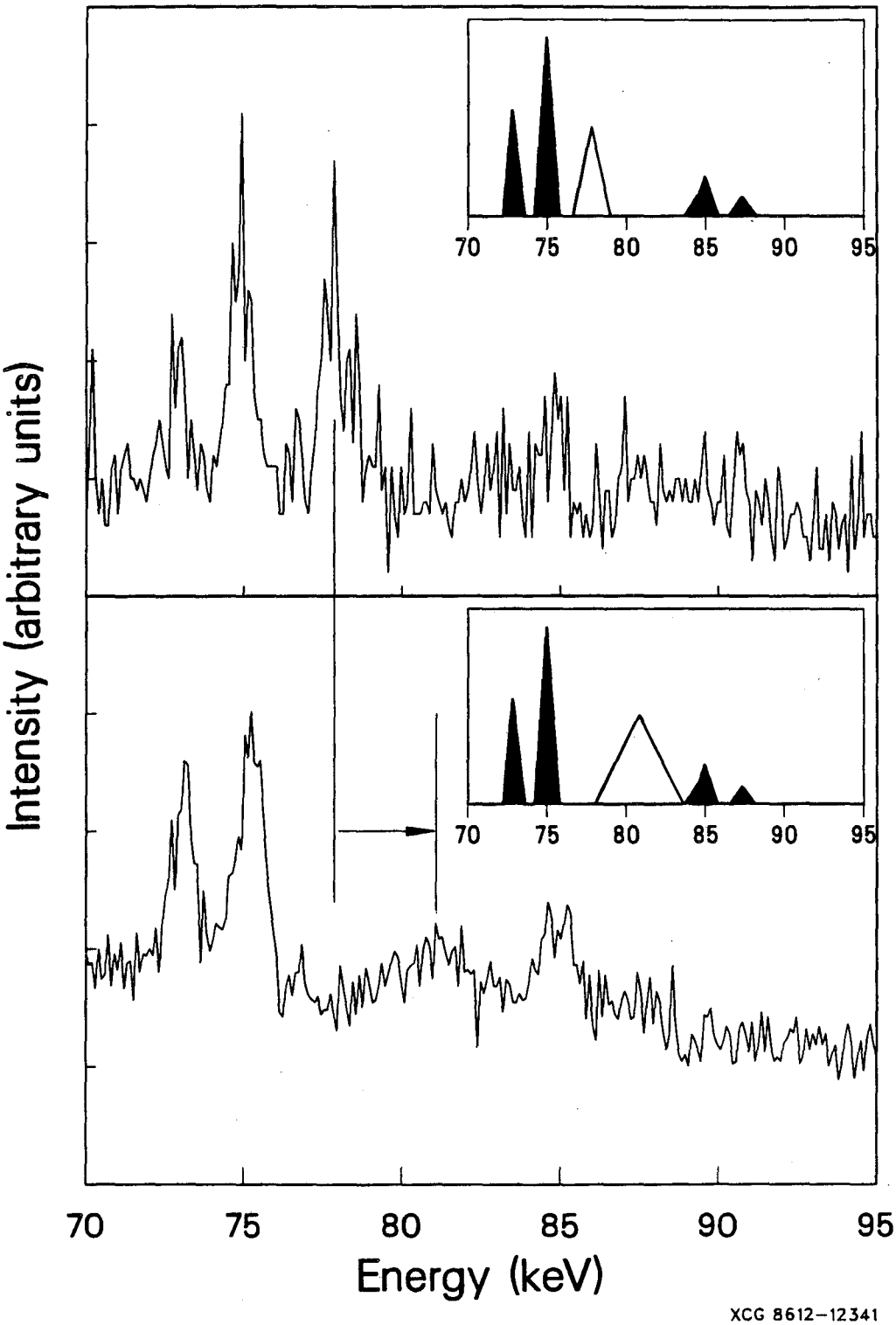
Intensity (arbitrary units)
70
75
80
85
90
95
Energy (keV)
XCG 8612-12341

Figure 6.1

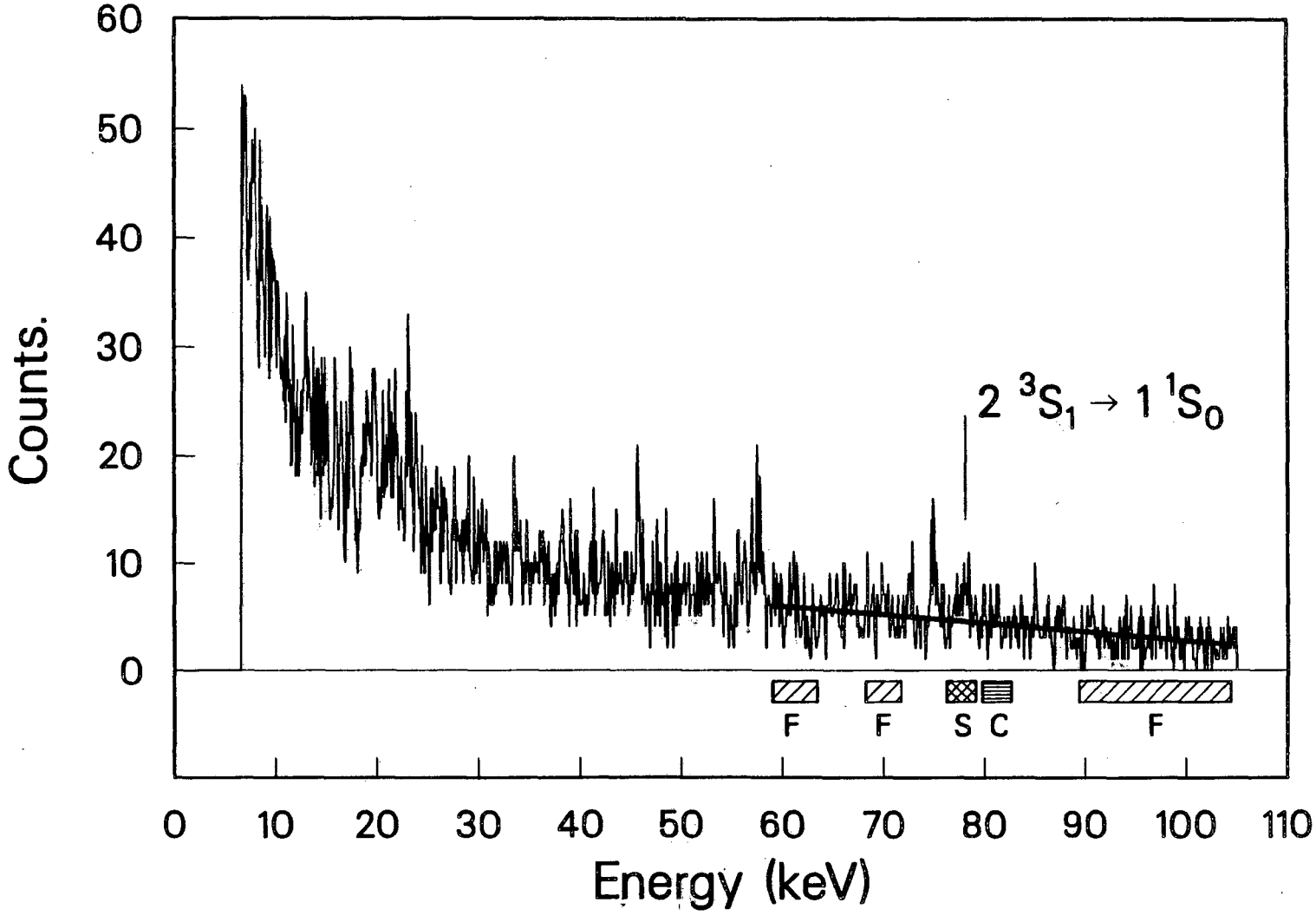
Counts.
60
50
40
30
20
10
0
$2\ ^3S_1 \rightarrow 1\ ^1S_0$
F
F
S
C
F
0
10
20
30
40
50
60
70
80
90
100
110
Energy (keV)
XCG 8612-12342

Figure 6.2

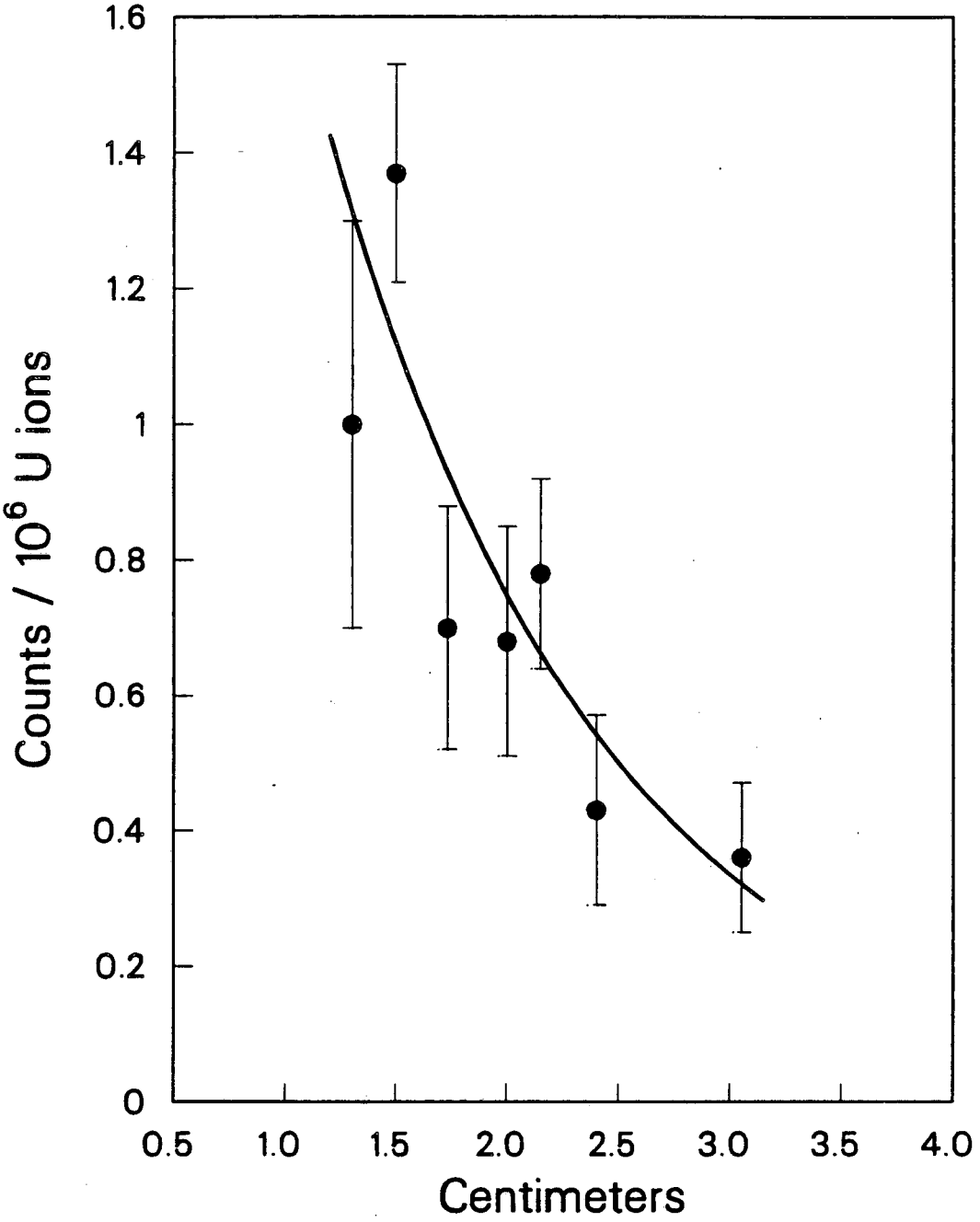

XCG 8612-12337

Figure 6.3

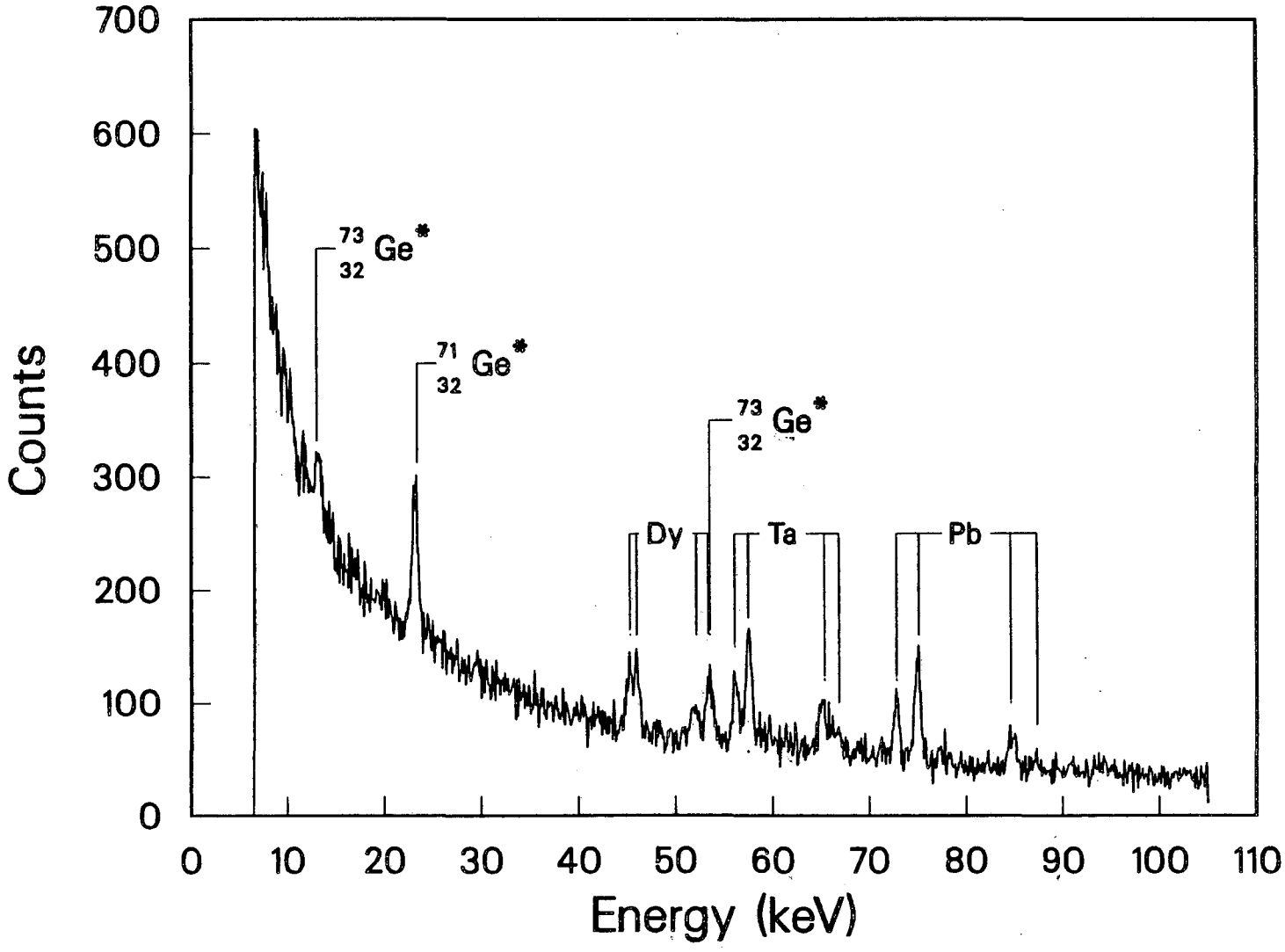
700
600
500
400
300
200
100
0
Counts
0
10
20
30
40
50
60
70
80
90
100
110
Energy (keV)
73 32 Ge*
71 32 Ge*
73 32 Ge*
Dy
Ta
Pb
XCG 8612-12340

Figure 7.1

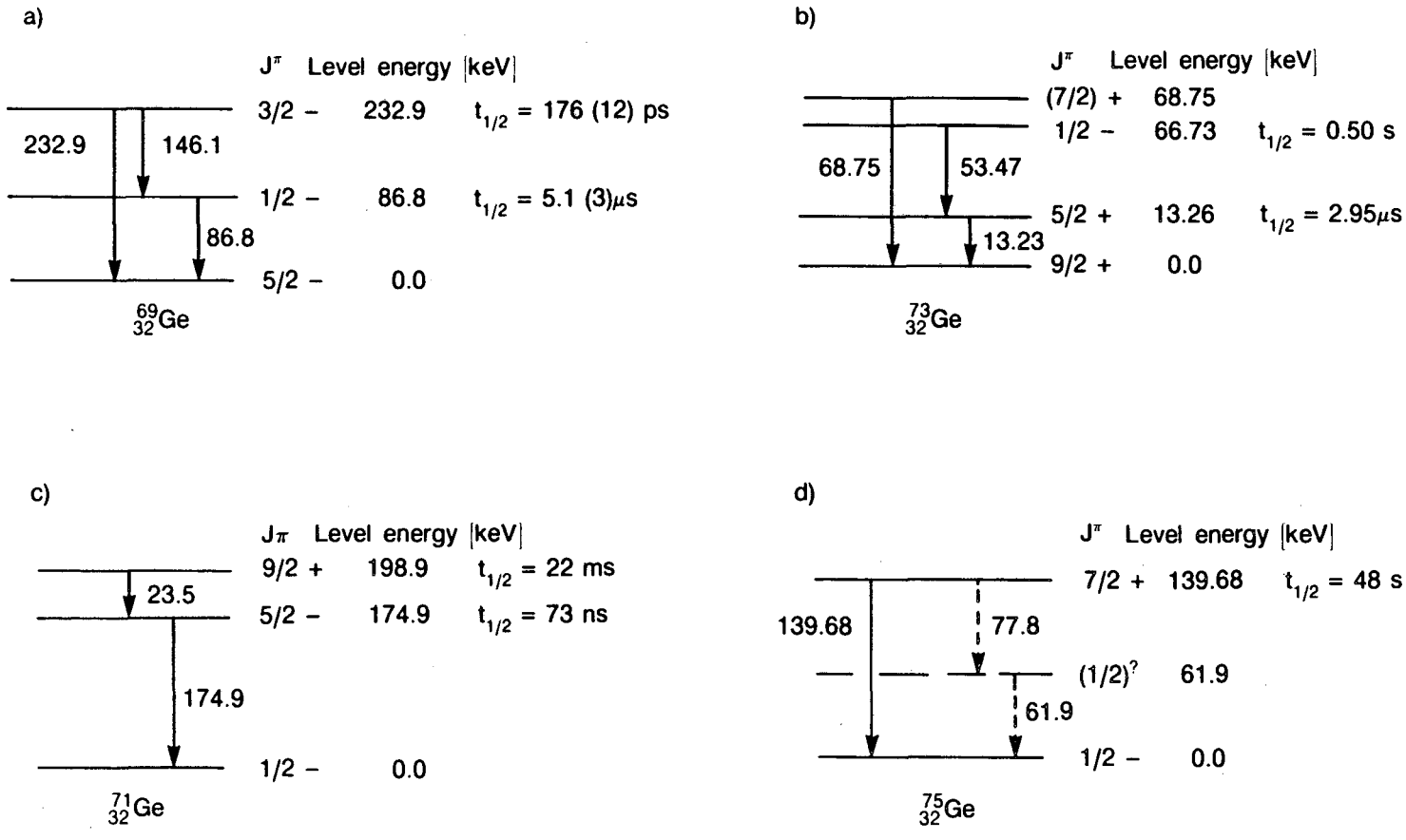
a)
J^π Level energy [keV]
3/2 − 232.9 $t_{1/2}$ = 176 (12) ps
232.9
146.1
1/2 − 86.8 $t_{1/2}$ = 5.1 (3)μs
86.8
5/2 − 0.0
$^{69}_{32}$Ge
b)
J^π Level energy [keV]
(7/2) + 68.75
1/2 − 66.73 $t_{1/2}$ = 0.50 s
68.75
53.47
5/2 + 13.26 $t_{1/2}$ = 2.95μs
13.23
9/2 + 0.0
$^{73}_{32}$Ge
c)
$J\pi$ Level energy [keV]
9/2 + 198.9 $t_{1/2}$ = 22 ms
23.5
5/2 − 174.9 $t_{1/2}$ = 73 ns
174.9
1/2 − 0.0
$^{71}_{32}$Ge
d)
J^π Level energy [keV]
7/2 + 139.68 $t_{1/2}$ = 48 s
139.68
77.8
$(1/2)^?$ 61.9
61.9
1/2 − 0.0
$^{75}_{32}$Ge
XBL 8612-5020

Figure 7.2

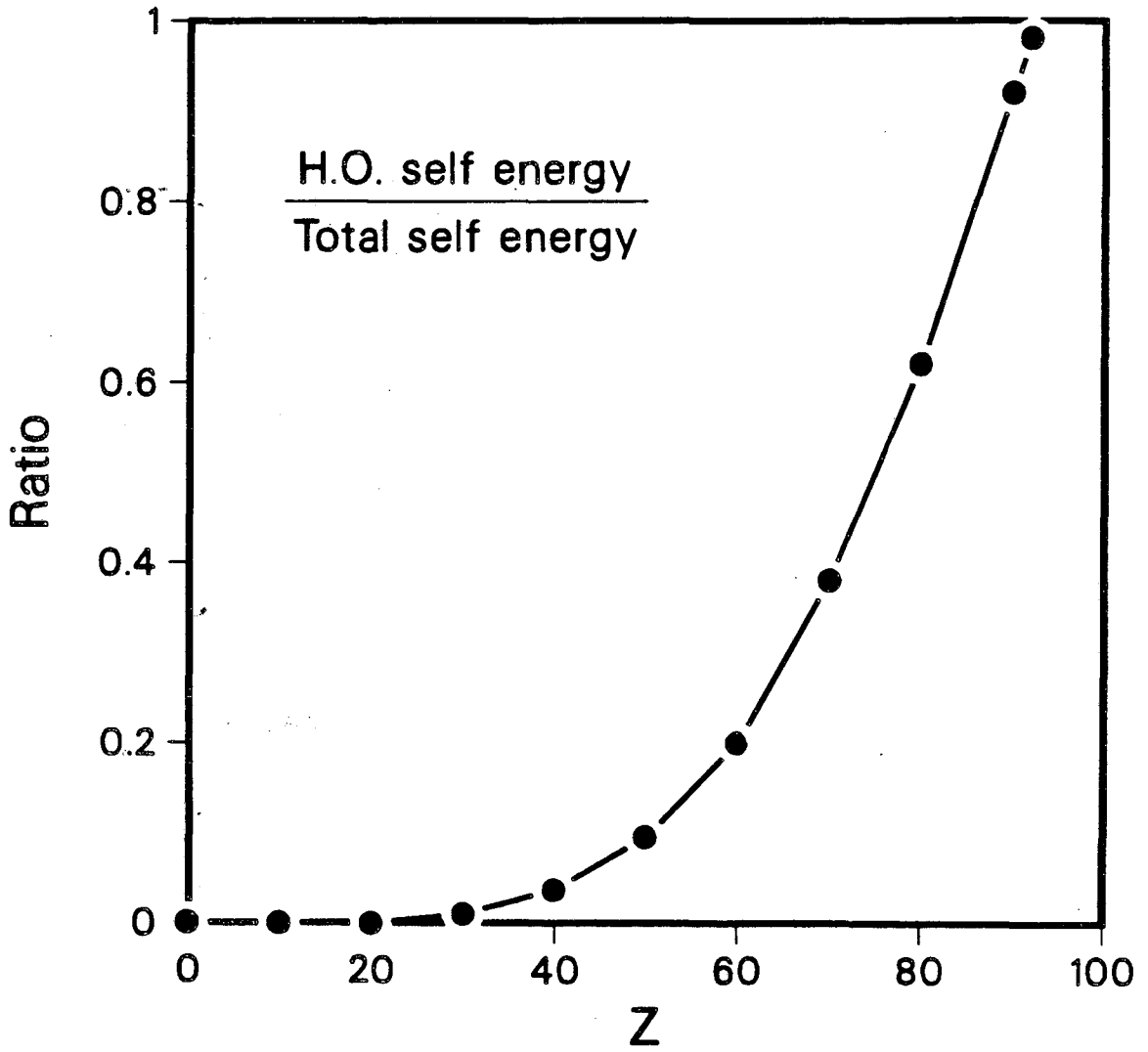
H.O. self energy
Total self energy
Ratio
1
0.8
0.6
0.4
0.2
0
0
20
40
60
80
100
Z
XCG 838-7228

Figure 9.1

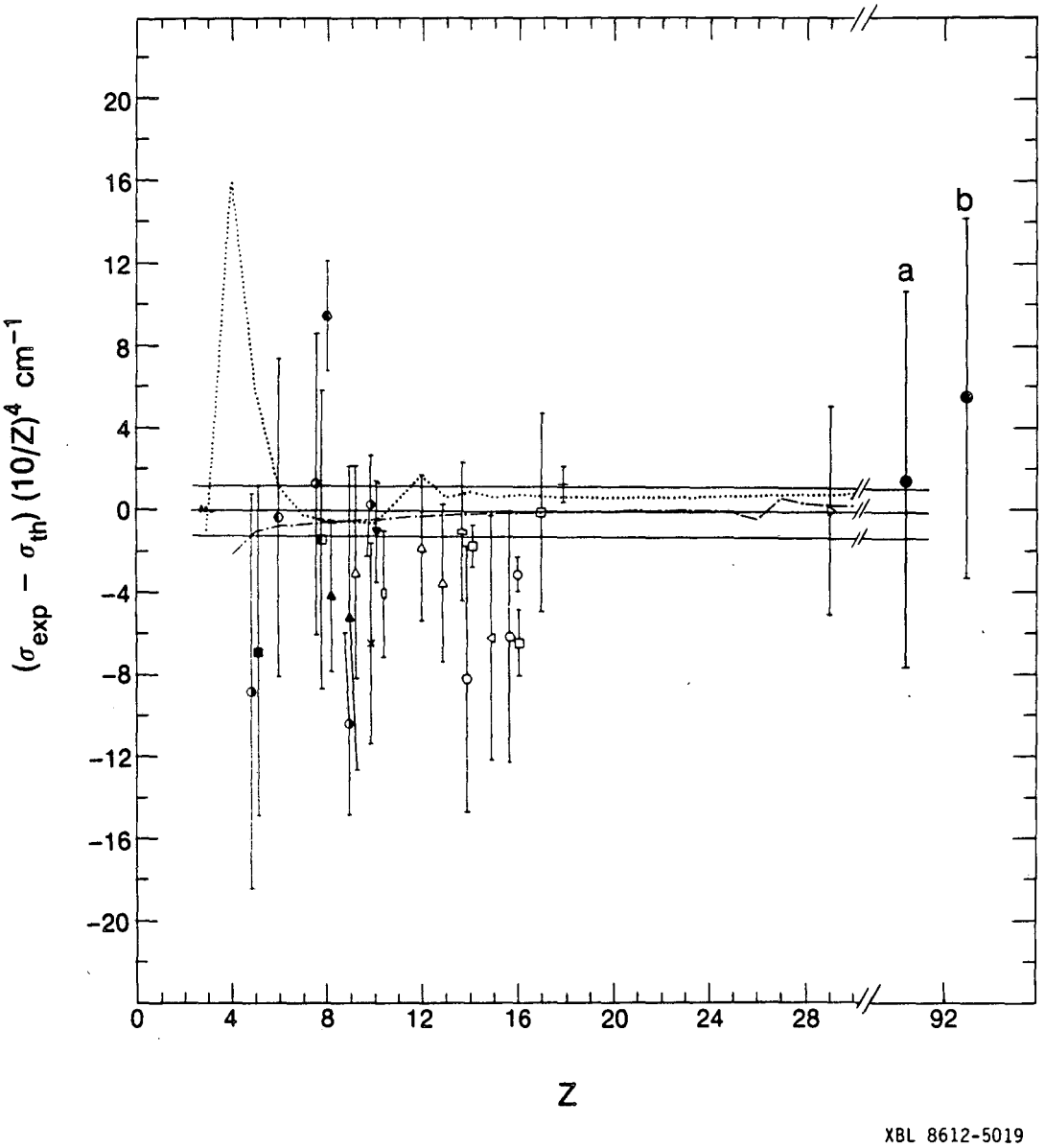
20
16
12
8
4
0
-4
-8
-12
-16
-20
0
4
8
12
16
20
24
28
92
a
b
Z
$(\sigma_{exp} - \sigma_{th})(10/Z)^4$ cm^{-1}
XBL 8612-5019

Figure 9.2

Z	Symbol for the point	Reference
2	Tiny square	R.A. Holt, S.D. Rosner, T. D. Gaily, A. G. Adam, Phys. Rev. A 22, 1563 (1980).
2	Tiny dot	E. Riis, H.G. Berry, O. Poulsen, S.A. Lee, S.T. Yang, Phys. Rev. A 33, 3023 (1986).
5	Hexagon, white-black	B. Edlen, Nova Acta Regiae Soc. Ups. 9, (1934).
5	Black Square	M Eidelsberg, J. Phys. B 7, 1476 (1974).
6	Hexagon, black-white	B. Edlen, B. Lofstrand, J Phys. B 3, 1380 (1970).
8	Circle, white-black	W. Engelhardt, J. Sommer, Astrophys J. 167, 201 (1971).
8	Square, black-white	S.C. Baker, J. Phys. B 6, 709 (1973).
8	Black Hexagon	G.D. Sandlin, G.E. Brueckner, R. Toulsey, Astrophys. J. 214, 898 (1977).
8	Black Triangle, point up	M.F. Stamp, I.A. Armour, N.J. Peacock, J.D. Silver, J. Phys. B 14, 3551 (1981).
9	Circle, white-black	W. Engelhardt, J. Sommer, Astrophys J. 167, 201 (1971).
9	Black Triangle, point up	M.F. Stamp, I.A. Armour, N.J. Peacock, J.D. Silver, J. Phys. B 14, 3551 (1981).
9	Triangle, point up	H.A. Klein, F. Moscatelli, E.G. Myers, E.H. Pinnington, J.D. Silver, E. Talbert, J. Phys. B 18, 1483 (1985).
10	Circle, white-black	W. Engelhardt, J. Sommer, Astrophys J. 167, 201 (1971).
10	"X" symbol	H.A. Klein, S. Bashkin, B.P. Duval, F. Moscatelli, J.D. Silver, H.F. Beyer, F. Folkmann, J. Phys. B 15, 4507 (1982).
10	Black Triangle	G.D. Sandlin, R. Tousey, Astrophys. J. 227, L107 (1979).
10	Vertical Rectangle	H.G. Berry, J.E. Hardis, Phys. Rev A 33, 2778 (1986).
12	Triangle, point up	H.A. Klein, R. Moscatelli, E.G. Myers, E.H. Pinnington, J.D. Silver, E. Trabert, J. Phys B 18, 1483 (1985).
13	Triangle, point up	H.A. Klein, R. Moscatelli, E.G. Myers, E.H. Pinnington, J.D. Silver, E. Trabert, J. Phys B 18, 1483 (1985).
14	Horizontal Rectangle	S.I. Armour, E.G. Myers, J.D. Silver, E. Trabert, Phys. Lett. 75A, 45 (1979).
14	Hexagon	A.E. Livingston, S.J. Hinterlong, J.A. Poirier, R. Deserio, H.G. Berry, J. Phys. b 13, L139 (1980).
14	Square	R. Deserio, H.G. Berry, R.L. Brooks, J. Hardis, A.E. Livingston, S.J. Hinterlong, Phys. Rev. A 24, 1872 (1981).
15	Triangle, point left	A.E. Livingston, S.J. Hinterlong, Nucl. Instr. Meth. 202, 103 (1982).
16	Hexagon	A.E. Livingston, S.J. Hinterlong, J.A. Poirier, R. Deserio, H.G. Berry, J. Phys. b 13, L139 (1980).
16	Circle	E.J. Galvez, A.E. Livingston, A.J. Mazure (To be published)
16	Square	R. Deserio, H.G. Berry, R.L. Brooks, J. Hardis, A.E. Livingston, S.J. Hinterlong, Phys. Rev. A 24, 1872 (1981).
17	Square	R. Deserio, H.G. Berry, R.L. Brooks, J. Hardis, A.E. Livingston, S.J. Hinterlong, Phys. Rev. A 24, 1872 (1981).
18	Dash	H.F. Beyer, F. Folkmann, K.H. Schartner, Z. Phys. D __65 (1986).
29	Triangle, point right	J.P. Buchet, M.C. Buchet-Poluizac, A. Denis, J. Desesquelles, M. Druetta, J Grandin, X. Husson, D. Lechler, H.F. Beyer, Nucl. Instr. Meth. B 9, 645 (1985).

Figure 9.3

This report was done with support from the Department of Energy. Any conclusions or opinions expressed in this report represent solely those of the author(s) and not necessarily those of The Regents of the University of California, the Lawrence Berkeley Laboratory or the Department of Energy.

Reference to a company or product name does not imply approval or recommendation of the product by the University of California or the U.S. Department of Energy to the exclusion of others that may be suitable.

LAWRENCE BERKELEY LABORATORY
TECHNICAL INFORMATION DEPARTMENT
UNIVERSITY OF CALIFORNIA
BERKELEY, CALIFORNIA 94720